STRUCTURE OF TURBULENCE IN THE MARINE ATMOSPHERIC SURFACE LAYER

by

Ravi Shankar Boppe

Dissertation submitted to the faculty of the
Virginia Polytechnic Institute and State University
in partial fulfillment of the requirements for the degree of

DOCTOR OF PHILOSOPHY

in

AEROSPACE ENGINEERING

APPROVED:

Dr. Wayne L. Neu, Chairman

Dr. R. L. Simpson

Dr. W. J. Devenport

Dr. S. Liapis

Dr. S. A. Ragab

December, 1995

Blacksburg, Virginia

STRUCTURE OF TURBULENCE IN THE MARINE ATMOSPHERIC SURFACE LAYER

by

Ravi Shankar Boppe

Committee Chairman: Dr. Wayne L. Neu

AEROSPACE ENGINEERING

(ABSTRACT)

Turbulence research in the laboratory has confirmed the existence of quasi-coherent structures amidst the chaos of a turbulent boundary layer. It has been observed that a quasi-periodic phenomena called "bursting" accounts for a major contribution to the turbulent Reynolds stress and the production of turbulent kinetic energy. Bursting is the term used for a sequence of events, where a low-speed streak of fluid from the near wall region lifts away from the wall, slowly at first, and then rapidly moves away from the wall as it convects downstream where it becomes unstable and breaks up violently upon interaction with the outer flow. This ejection of low speed fluid into the mean flow is responsible for locally high values of turbulent kinetic energy. Although a great deal is known about these structures in laboratory flows, little has been done to investigate if such structures are universal in turbulent flows, i.e., their existence in large Reynolds number flows such as the turbulent air flow over the ocean. It would seem, intuitively, that such structures, if present in the marine atmospheric boundary layer, would play a major role in the transfer of momentum, mass and heat across the air-sea interface. It is speculated that these motions may also be associated with large scale organized motions in wall bounded turbulent shear flows. The effort aimed at elucidating the physics underlying such structures would be invaluable in contributing to our understanding of the air-sea flux mechanism.

In this dissertation, standard ejection detection schemes like the quadrant, the VITA and the modified u-level techniques have been applied to turbulent wind data measured over the ocean to confirm the existence of burst like structures. The proportions of contributions to the Reynolds stress from the four quadrants of the $u'w'$ plane are in close agreement with the corresponding contributions for a laboratory flow. Ejection detection followed by the grouping of ejections into bursts yielded a mean burst period of 47 s, at a height of 8.2 m above the water surface, where the mean wind velocity was 6.74 m/s. This burst period corresponds well with the peaks obtained from the autocorrelation of the streamwise velocity signal and the first moment of the stress spectrum, confirming the quasi-periodic nature of this phenomena. Furthermore, phase averages of these events show a structure which is similar to the structure of events detected in laboratory flows.

The ejection periods are seen to decrease with increasing wind speed. The burst periods decrease at first with increasing wind speed and then appear to attain a constant value after a wind speed of 6-7 m/s. This has been attributed to the breakdown of the grouping algorithm at higher wind speeds. Ejection and burst frequencies exhibit no discernible dependence on the surface wave field.

Ejection and sweep motions have been studied at various length scales. The original velocity signal is bandpass filtered for various frequency bands. For each band, the percentage contributions to the Reynolds stress from the quadrants of the $u'w'$ plane are close to the corresponding quadrant contributions of the other bands. This indicates similar turbulence structure at different scales. The velocity signals for each band have been normalized by their root mean square (RMS) value. Visualizing the signals on nondimensional time shows the signals from each band to be very

similar. These results can also be interpreted as evidence for the ejection and sweep motions existing simultaneously at different scales, indicating the fractal nature of these events.

Large scale motions, which appear to be associated with ejection and sweep motions, have been identified in the marine atmospheric surface layer using velocity probe measurements at multiple heights. Visualizing these velocity signals suggests that the organized features extend across the depth of the surface layer. Converting the temporal signals to spatial fluctuations suggests that these structures are inclined at an angle while convecting downstream. The inclination angle near the surface ($z < 18$ m) is approximately 15° and it increases with increasing height to about 45° when $z = 45m$. The spatial velocity fluctuations also indicate that these organized features may be large transverse vortical arches.

ACKNOWLEDGEMENTS

I would like to express my deepest appreciation for all of the advice, encouragement and support given to me by my advisor, Dr. Wayne L. Neu. I would like to thank Dr. Roger L. Simpson and Dr. Saad A. Ragab for their private assistance which has helped me in the overall understanding of the research. I would also like to thank Dr. William J. Devenport and Dr. S. Liapis for their criticism of this dissertation.

I would like to thank my peers and friends for making my stay in Blacksburg a memorable one. Finally, I would like to acknowledge the constant encouragement and support from my parents, which they have provided throughout my education.

The data analyzed in this dissertation were collected under the direction of Russell Snyder with support from the National Science Foundation (OCE-8817273). The analysis was supported by the Office of Naval Research (N00014-93-1-0239).

To My Parents and Sister,
for their love and support.

NOMENCLATURE

u	Streamwise instantaneous velocity.
v	Cross flow component of instantaneous velocity
w	Normal component of instantaneous velocity
u'	Streamwise fluctuating velocity.
v'	Cross flow component of fluctuating velocity
w'	Normal component of fluctuating velocity
u_{rms},w_{rms}	Long time rms of u' & w'.
H	Quadrant technique threshold.
k	VITA threshold.
L	Modified u-level threshold.
$q(t)$	A fluctuating quantity.
T_A	Averaging time in VITA.
$\hat{q}(t, T_A)$	Variable interval time average of $q(t)$.
t_e	Time between ejections.
t_0	Mean duration of an ejection.
t_{max}	Maximum time between ejections from same streak.
T_e	Mean ejection Period.

T_B	Mean Burst Period.
δ	Boundary layer thickness.
ρ	Density.
ν	Kinematic coefficient of viscosity for air.
u_*	Friction velocity ($\sqrt{\frac{\tau_w}{\rho}}$), ($-\overline{u'w'}$ in the atmospheric surface layer).
u^+	u/u_*.
z	Height above the surface
z^+	zu_*/ν.
Re	Reynolds number.
Re_θ	Reynolds number based on momentum thickness.
$< q(\tau) >$	Conditional average of a fluctuating quantity q.
f	Frequency
S_u	u' autospectrum.
C_{uw}	$u'w'$ cospectrum.
T_B^+	Nondimensional mean burst period using inner variables.
T_B^*	Nondimensional mean burst period using outer variables.
C	Phase velocity of dominant wave frequency
L	Monin-Obukhov length
z_0	Roughness length parameter
z/L	Stability parameter
$H_{\frac{1}{3}}$	Significant wave height
ω_m	Modal wave frequency
g	Acceleration of gravity

TABLE OF CONTENTS

LIST OF FIGURES

Chapter 1

INTRODUCTION

Turbulent boundary layers have been the subject of extensive study in the field of fluid dynamics. The importance of turbulence in the transport of mass, momentum and heat in most engineering and geophysical flows makes it worthwhile to better understand the basic phenomena of turbulence.

One of the most remarkable advances in the field of fluid dynamics has been the discovery of quasi-coherent structures in turbulence. Visual observations and numerical simulations have shown that spatially-organized large-scale motions in turbulent flows are apparently responsible for the maintenance (production/dissipation) of turbulence. The study of such structures, if they are indeed responsible for the turbulence generation, is of fundamental importance to the understanding of the dynamics governing the phenomena of turbulent fluid flow.

Though a great deal of information has been gathered about these structures by visual investigations and conditional sampling of velocity probe data, little is known about their evolution, their dynamics and their interaction with surrounding flow. Most of the characterization of these organized motions is from studies conducted in

the laboratories, and little has been done to establish whether these structures are universal.

As these structures play a dominant role in the flux mechanism in a turbulent boundary layer, it would seem, intuitively, that, their study at high Reynolds number flow, such as the marine atmospheric boundary layer, would be an important step in better understanding the transfer of momentum, moisture and heat across the air-sea interface and also in characterizing the ocean surface properties.

1.1 Background

1.1.1 General

Turbulence in fluid flows has long been thought to be a random and chaotic phenomena stemming from the observations of Osborne Reynolds that fully developed turbulent flow is composed of a mean motion and a stochastic fluctuation. Although these flows are governed by the Navier-Stokes equations, the analytical-intractability of this non-linear system of equations forced researchers to settle for description and prediction of certain features using experimental techniques. The small temporal and spatial scales which influence the dynamics prevent the direct computation of the Navier-Stokes equations for flows of practical interest. The present trend is to use approximations of the governing equations, the so called Reynolds averaged Navier-Stokes (RANS) equations for computational purposes. The averaging process introduces additional terms (the apparent shear stress or the Reynolds stress) into the equations which are unknown in the closed form and must be modeled. The models for the Reynolds stress are semi-empirical relations, which are based on dimensional

analysis, with the coefficients being fixed by statistical regression of the available experimental data.

The lack of insight into the physical process of turbulence hampered the improvement of models as this could be brought about only by modeling the physics closer to what it actually is. A considerable amount of effort has been spent during the past three decades with the help of flow visualization techniques to understand the kinematics and dynamics of turbulent flows. Flow visualization studies have revealed, contrary to prior perception, the existence of organized flow structures in turbulent flows. These structures have been seen to play a key role in the production of turbulent Reynolds stress (TRS) and production/dissipation of turbulent kinetic energy (TKE). The existence of these flow structures has been confirmed by direct numerical simulation (DNS) at low Reynolds numbers. The limitations of present day computers prevent the simulation at higher Reynolds number. Though the existence of these structures has been repeatedly confirmed in the laboratory there is little consensus on their spatial and temporal scaling. Clearly there exists a need to establish if these motions are universal.

1.1.2 Flow visualization studies

Insight into the dynamics of turbulent boundary layers was pioneered by researchers at Stanford University in the sixties using the hydrogen bubble flow visualization technique. Kline *et al.* [1967] divided the flat plate boundary layer into a number of regions. In the region $0 < z^+ < 10$ they reported the presence of a regular pattern of fluid motion distributed in the spanwise direction. These patterns consisted of low speed fluid alternating with high speed fluid. The streaky patterns, which were

seen to be regular in space, were observed to be destroyed and re-established with a random distribution in time. The low speed streaks were observed to develop a wavy configuration and then suddenly lift away from the wall and move outward into a region somewhat further away from the wall where they violently broke up by interaction with the outer flow. Kline *et al.* further suggested that this ejection process is a primary mechanism for the production of turbulent kinetic energy. Corino & Brodkey [1969] observed similar phenomena in the wall region of turbulent pipe flow. Studying the turbulence production near the wall for a flat plate, Kim *et al.* [1971] termed this sequence of events, from the formation of these streaks to their breakup, *bursting*. They observed that in the region $0 < z^+ < 100$ essentially all turbulence was produced during the intermittent bursting periods. Corino & Brodkey found that roughly 70% of the contribution to the Reynolds stress was from ejection related events. Grass [1971] observed that these motions were found in flows over boundaries of various roughness. He conjectured that the ejection process could represent a universal and dominant mode of momentum transport outside the immediate wall region and possibly extending across the entire depth of the boundary layer.

These results encouraged further studies aimed at understanding the dynamics of the ejection process and its relation with other possible large-scale motions in the turbulent boundary layer. This led to the recognition of other coherent structures such as the horseshoe shaped vortex [Head & Bandyopadyadhay, 1981] and internal shear layers [Alfredsson & Johansson, 1984], which were thought to play an important role in the turbulence generation mechanism. Although it was agreed that these motions were the pumps transferring energy from the mean flow in the outer region into chaotic motions, there was little consensus on their spatial and temporal relations.

Furthermore, the complexity of the flow along with conflicting interpretation of the available data led to confusion and speculation about the role of the different coherent structures in the dynamics governing turbulent boundary layers.

This scenario led Kline and co-workers to undertake a "community-wide" survey in 1986 to extract the facts, established through reliable data, from the speculations and extrapolations of available data. Based on this study and from animations of direct numerical simulation of a low Reynolds number flat plate boundary layer flow [Spalart, 1988], Kline & Robinson [1988] were able to classify eight categories of quasi-coherent structures in a turbulent boundary layer. A detailed review by Robinson [1991] depicts the widely accepted picture of these coherent structures.

1.1.3 Identifying bursts using velocity probe data

Although flow visualization has been effective in the laboratory at giving a general description of the organized flow structures in the disorder of turbulent flow, it does not have the capability to provide detailed information on the velocity characteristics of a burst event. Also, it fails to discern events in higher Reynolds number flows. This difficulty prompted studies to be conducted using probes with the intention of measuring the velocity and pressure fields associated with burst events. These measurements in conjunction with a reliable detection algorithm provided the capability to detect events at higher Reynolds number and had the additional advantage of educing the spatial structure of these motions.

Characterizing bursts from velocity probe data was first attempted by Kim *et al.* [1971] using short time autocorrelation performed on the streamwise component of the velocity signal. Kim *et al.* found that the first positive peak in the autocorrelation

had a lag time which corresponded well with the value of the burst period obtained from flow visualization. Strickland & Simpson [1975] found a correspondence between the peaks of the first-moment of the long sampling time wall stress spectral density and the short sampling time autocorrelation. These techniques are useful only in estimating the mean burst period but are incapable of detecting individual events.

Before proceeding further, it is necessary to to make the distinction, as noted by Offen & Kline [1975], between bursts and ejections. A burst (defined as the breakup of a low speed streak) may contain one or more than one ejection of fluid. Multiple ejections from the same burst appear in groups. Groups of ejections occur more often than single ejection bursts with increasing distance from the wall. The detection algorithms discussed below are, in many cases, detecting ejections rather than bursts. These detected ejections may then be grouped into bursts as was done by Bogard & Tiederman [1986], Luchik & Tiederman [1987] and others.

Several techniques for detecting individual events, bursts or ejections, in velocity probe data have been developed using simultaneous velocity measurement and flow visualization. The detection techniques are based on the fact that the event results in a unique velocity signal pattern which can be recognized by a detector function. Blackwelder & Kaplan [1976] used the Variable Interval Time Averaging (VITA) technique on the streamwise velocity signal to look for large local variances associated with ejections. Johansson & Alfredsson [1982] observed that large local variances were associated with both accelerating and decelerating events and proposed that the streamwise velocity should be accelerating with a large local variance to be classified as an ejection event. Lu & Willmarth [1973] recorded an ejection event whenever the streamwise velocity was below a certain preset threshold level. This technique known

as the u-level technique gave multiple detections for a single ejection event and was modified by Luchik & Tiederman [1987] such that the detector function was turned on when the streamwise velocity was below a certain threshold level and turned off when it was greater than 0.25 times the preset threshold. This technique called the modified u-level technique gave detections which corresponded well with those of flow visualization.

The quadrant technique, described by Wallace *et al.* [1972] and Lu & Willmarth [1973], is based on the magnitude of the second quadrant (i.e., $u' < 0$ and $w' > 0$) $u'w'$ product falling below a preset threshold level to detect an ejection. It was shown to be the most reliable and effective detection algorithm in the study of Bogard & Tiederman [1986]. They compared the ejections detected by the quadrant technique, the VITA technique and the u-level technique, to those observed by flow visualization. The recent technique of Zoran Zarić discussed by Falco & Gendrich [1988] is also an effective way to detect burst events. This technique looks at levels of the product $u'du'/dt$ (an indicator of the rate of change of the turbulent kinetic energy) which was observed to be highly intermittent in nature.

1.1.4 Bursting at High Reynolds Number Flows

There has been very limited focus on detecting these events in flows of higher Reynolds numbers. Gordon [1974], investigating the turbulent structure of the estuarine tidal flow attributed periods of high momentum transport to bursting phenomena on a geophysical scale. These flows have a Reynolds number typically on the order of 10^7–10^8. Heathershaw [1974] observed similar bursting phenomena in the bottom turbulence of the Irish Sea and estimated that roughly 70% of the Reynolds

stress contribution was from ejection events. Gordon [1975] estimated a burst period of 70 seconds for the estuarine tidal flow and also conjectured that the dimensionless burst period was independent of or a weak function of Re_θ. Jackson [1976] observed the water surface macro turbulence phenomena ("boils") on the surface of the lower Wabash river (Illinois) and interpreted them as surface manifestation of bursts. The scaled frequency of these "boils" was in good agreement with previous laboratory results.

Organized motions have been observed in temperature traces at several heights in the atmospheric surface layer by Phong-anant *et al.* [1980]. They associated a gradual rise in temperature followed by a relatively sharp decrease (ramp-like feature) as the signature of a large structure in the flow. They hypothesized that this structure could resemble a three-dimensional horse-shoe vortex when observed in a coordinate system moving with the average convective velocity of that structure. Chambers & Antonia [1981] studied flow over the ocean surface and found a high probability that both second and fourth quadrant surface stress events (ejections and sweeps) occurred together with similar events for heat flux.

Narasimha & Kailas [1987] have analyzed the velocity probe data in a near-neutral atmospheric boundary layer using the VITA technique to identify events of high momentum flux. They estimate a mean period of 70 seconds. Narasimha & Kailas [1990] using the same data, have examined the time between two successive events and found the distribution to have two distinct peaks. They conjectured that such events either occur in groups (i.e., in quick succession) or are single events independent of others. Katul *et al.* [1994] studied the sensible heat flux above a desert surface. They identified the flux bursts using the quadrant technique. They propose that the

mean burst period may be a function of atmospheric stability. Numerous studies [e.g., Duncan & Shuepp, 1992; Paw U *et al.*, 1992; Gao *et al.*, 1992] have also been directed towards identifying intermittent events over forest canopies.

1.2 Motivation for present study

Despite the intense research effort focused on the coherent structures and the considerable success in quantifying bursts using the detection algorithms, much of the dynamics governing these motions is still a mystery. Moreover, the scaling of these events is still a matter to be resolved. The long-standing controversy concerning the relative importance of the inner and outer layers of the turbulent boundary layer as causal factors in the dynamics of turbulent motions has come to be known as the "inner/outer controversy". The outer-dominant view is that the inner layers are driven by the fluctuations of the outer layers. The inner-dominant view is that most of the turbulence production occurs in the inner layer and then diffuses outward. The outer-dominant view suggests that the burst frequency would scale on the outer variables, U_e and δ, whereas, the inner-dominant view suggests that the burst frequency would scale on the inner variables, u_* and ν. However, recent findings [Robinson, 1991] suggest that the scaling of burst events may also be a function of the Reynolds number. In light of the scales involved in the atmospheric boundary layer, it is unlikely that the molecular viscosity would play a role.

The present investigation aims at studying burst structures and the associated large scale motions in the marine atmospheric surface layer. The major feature that distinguishes the marine atmospheric surface layer from its continental counterpart is the presence of ocean waves, which give it a wet and mobile lower boundary. The

surface heat flux is not as important over water as over land [Garratt, 1992] and hence the density effects are also less important. The marine atmospheric surface layer is much nearer neutral stability, over large areas of the ocean, than the boundary layer over land. This is an important feature in subjecting the geophysical boundary layer to traditional laboratory analysis.

The lowest 1 km. or so of the marine atmosphere is turbulent and experiences surface effects through vertical exchange of momentum, heat and moisture. While the structure of this turbulence is similar to that in a laboratory flat plate boundary layer [e.g., Takeuchi *et al.*, 1977; Chambers & Antonia, 1981; Kawamura *et al.*, 1981], except for, perhaps in the few millimeters adjacent to the surface, the laboratory definitions of the extent of various regions based on z^+ (inner scaling) appear to be inappropriate in the atmospheric boundary layer. For example, the log region in an atmospheric boundary layer typically extends over 100 meters above the surface ($z^+ > 10^6$) [e.g., Panofsky & Dutton, 1984]. In a typical laboratory flow however, the log region extends only to $z^+ \approx 500$ [e.g., Kline *et al.*, 1967]. Thus, at a few meters above the surface in the atmospheric surface layer, while at a huge height in terms of z^+ (order of 10^5), one is still quite low in terms of the boundary layer profile.

As the governing physics for both laboratory flows and environmental flows is the same, intuitively, it would seem that the turbulent flow structure would be similar in nature. Characterization of burst structures in the marine atmospheric surface layer, will not only help establish the universal nature of these events, but may also help resolve the so called "inner-outer" controversy associated with the scaling of these events. Identifying large structures, which embody the ejection and sweep motions, in the atmospheric surface layer will be useful as a testbed for comparison with

numerical simulations and consequently in refining turbulence models. Furthermore, the study of such structures, in the marine atmospheric boundary layer, is in itself of great importance to understanding air-sea momentum transfer, pollutant mixing and dispersion, and the transfer of heat and moisture across the air-water interface.

Chapter 2 gives a brief overview of the quasi-coherent structures in a turbulent boundary layer, as described by Kline & Robinson [1989]. Chapter 3 gives a description of the experiments involved in gathering the turbulent wind data which have been used in the present study to study the burst structures. Chapter 4 gives an outline of the different detection algorithms used to detect ejection events in turbulent velocity probe data. Chapter 5 describes the characteristics of the burst events which have been identified during the course of the present study. The detection techniques described in chapter 4 have been applied to the turbulent wind data. Detection of ejections followed by their grouping into bursts indicates a highly intermittent phenomena which has a dominant contribution to the Reynolds stress. Quasi-periodicity in the velocity signal determined using autocorrelations and spectral analysis give the dominant frequency content close to the observed frequency of the bursts. Spatial velocity characteristics of these burst structures have been educed by phase averages of conditionally sampled velocity data. Scaling of these events using the inner and outer variables has also been examined.

Chapter 6 describes the effect of wind speed and surface wave conditions on the burst periods. This study finds that the ejection period decreases with increasing wind speed. Surface wave conditions seem to have no affect on the ejection period. Chapter 7 examines the structure of turbulence over the ocean at different scales. Ejection and sweep motions seem to coexist at different scales, suggesting a fractal nature

of these events. Chapter 8 describes an attempt at identifying and characterizing large scale motions which are associated with bursting phenomena. Spatial structure has been studied by transforming temporal measurements using Taylor's hypothesis. Results indicate that ejections and sweeps may be a consequence of large vortical arch like structures. Finally, the dissertation is closed with some concluding remarks and suggestions for future work.

Chapter 2

QUASI-COHERENT STRUCTURES

The studies of turbulent shear flows have revealed the existence of organized motions or eddies in the flow. These motions have been repeatedly confirmed to exist using flow visualization techniques and also in animations of a direct numerical simulation of a canonical flat plate boundary layer. Studies over the years have led to the belief that these quasi-coherent structures play an important role in the turbulence generation mechanism.

Although the significance of these structures in the transport of turbulent phenomena is widely accepted, there is little consensus on their spatial and temporal structure. Furthermore, the different types of these orderly structures which exist within the disorder was also a subject of debate. The state of knowledge led to a lot of speculation about the types of motion and their importance in the dynamics. Kline and co-workers undertook a "community-wide" survey in 1986 to extract the facts from the studies conducted around the world. One of the major goals of the study was to categorize the different coherent structures in the turbulent boundary layer and to identify their role in the turbulence generation mechanism. The following sec-

tion briefly describes the motions observed in a flat plate boundary layer as described by Kline & Robinson [1988]. The illustrations are the hypothetical models, for these structures in a flat plate boundary layer with zero pressure gradient, proposed by Robinson [1990].

2.1 Eight Categories of Quasi-Coherent Structures in the Turbulent Boundary Layer.

1. **Low-speed streaks in the near wall region** ($z^+ < 10$): Low speed streaks are regions of slow moving fluid relative to the surrounding fluid. It is estimated that the streaks have a speed typically about one-half the local mean speed. The streaks are speculated to be traces left behind by vortex elements. The mean spanwise width of these streaks has been estimated to be nearly 100 wall units and has been found to be constant for flows over a wide range of Re_θ. The streaks eventually move away from the wall and break up as they move downstream.

2. **Ejections:** When the low speed streaks migrate slowly away from the wall as they move downstream, at a certain stage they rise rapidly away from the wall in a ejection like motion often called "lifting". The lifted streak then undergoes a rapid wave-like motion and eventually breaks down which leads to the appearance of finer scales of motion indicating locally high values of turbulent production. The entire process of streak formation through break down has been termed "bursting". The ejections manifest themselves as a negative fluctuation from the mean in the streamwise velocity ($u' < 0$) and a positive fluctuation from the mean in the velocity component normal to the wall ($w' > 0$).

3. **Sweeps:** Continuity suggests that outward ejection of low momentum fluid must be compensated by wallward sweeps. Unfortunately, the dynamics of the sweep events are poorly understood owing to the difficulty in observing the penetration of the outer flow towards the wall using flow visualization techniques.

4. **Vortical structures :** Kline & Robinson [1989] have defined a vortical structure as "made up of vortex elements with more than one orientation". Though there is confusion regarding their shapes and orientations, the commonly accepted vortical structure is the "horseshoe-shaped" vortical structure or the "arch". These structures have been called the "molecules of turbulence" and are said to be the prime structures for turbulence generation. In flows of considerably high Reynolds number, the arch is thinner and elongated, appearing more like a hairpin and is known as a hairpin vortical structure. Due to the extremely complicated nature of the flow, these structures cannot be discerned by visual observations. The spatial description of these structures have been extracted from the velocity signal using phase averages of conditionally sampled signal. Figure 2.1 shows a conceptual model of the arch and the motions associated with it. It can be seen from this conceptual model that the sweeps are the downstream side ($u'w'4$) and ejections are the upstream side ($u'w'2$) of such a vortical structure.

5. **Internal shear layers near the wall :** These are regions near the wall where the shear rate ($\frac{du}{dy}$ and $\frac{du}{dz}$) is significantly higher than the local mean value. Although the existence of these structures has been reported by many observers, the inability of the conditional sampling techniques to distinguish between these

structures and other motions of similar nature has led to a lot of speculation about their spatial relation with other structures and their role in the turbulence generation mechanism.

6. **Near wall pockets :** Pockets have been described as regions in the sublayer which are void of any marker particles distributed in the flow to make the flow visible. The pockets have a mean spanwise width of 60 wall units. This agreement of the spanwise dimension with the low-speed streaks suggests the formation of ring vortices from pinching off of horseshoe vortices which form at the sides and upstream and downstream ends of pockets.

7. **Large-scale-motions in the outer boundary layer :** Large scale motions or large eddies are responsible for entrainment or transfer of vorticity to fluid which is originally irrotational. Figure 2.2 shows a model of the large scale motion. These structures are typically arch shaped. The irrotational fluid is entrained on the downstream side of the head and also alongside the necks of these vortical arches. Dissipation is high in the stretching necks of the arch shaped vortices, but low in the transverse heads where the vortex stretching is weak.

8. **Large discontinuities in streamwise velocities :** Observations of the near-wall region in a turbulent boundary layer have seen sharp jumps in the streamwise velocity, often called "backs", which extend from the wall through the entire layer. These backs are thought to be the upstream faces of large-scale motions. Figure 2.3 illustrates the relation between the backs and large scale motions. There seems to be a significant relation between backs, bulges (see figure) and high turbulence production events near the wall. It is speculated that large

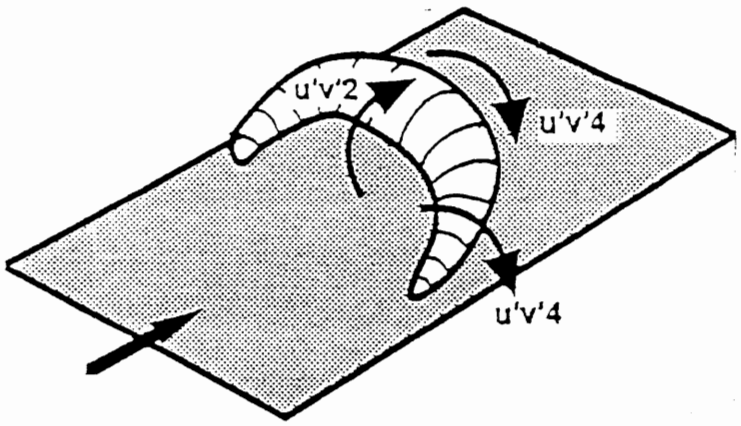

Figure 2.1: Ejections and Sweeps associated with an arch like vortical structure. [from Robinson, 1990]

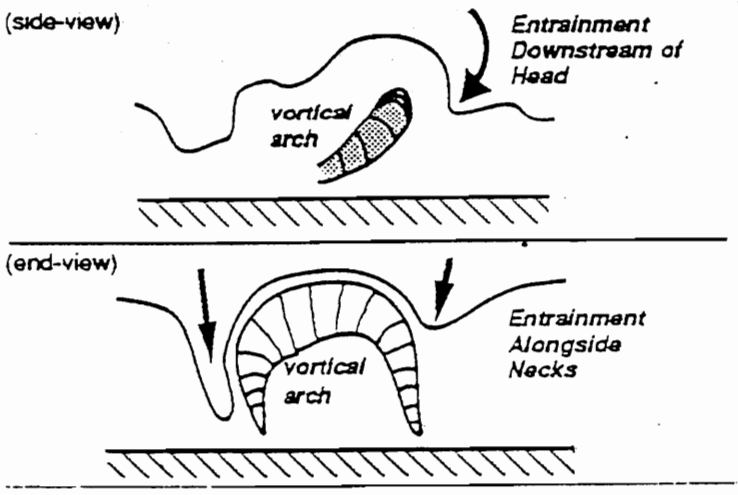

Figure 2.2: Entrainment process associated with vortical arch in the outer-region of a turbulent boundary layer. [from Robinson, 1990]

discontinuities lie at the center of large scale motions.

Data gathered so far confirms the existence of all eight quasi-coherent structures in a flat plate boundary layer at low Re_θ but have not revealed the spatio-temporal relations of these structures and their role in the dynamics of turbulence, furthermore, the tendency to emphasize the role of one motion over the other in the production process has given rise to numerous hypothesis for the evolution of these structures. Based on the studies of animations of direct numerical simulation of a turbulent boundary layer on a flat plate [Spalart, 1988], Robinson [1990] hypothesized the dynamics which are briefly described in the following section.

2.2 Dynamical Speculation

- **Near-wall arch formation :** The transverse vortical structures form on the top of the near wall low speed streaks due to the inflectional velocity profile associated with the sharp velocity gradients at the interface between streaks and the high speed fluid surrounding it. Figure 2.4 illustrates the process as described by Robinson [1990].

- **Quasi-streamwise vortex formation :** When a vortical arch, which forms on a low speed streak, convects downstream, the high gradient in streamwise velocity, across the boundary layer near the wall, stretches the leg and eventually leads to the formation of a quasi-streamwise vortex. Another possibility suggests that the neck of a vortical arch descends into the low momentum near wall fluid and as it convects downstream, the rapid stretching of the neck leaves an elongated vortex near the wall. This suggests that this process may repeat over

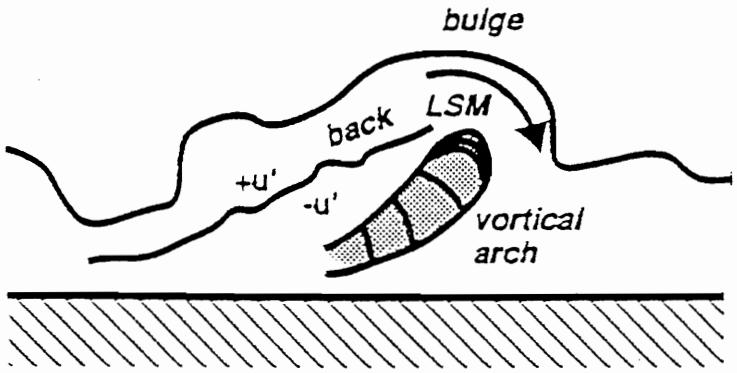

Figure 2.3: Association between large-scale vortical arches and "backs" at the instantaneous edge of a boundary layer. [from Robinson, 1990]

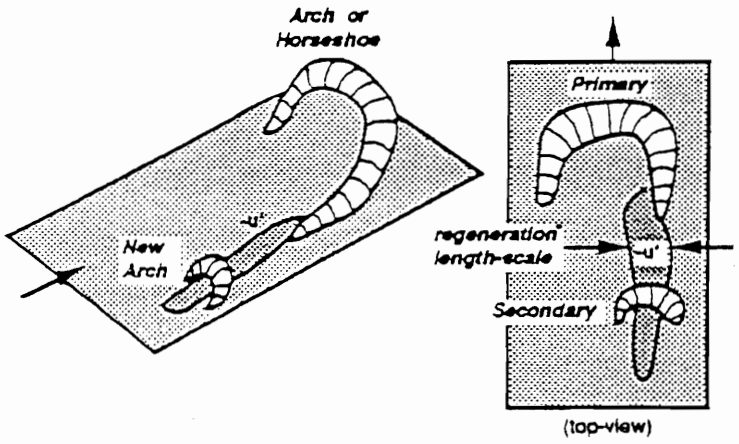

Figure 2.4: Formation of near wall vortical arches on a low speed streak. [from Robinson, 1990].

and over giving rise to many quasi-streamwise vortices generated by a single vortical arch. Figure 2.5 illustrates the hypothetical model for this process.

In summary, the hypothetical turbulence generation mechanism and the Reynolds stress production associated with the coherent structures is illustrated in Figure 2.6 where a vortical arch gives rise to a trailing quasi-streamwise vortex. Quasi-streamwise vortices collect and liftup low-momentum fluid from the near wall region leaving behind a low speed streak. High speed streaks create a shear layer which rolls up into a new vortical arch.

In effect, it is hypothesized that the cycle of turbulence production is driven by the formation and regeneration of vortical structures. Although the models proposed are for the idealized flat plate boundary layer at low momentum thickness Reynolds number, Re_θ, certain features of the model may be universal.

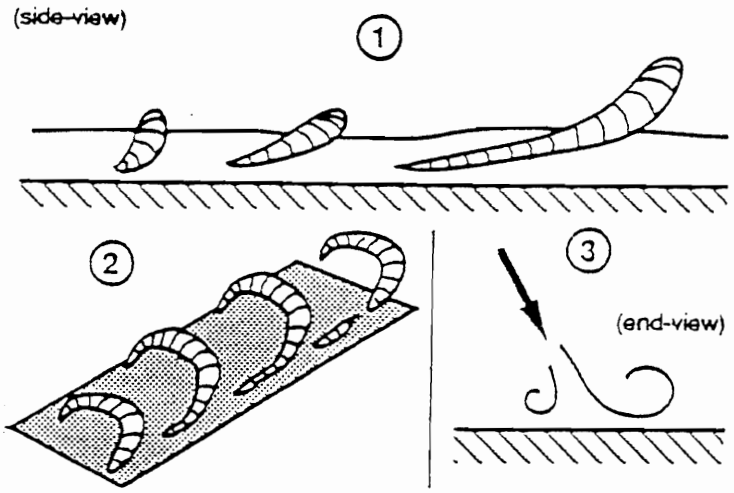

Figure 2.5: Possible formation mechanisms for near-wall quasi-streamwise vortices. 1) Stretched leg of a new vortical arch. 2) descendent from the neck of a mature vortical arch. 3) re-direction of wallward fluid by continuity. [from Robinson, 1990]

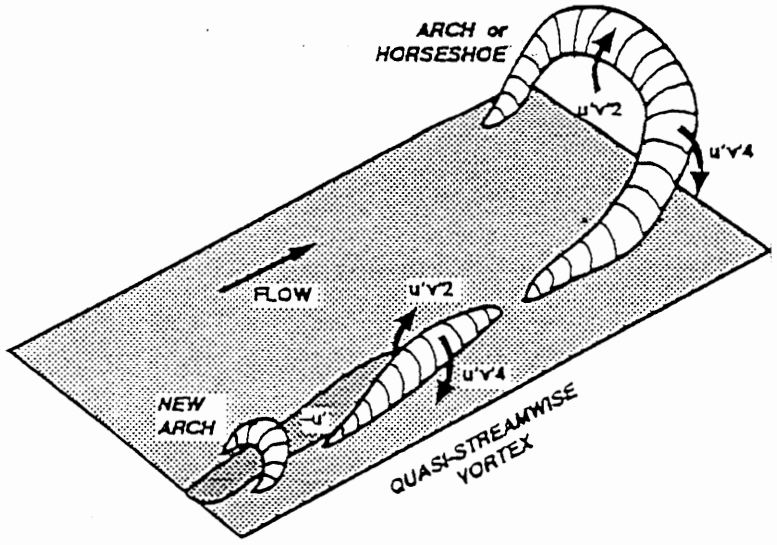

Figure 2.6: Turbulence generation mechanism for a flat plate canonical boundary layer. [from Robinson, 1990]

Chapter 3

DATA SETS

The present study involves analysis of data that were collected during the course of two different experiments, viz., the Bight of Abaco experiments and the Risø Air-Sea Experiments. The following sections present a brief description of these experiments.

3.1 Bight of Abaco Experiments

The wind and wave data were obtained during the course of experiments performed as a part of a larger research program to predict the evolution of the surface gravity wave field [Snyder *et al.*, 1990]. The experiments were performed in the Bight of Abaco during the springs of 1990 and 1991. The main objective of these experiments was to record the turbulent wind and the surface wave spectrum over an extended region of space and period of time. As such, many meteorological parameters, including boundary layer height, were not measured.

3.1.1 Site description

The control region of the field experiment was the Bight of Abaco, which is a 100-km by 40-km semi-enclosed section of the Little Bahama Bank lying between the Great Abaco Island to the east, Little Abaco Island to the north and Grand Bahama Island to the Northwest. The wind and wave data were recorded at several locations in the Bight to have a record of the complete evolution of the synoptic wave field. The wave data were recorded using floating, 10-sensor arrays, and the turbulent wind data were recorded with the help of "weather stations" specially designed for this experiment. (Details of the instrumentation and logistics are described in Snyder *et al.*, 1990). Figure 3.1 shows the distribution of the wave arrays and the weather stations in the control region for the experiments conducted during the spring of 1990.

Figure 3.2 shows a sketch of the weather station. The station is supported by a tripod stand resting on the seabed. A 1 m diameter instrument platform supporting the instruments for data acquisition and telemetry was secured by guyed risers from each of the tripod stands. The instrument panel had an elevation of 1.5 m to keep it above the water. A solar panel, battery, antenna and K-Gill propeller anemometer were mounted on this platform.

The K-Gill propeller vane anemometer (R. M. Young Company), which was driven by the turbulent wind, was nominally at a height of 8.2 m above the water surface. The anemometer was mounted atop a guyed 1-inch-diameter pole, which produced minimal flow distortion effects. This pole extended above a 1-m diameter platform supporting the instruments for data acquisition and telemetry which was mounted on a guyed riser from the tripod stand. The instruments were remotely operated via

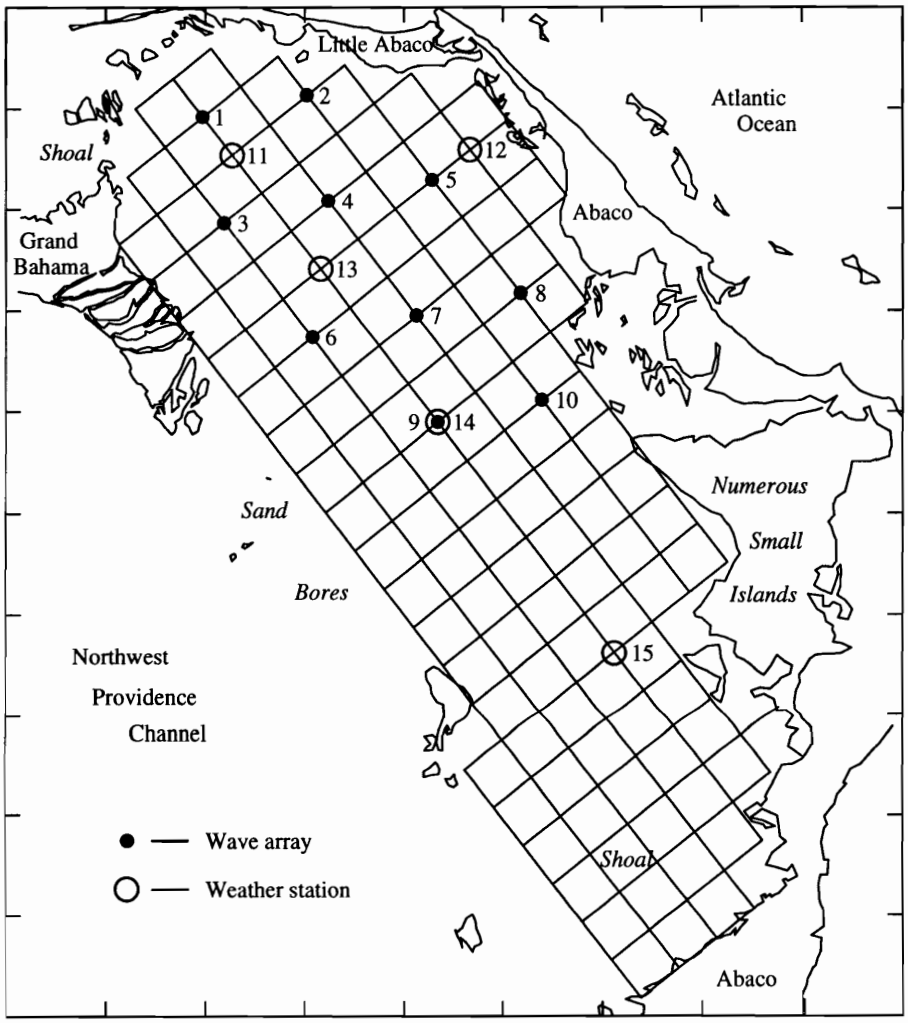

Figure 3.1: Station location for the spring 1990 field experiments. Grid is 4.8 × 4.8 km, border scale is 10 km per division.

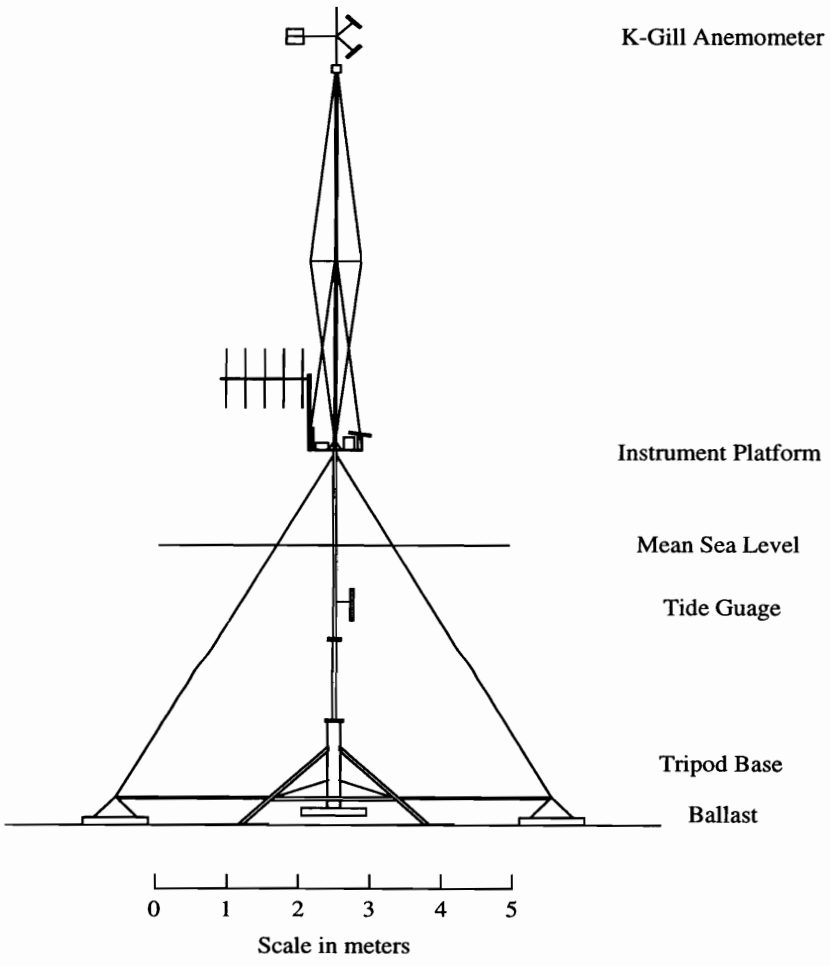

Figure 3.2: Weather Station sketch.

a radio link. Each instrument, when so instructed, performed data collection for a specifiable time interval, storing the data on board until it was instructed to telemeter the data to the base station.

The turbulent wind data was gathered for periods of thirty minutes at a frequency of 5 Hz. Stations 13 and 14 recorded continuous data while stations 11 and 12 recorded data for 30 minutes each hour. The wind component signals bearing the direction and the output from each anemometer were low-pass filtered prior to sampling using a four-pole Bessel filter with a cutoff frequency at 2 Hz.

For the period selected to study the burst structures, the air and water surface temperatures were nearly equal but warm ($\approx 25°C$). Owing to the latent heat flux, the surface layer was slightly unstable; z/L (where L is the Monin-Obhukov length) was estimated to be -0.1, which may be considered to be near-neutral stability for the surface layer. This indicates that shear effects are dominant when compared to buoyancy-related effects near the surface. This is important in subjecting the geophysical boundary layer to traditional laboratory analysis.

3.1.2 Data Reduction

Instantaneous values of the wind direction, elevation angle, and magnitude were calculated from the recorded output levels of the wind vane and two propeller signals from each anemometer. The wind magnitude and elevation angle were obtained by using a unique table lookup scheme developed directly from the wind tunnel calibration of the anemometer [Wei, 1990]. The effect of a wind speed dependence on the angular response function of the propellers is built into this technique, and thus it may be more accurate at lower wind speeds than the inversion of a typical system of

propeller response functions used extensively in previous applications of this type of anemometer.

The instantaneous wind vectors having direction clockwise from north, elevation angle and the magnitude were then averaged over an entire 30 minute record to get the mean wind vector $\boldsymbol{U}$. The instantaneous wind vectors were then transformed to a coordinate system defined by the mean wind vector and expressed as $\boldsymbol{U} = (u,\ v,\ w)$ where u is along the mean wind vector, v in the horizontal cross flow direction and w in the vertical direction for a right hand system. Each component was then stored as a mean and fluctuating part, i. e.

$$\begin{aligned} u &= \bar{u} + u' \quad ; \\ v &= \bar{v} + v' \quad ; \\ w &= \bar{w} + w' \quad ; \end{aligned}$$

A summary file was created for each station containing the mean wind speed, azimuth, elevation angle, the variance of the fluctuating quantities and the cross-correlations ($\overline{u'w'}$ and $\overline{v'w'}$).

3.2 Risø Air-Sea Experiment (RASEX)

The turbulent wind data at multiple heights were measured at the offshore wind farm setup at Vindeby in Denmark. Experiments were conducted during the spring and fall of 1994. A detailed description of the site and logistics can be found in Barthelmie *et al.* [1994].

3.2.1 Site Description

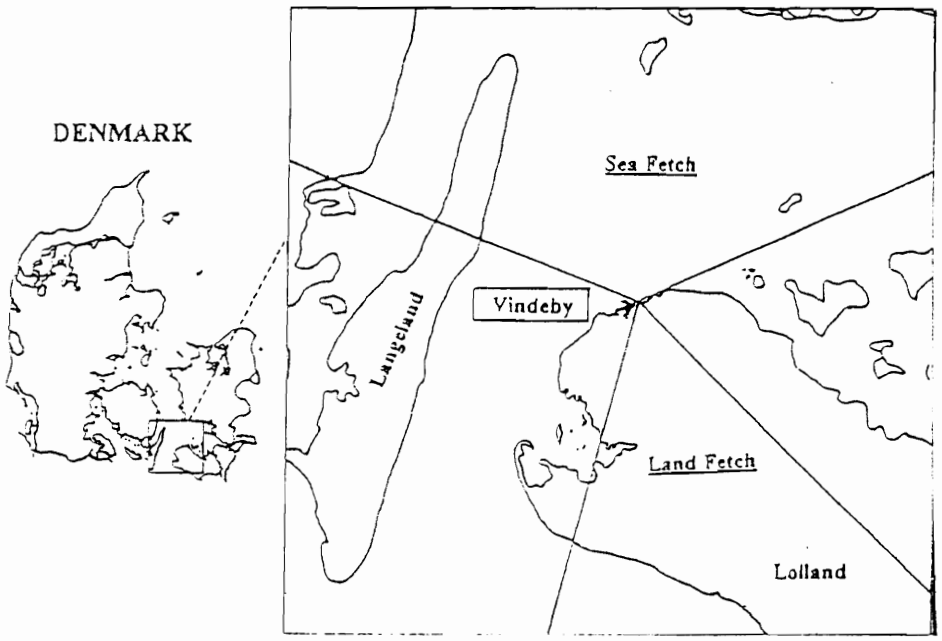

Figure 3.3: Location of Vindeby, Denmark [Barthemie *et al.*, 1994]

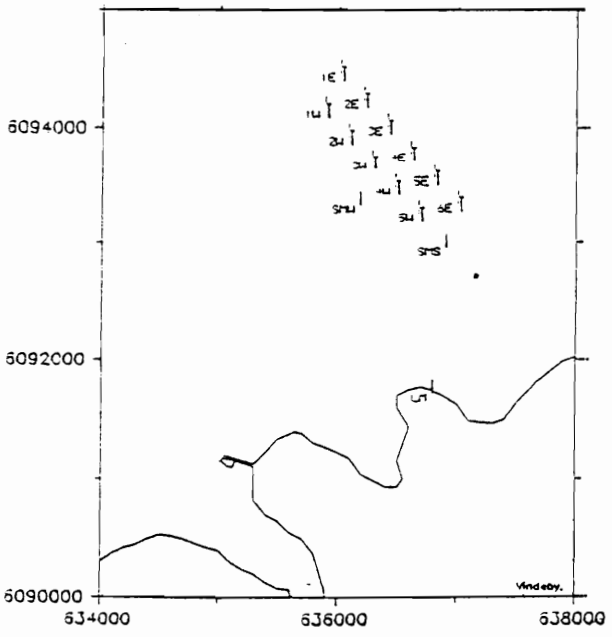

Figure 3.4: The configuration of the wind farm and position of the masts at Vindeby [Barthelmie *et al.*, 1994].

The Vindeby offshore wind farm is located off the northwestern coast of the island of Lolland. Figure 3.3 and Figure 3.4 show the location of the the wind farm along with the configuration of the wind turbines and the masts. The eleven wind turbines (labeled 1E-6E, 1W-5W) are arranged in two rows oriented along an axis of $325-145°$. The most southerly turbine in the array is approximately 1.5 km from land and the turbine spacing is 300 m both along and between the rows. The water depth is between 2.1 and 5.1 m.

Data pertinent to the present study were collected on the three meteorological masts, one on land and two offshore. The land mast is located nearly 2 km south of the southernmost turbine in the array. The offshore masts are placed at distances equal to the turbine spacing, one to the west and one to the south of the first row. Due to their locations, the masts have been labeled Land Mast (LM), sea mast south (SMS) and sea mast west (SMW). The minimum distances from land to SMS and SMW are approximately 1.27 km and 1.63 km respectively. Topography at Vindeby is flat and lies close to sea level and hence no topographic enhancement of wind speed is expected. To the south of the LM the terrain is mainly open farmland with a few scattered houses and trees, with open sea to the north. The coastline runs approximately along the line of 285–105°. Long open sea fetch was desirable for the present investigations so as to have the wave conditions as close as possible to fully-developed. Wind with azimuth ranging from 225–345° had a fetch ranging 15–25 km. These directions were used for choosing the data records for analysis.

3.2.2 Instrumentation

Instruments installed on the three meteorological masts (LM, SMS and SMW) measured mean wind speed at three different levels, wind direction from two different levels, temperature difference and absolute temperature. Three extra anemometers were provided on the sea masts to obtain a detailed wind profile.

In addition to having the same instruments as SMS, SMW was equipped with six 3D fast response sonic anemometers* (F2360a GILL 3 Axis Ultrasonic anemometer) which could measure vector wind speed/direction fluctuations along with temperature fluctuations. The anemometer could measure wind speeds ranging 0 to 60 m/s with a resolution of 0.01 m/s. SMW was also equipped with a downward looking IR thermometer for water surface temperature measurements and instruments to measure water temperature at different depths, wave heights (with an ultrasonic wave height sensor) and an electromagnetic current meter.

The data acquisition system logged over 100 simultaneous signals from 6 different locations with physical separations of up to 3 km. This was done using 4 PCs, one in each of the turbines 4W, 5W and 5E and one in the measuring hut at the foot of the land mast. Data from the sea masts and the turbine signals were acquired by the turbine PCs and transmitted to the land mast on a fiber optic link. The land mast PC, in addition to acquiring all the local meteorological signals, simultaneously received the serial signals from 4W, 5W and 5E. This way all signals were available at the land mast to ensure synchronization. All PCs ran the Risø PC-DAQ data acquisition software.

*For more information about anemometers, refer Wyngaard [1981], Kaimal & Finnigan [1994].

For details about data conversion systems, refer Barthelmie *et al.* [1994]. Samples were taken at the rate of 20 Hz. and stored as half-hourly means together with selected higher resolution time-series. Data were stored on the media as a series of 4-byte reals, which used standard IEEE single precision format for DOS.

3.2.3 Data Reduction

As in the Bight of Abaco experiment, instantaneous values of the wind direction, elevation angle and magnitude were calculated from the information recorded by the channels for the 3D anemometer.

The instantaneous wind vectors having direction clockwise from north, elevation angle and the magnitude were then averaged over an entire 30 minute record to get the mean wind vector $\boldsymbol{U}$. Each component was then stored as a mean and fluctuating part as was done previously. The instantaneous temperature was also broken into a mean and fluctuating component.

Chapter 4

CONDITIONAL SAMPLING TECHNIQUES

Visual investigations of turbulent flow have provided valuable information regarding the spatio-temporal characteristics and evolutionary information of turbulence structure. However, this method has difficulty discerning events in higher Reynolds number flows. Also, this technique is unsuitable for the determination of the velocity field.

The contribution of velocity probe measurements has been invaluable in alleviating this problem to a certain extent. Although the flow field is highly three dimensional, single point velocity measurements have provided qualitative and quantitative information about turbulent flows. Conditional sampling schemes have been devised to extract important information from the probe data to elucidate the dynamics of the flow.

Algorithms for detection of a coherent structure are primarily associated with the fact that there is a recognizable pattern or intensity in the fluctuating components of the velocity signal whenever a burst event passes through the point of detection. Numerous detection schemes have been developed to educe the characteristics of a

structure from the stochastic background and the popular and reliable schemes to emerge are the quadrant and u-level techniques of Willmarth & Lu [1972] and the VITA technique of Blackwelder & Kaplan [1976]. Other schemes to have emerged from recent studies and not as widely used are the technique of Zarić [Falco & Gendrich, 1988] and detection using wavelet transform [Turner & Leclerc, 1994].

The following sections briefly describe these schemes which have been applied to the data in the present investigation to identify the burst structures in the marine atmospheric surface layer (MASL).

4.1 The Quadrant Technique

The Quadrant technique evolves from the studies of Willmarth & Lu [1972] who studied the association of the Reynolds stress production to the fluctuations u' and w'. Quadrant analysis classifies events, as ejections, sweeps and inward/outward interactions on the $u'w'$ plane, which transport momentum toward and away from the wall. The product $u'w'$ is proportional to the instantaneous contribution to the Reynolds stress and in a frame of reference moving with the mean velocity, describes the instantaneous momentum flux. Figure 4.1 shows those fluctuations in space, moving with the local mean velocity, which are associated with a vortical structure. An ejection is the lifting of low-momentum fluid away from the near-wall region. These motions result in an instantaneous defect from the mean velocity in the streamwise direction and a positive fluctuation in the normal direction when they pass through the point of detection. This physical event corresponds to a quadrant 2 event on the $u'w'$ plane.

The quadrant-2 technique is a detector function which records an ejection whenever u' is negative, w' is positive (second quadrant on the $u'w'$ plane) and the $u'w'$

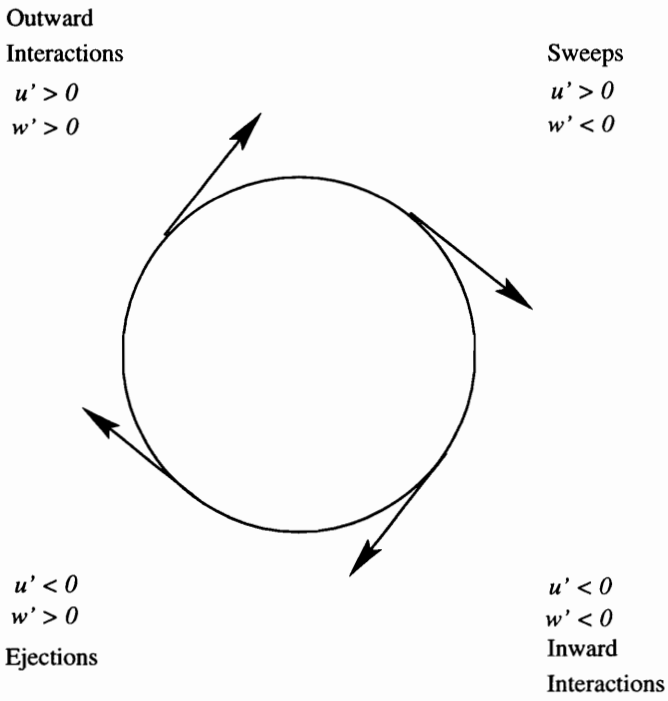

Figure 4.1: Spatial representation of the fluctuations of a vortical structure in a frame of reference at the center of the structure, moving with its velocity

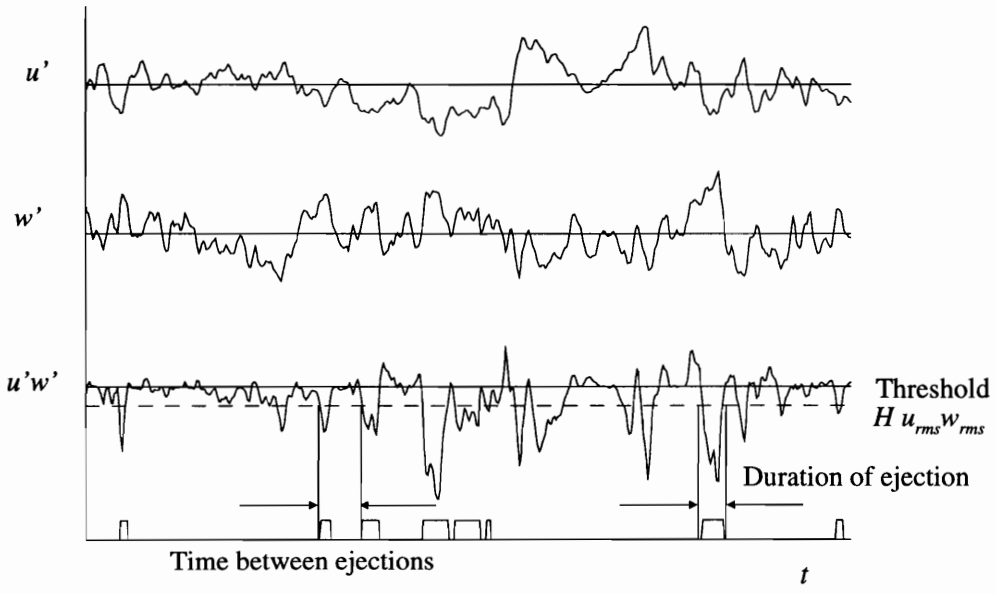

Figure 4.2: The duration of the events detected by the quadrant technique.

product has a magnitude greater than the product of the root-mean-square (RMS) of the normal and streamwise components of the velocity and a threshold H. In a functional form the detector function is given as :

$$D(t,H) = \begin{cases} 1 & |u'w'(t)| > Hu_{rms}w_{rms}; \quad u' < 0, w' > 0. \\ 0 & \text{otherwise} \end{cases} \tag{4.1}$$

where u_{rms} and w_{rms} are the long time RMS of the u' and w' fluctuations respectively. The threshold H has been called the hole size in the analysis of the contribution to the Reynolds stress from each quadrant by Willmarth & Lu [1973]. An estimate of H which has proved reliable is the average value of the quadrant-2 level as suggested by Comte-Bellot *et al.* [1978]. They proposed,

$$H = \frac{|(\overline{u'w'})_2|}{u_{rms}w_{rms}} \tag{4.2}$$

where the subscript 2 indicates that the averaging involves only second-quadrant motions. It has been found that using (4.2) results in a $H \approx 1$ for a wide range of flows. Figure 4.2 illustrates the events and their durations as recorded by this scheme. Defined on this figure are time between ejections and duration of an ejection.

This technique has proved to be superior to other schemes as it detects the physical situation associated with an ejection, however the major drawback of this technique is that it requires the record of both the streamwise and the normal components of the velocity which increases the experimental difficulty.

4.2 VITA Technique

Since its introduction by Blackwelder & Kaplan [1976], the Variable Interval Time Averaging (VITA) technique has proved to be reliable in detecting the passage of a

structure through the point of detection. The scheme is based on the fact that the passage of a coherent structure through the detection point causes a rapid change in the instantaneous streamwise component of the velocity which can be detected by the level of local variance.

The variable interval time average of any fluctuating quantity is defined as,

$$\hat{q}(t, T_A) = \frac{1}{T_A} \int_{t-\frac{T_A}{2}}^{t+\frac{T_A}{2}} q(\tau) d\tau. \tag{4.3}$$

where T_A is the averaging time. This scheme when applied to the streamwise fluctuating velocity gives a measure of the turbulent energy during the averaging time. The local variance of the u' signal is then given by,

$$\mathrm{VAR}(t, T_A) = [\hat{u'^2}](t) - [\hat{u'}(t)]^2. \tag{4.4}$$

if this variance is to be some measure of the passage of an event in the flow, then the averaging time must be of the order of the duration of the event. It must be noted, however, that this scheme acts as a low pass filter for the signal with a cutoff frequency at $1/T_A$ and hence very large values of T_A will tend to miss the detection of events. Robinson [1986] proposed that a choice of T_A is to be a value such that the qualitative shape of the ensemble average of the streamwise velocity signal, is not affected greatly by variations in T_A.

It was observed by Alfredsson & Johansson [1982] that high levels of local variance could be associated with both accelerating as well as decelerating events in the flow. In order to detect ejection related events, they augmented the detector function of Blackwelder & Kaplan with the condition that the streamwise fluctuation should be accelerating to validate an ejection. The detector function for the VITA technique is

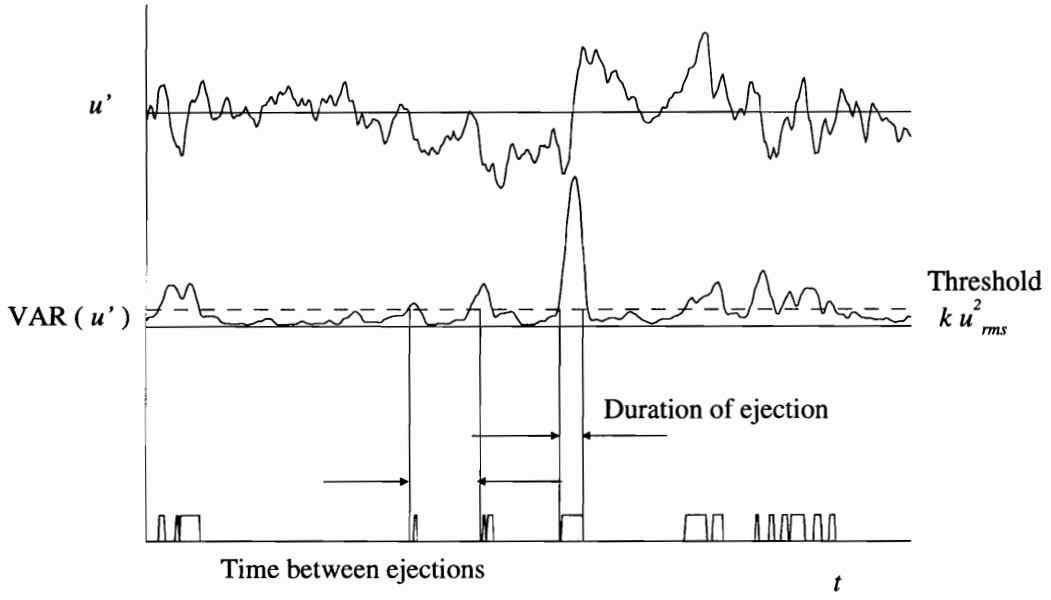

Figure 4.3: Duration of the events detected by the VITA technique

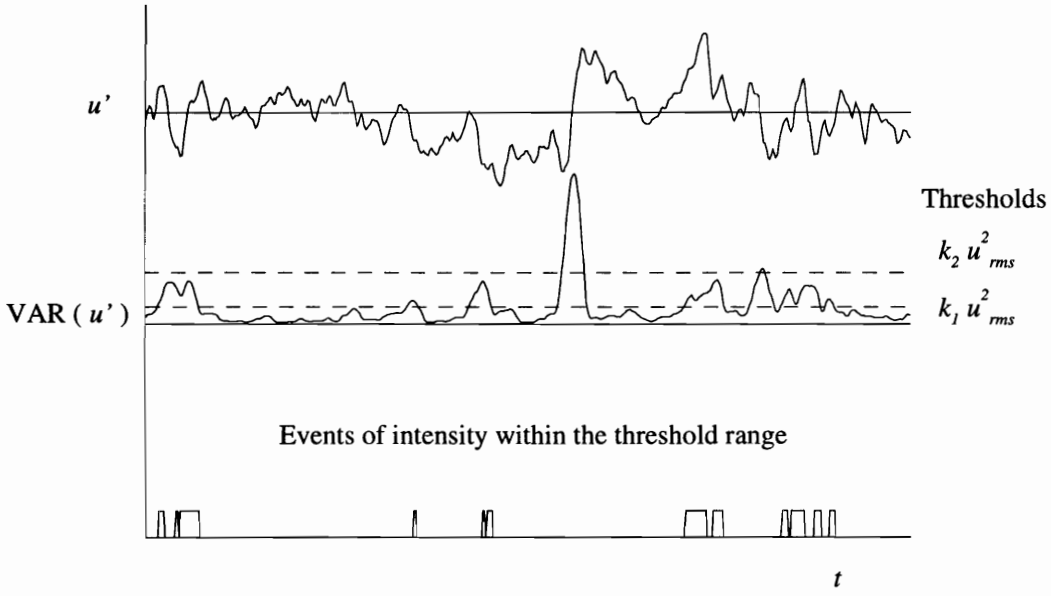

Figure 4.4: Modification to the VITA technique by Robinson [1986] to detect events of a particular intensity

then,

$$D(t,k,T_A) = \begin{cases} 1 & \text{VAR}(t,T_A) > ku_{rms}^2; \frac{du'}{dt} > 0. \\ 0 & \text{otherwise.} \end{cases} \tag{4.5}$$

The value of the threshold k sets the trigger level for the detector function. Figure 4.3 illustrates the events recorded by the VITA technique. To look for events of a particular intensity (which may be a characteristic of some coherent motion) Robinson [1986] proposed windowing of the threshold level. This modification, as illustrated in Figure 4.4, sets two levels of thresholds $k_1 u_{rms}^2$ and $k_2 u_{rms}^2$ and records an event when the local variance falls between these threshold values.

The major advantages the VITA technique has over the quadrant technique is that it requires only the streamwise component of the velocity and that it can be applied to other variations in the signal (e.g., $u'du'/dt$) to detect structures. However its success in detecting events depends on the choice of the two independent parameters k and T_A.

4.3 *u*-level Technique

The u-level technique of Willmarth & Lu [1971] is one of the simplest sampling schemes devised to detect the passage of a burst event through the point of ejection. The technique is based on the fact that an ejection results in a decrease in the streamwise component of the velocity and these defects when below a certain level validate an ejection. In a functional form the scheme is,

$$D(t,L) = \begin{cases} 1 & u' < -Lu_{rms} \\ 0 & \text{otherwise} \end{cases} \tag{4.6}$$

where L is the threshold constant. It was observed by Luchik & Tiederman [1987] that the detector function when modified such that it is turned on when

$$u' < -Lu_{rms}$$

and turned off when

$$u' \geq -0.25Lu_{rms}$$

resulted in detections which corresponded closely with the events observed through flow visualization. This scheme was called the modified u-level or the mu-level technique. Figure 4.5 illustrates the detection scheme to record ejections. The advantage of this scheme is that it requires only the streamwise component of the velocity.

4.4 Z. Zarić TKE method

The algorithm is based on the underlying assumption that the passage of a burst event is accompanied by an increase in the time rate of change of the turbulence energy, and the end of the event is marked by the reduction in the turbulence energy levels, [Falco & Gendrich, 1988].

A measure of the rate of change of turbulence energy can be estimated using the major component of the turbulent kinetic energy;

$$\frac{du'^2}{dt} = 2u'\frac{du'}{dt} \tag{4.7}$$

The quantity $u'du'/dt$ was found to be more intermittent than the velocity fluctuation or the velocity gradient fluctuation signal in the turbulent region of the flow. Figure 4.6 shows this and how it is correlated to the quantity $u'w'$.

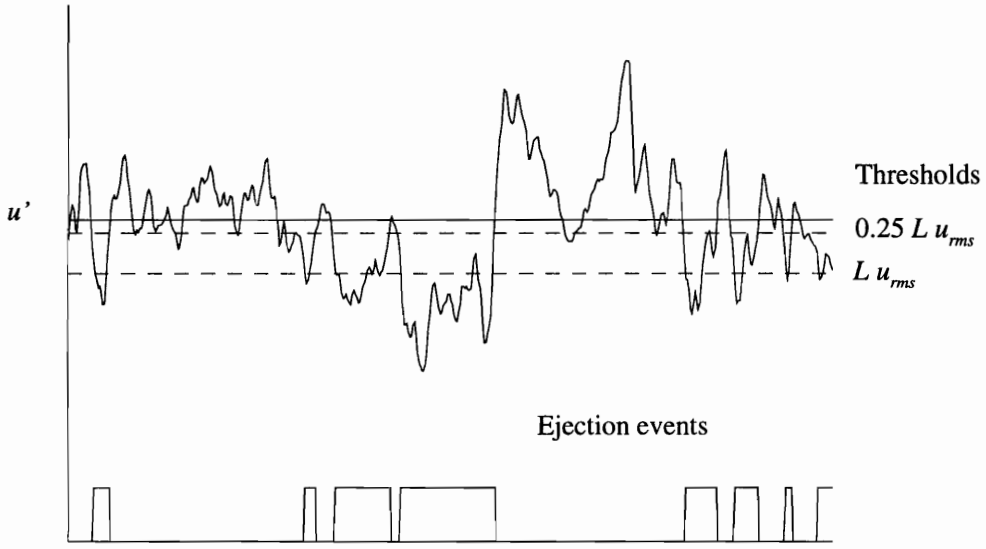

Figure 4.5: Duration of the events detected by the Modified u-level technique

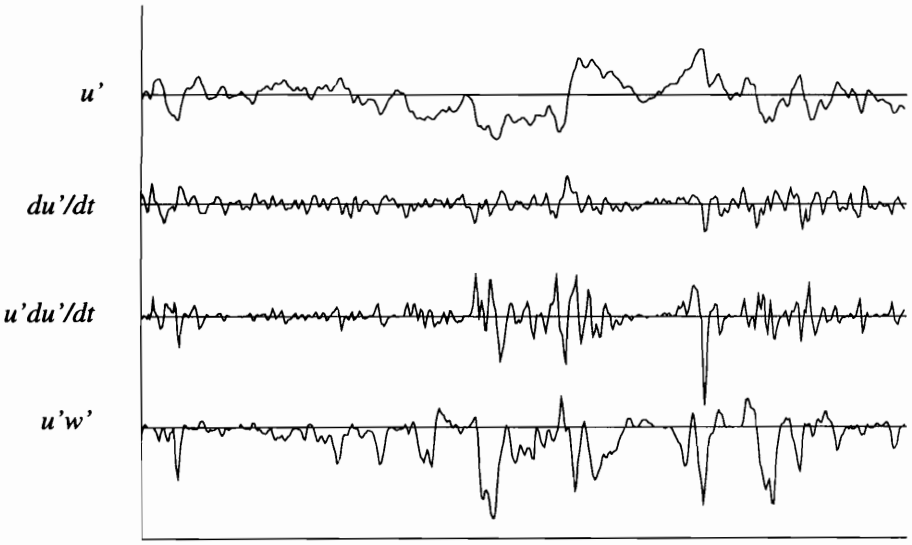

Figure 4.6: Fluctuating signals u', du'/dt, $u'du'/dt$ and $u'w'$.

This algorithm has the inherent advantage that, it needs only the streamwise component of the velocity signal and it uses more of the available information contained in the u' signal compared to other algorithms. The parameters whose level and sign trigger a detection are $u'du'/dt$, u' .

It is hypothesized that $u'du'/dt$ attains a high magnitude when a event associated with a coherent structure passes over the probe. The nature of the event is detected by the sign of u', i.e., for $u' > 0$ the event is a sweep and for $u' < 0$ it is an ejection event. In a functional form, the scheme is:

$$D(t, C) = \begin{cases} 1 & |u'du'/dt| > C\ (u'du'/dt)_{rms} \\ 0 & \text{otherwise} \end{cases} \tag{4.8}$$

where C is an arbitrary nondimensional threshold. Studies have suggested values of C ranging from 0.6 – 1.0 for reliable detection. As noted by Falco & Gendrich [1988], the intensity of the two possible events, ejections and sweeps, might be different and also they might be dependent on the distance from the wall, and the threshold might have to be adjusted depending on the event being sought.

4.5 Wavelet Transform Method

It is well known that turbulent flow is composed of organized (coherent) structures and weaker random superimposed background fluctuations. Measurements of turbulence at high frequency yield data revealing these intermittent and multi-scale processes. Analysis of these time series using standard detection schemes (like the quadrant and VITA), detect localized gradients in a fluctuating quantity. These gradients are associated with coherent structures and then ensemble averages are used to show phase relations. A shortcoming of such procedures is that the technique

used, to a large extent, determines the phase information. Moreover, all temporal information associated with the individual event is lost. This has been considered a major drawback which ill-suits investigating intermittent processes.

Wavelet conditional sampling provides a more objective technique to identify coherent structures in a "noisy" time series. Other techniques first require identification and then phase averaging to separate the organized features from the background turbulence, whereas wavelet analysis achieves this without any phase averaging.

The concepts of wavelets, though present since the time of Haar [1909], have received serious attention during the eighties [Grossmann *et al.*, 1989]. A detailed review of the theory and applications can be found in Farge [1992]. A brief description of the method is presented below.

The wavelet transform is based on the concept of a local* transform. This has the inherent advantage of extracting information about the scale, intensity, and location of desired features embedded in a time series.

If $g(t)$ represents a fundamental wavelet which satisfies certain mathematical conditions, then its family $(g_{a,b})$, produced by translation and dilation may be represented by

$$g_{a,b}(t) = \frac{1}{\sqrt{|a|}} g(\frac{t-b}{a}) \tag{4.9}$$

The nondimensional parameter a is called the dilation factor, which affects the size and amplitude. The parameter b is a translation parameter, which sets the origin of the function. It is desirable that the family of wavelets form an orthonormal basis

*Fourier transform gives the representation of a signal as a sum of extended trigonometric (basis) functions, whereas, the Wavelet transform expresses a function as a superposition of localized, pulse-like functions called wavelets, [Turner & Leclerc, 1994]

of the set of square integrable functions $L^2(R)$.

The continuous wavelet transform of a function $f(t)$ is defined as

$$F(a,b) = \int_{-\infty}^{\infty} f(t) g_{a,b}(t) dt \tag{4.10}$$

$F(a,b)$ are called the wavelet coefficients. The convolution results in large magnitudes of coefficients corresponding to the scale parameter a, when features of approximately the same scale appear near the location defined by b. When there is little activity at a particular scale and position, the absolute values of the associated wavelet coefficients are small. The original signal f can be recovered from the coefficients using the inverse relation given by

$$f(t) = C_g^{-1} \int_{-\infty}^{\infty} [\int_{-\infty}^{\infty} F(a,b) g_{a,b}(t) db] \frac{da}{a^2} \tag{4.11}$$

where C_g is a normalizing factor.

The conditional sample scheme is based on the fact that, at each scale, coefficients with "unusually" large absolute values are associated with coherent structures. Coefficients with small absolute values are associated with background turbulence. After performing the wavelet transform, the coefficients are divided into two groups, strong and weak, depending on their absolute values. The threshold for this classification is set at some multiple of the root-mean-square of wavelet coefficients at that scale for the entire record.

The strong coefficients are:

$$|F(a,b)| > K F(a,b)_{rms}$$

and the weak coefficients are:

$$|F(a,b)| < KF(a,b)_{rms}$$

The inverse transform is then used for the high and low coefficients separately to extract the conditionally sampled "strong" and "weak" signal components. This procedure is illustrated schematically in Figure 4.7.

Figure 4.8 shows a signal which has been filtered using the routine DAUB4 from Press *et al.* [1992] which uses the filter coefficients given by Daubechies [1988]. The threshold parameter K has been set at 4 to get the filtered signal.

The conditional sampling schemes are very simple to implement and when used along with ensemble averaging have proved to be very useful in extracting the signatures of coherent motions from the stochastic background. It should also be noted, however, that the effectiveness of these schemes depends on the choice of the independent threshold parameters.

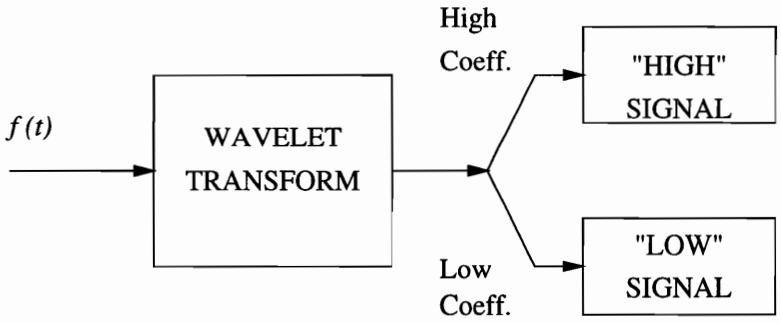

Figure 4.7: Schematic of wavelet conditional sampling.

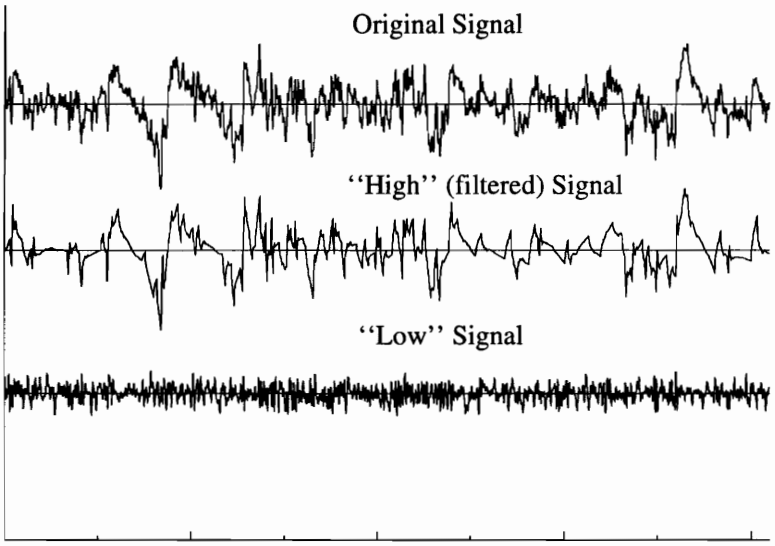

Figure 4.8: Filtering a turbulent signal using wavelet transform.

Chapter 5

BURSTS IN THE MARINE ATMOSPHERIC SURFACE LAYER

For the purpose of investigating the existence of coherent structures in the marine atmospheric surface layer, a data record 2-hours long was constructed using the Bight of Abaco (BOA) data. This long record was constructed from four successive, 30 minute records selected from a time during which the wind remained nearly constant for a relatively long period. The mean wind speed over each of the 30 minute periods varied from 6.57 to 6.85 m/s, averaging to a value of 6.74 m/s, and the direction azimuth was within a range of 4°, averaging to a value of 107° (clockwise from north). For the period being studied, $u_{rms} = 0.40$ m/s, $w_{rms} = 0.20$ m/s, and $-\overline{u'w'} = 0.035$ m^2/s^2. The significant wave height was 0.4 m. The modal frequency of the wave spectrum was 2.16 rad/s (or a period of 2.9 s). Using the dispersion relation, the phase velocity of the dominant wave C is 4.5 m/s, giving a wave age C/u_* of 24.

Figure 5.1, which shows a scatterplot of the data from one of the 30 minute duration files (BOA data) on the $u'w'$ plane, illustrates the typical skewing of the velocity fluctuations toward the second and the fourth quadrants. Ejections, the

second-quadrant motions, and the fourth-quadrant motions, called sweeps, contribute positively to the total Reynolds stress. The first and third-quadrant motions, termed outward and inward interactions, respectively, by Wallace *et al.* [1972], contribute negatively to the stress. Lu & Willmarth [1973] have shown that, on average, ejections account for 77% of the total $\overline{u'w'}$, whereas sweeps contribute 55% and the excess over 100% being balanced by the negative contributions from the interactions. In this study, these contributions towards the Reynolds stress, were found to be nearly the same in the marine atmospheric surface layer. For the 2-hour record constructed for analysis below, ejections account for 78%, sweeps for 52%, and the interactions are each -15%.

Corino & Brodkey [1969] found that roughly 70% of the contribution to the Reynolds stress was from ejection-related events in a turbulent pipe flow. Gordon [1975], investigating the estuarine tidal flow, found that 55% of the Reynolds stress was due to ejection events. Chambers & Antonia [1981] estimated that 80% of the Reynolds stress was from second-quadrant events in the marine atmospheric surface layer. Heathershaw [1974] also estimated that 70% of the stress was due to ejections in the bottom turbulence of the Irish Sea. Since the Reynolds number of these flows varies widely, the percentage contribution to the Reynolds stress from the different quadrants may be independent of the Reynolds number.

5.1 Detection of Ejections

Ejection events were identified in the velocity probe data using the quadrant technique, the modified u-level technique, and the VITA technique. It was found that the very low frequency velocity fluctuations of the wind over the ocean, which are absent

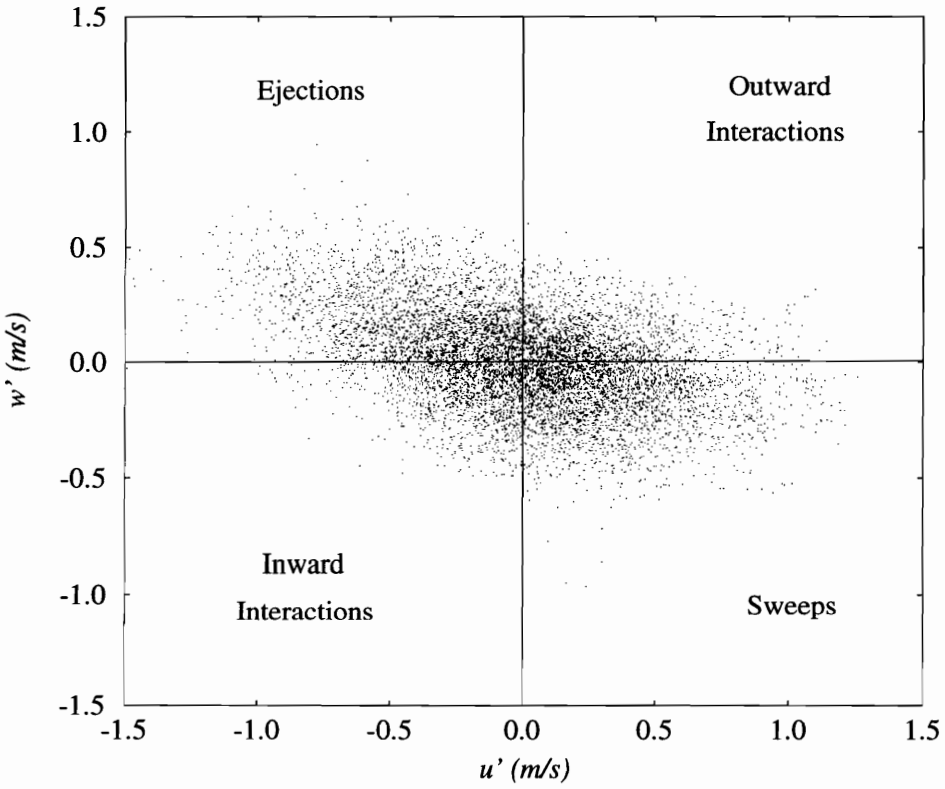

Figure 5.1: Scatter plot of the data points in one 30 minute record.

in the laboratory, create problems for the quadrant and u-level techniques. The effect of these fluctuations, which are presumably due, at least in part, to boundary layer rolls [e.g., Stull, 1988], is to temporarily increase or decrease the streamwise velocity, relative to a long time mean. This affects the condition of $u' < 0$ necessary for detecting ejections. These low-frequency trends in the data have been removed by subtracting from each point a moving average, centered at that point. This acts as a high-pass filter. The filtering was applied to both the u' and the w' signals before passing them through the detector function. A 1 minute moving average was found to remove the trends with little distortion of the higher-frequency fluctuations which trigger the detection algorithm. The motions under study are thus superposed on the longer-scale motions. It is possible that the burst events are modulated by these motions, but no evidence of this was found when the time history of ejections and bursts was compared to the low frequency velocity fluctuations that were filtered out. It was seen that the percentage contributions to the Reynolds stress from motions in each quadrant were changed only minimally by this filtering.

Applying the detection schemes to the data results in a timeline of ejections. Figure 5.2 shows u', w', the $u'w'$ product, and the level of the local variance (used by the VITA technique), along with the detections by the three algorithms for the first 600 s of the filtered data file. The detected ejections often appear in groups. Although the different techniques detect many of the same groups, their results differ significantly. While we can make this comparison of techniques at high Reynolds number, we have no reference (such as flow visualization) to compare their performance against. Since the quadrant technique makes use of two velocity components and was found to perform best at low Reynolds numbers [Bogard & Tiederman, 1986], the results to follow

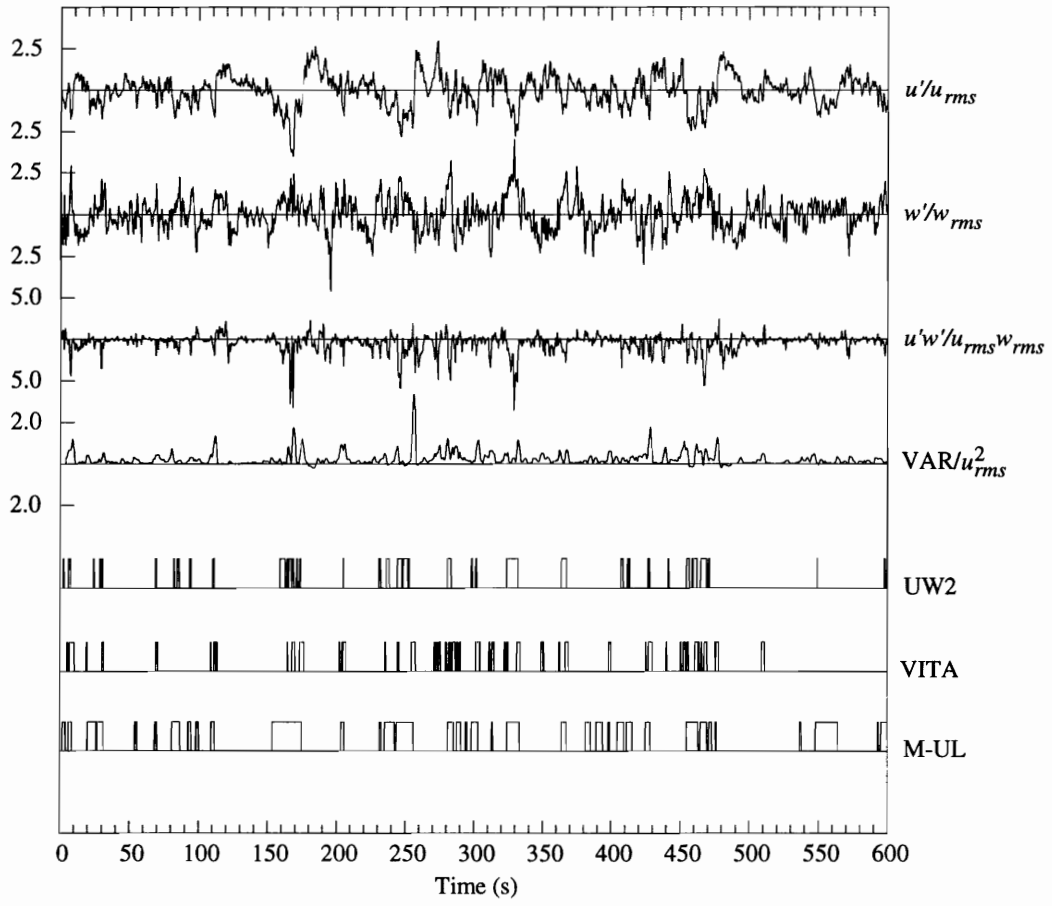

Figure 5.2: Timeline of the ejection events detected by the different detection techniques. See text for explanation.

have been obtained by applying only the quadrant technique.

The threshold for the quadrant technique H was estimated using eqn. (4.2) and was found to be 1.03. (This was rounded to 1.0 for the calculations.) The threshold L for the modified u-level technique was set as

$$L = \frac{\overline{|(u' < 0)|}}{u_{rms}} \tag{5.2}$$

where $\overline{(u' < 0)}$ is the average value of u' when it is less than zero. This resulted in $L = 0.86$. In the VITA technique the averaging time T_A was set at 4 s and the threshold k was set at 0.4.

It can be seen from Figure 5.2 that the ejections detected by each technique are of finite and variable duration. It can also be seen that most ejections occur in groups which are seen to be highly intermittent. Extending the analogy of a flat plate boundary layer to the marine atmospheric surface layer, the events detected as a group appear as if they are ejections from the same streak instability.

The mean duration of an ejection is $t_0 = 1.34$ s. A total of 546 ejections were detected in the 2-hour record giving the average time between ejections T_e a value of 13.19 s.

A histogram of the time between ejections t_e, defined as the time between the beginning of one ejection to the beginning of the next ejection, is shown in Figure 5.3. As expected, the histogram is highly skewed toward the lower values of the time between ejections and closely resembles an exponential distribution. Such a distribution of ejections can be grouped into bursts following the procedure described by Bogard & Tiederman [1986], hereinafter referred to as BT. The values of t_0 and T_e have been used below in grouping the ejections into bursts.

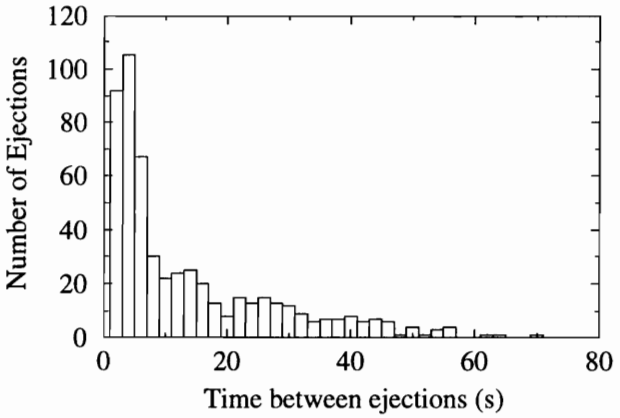

Figure 5.3: Histogram of the distribution of the time between ejections; threshold $H = 1.0$.

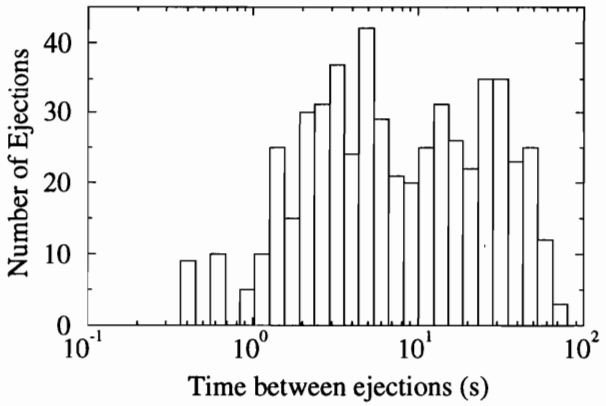

Figure 5.4: Histogram of the distribution of the time between ejections on a log axis; threshold $H = 1.0$.

5.2 Grouping Ejections Into Bursts

A burst, according to the definition of BT, is one or more than one ejection originating from the same streak instability. When the time between ejections is plotted on a logarithmic axis, as shown in Figure 5.4, the presence of two overlapping distributions, characterizing ejections from the same streak and those from different streaks, is seen. To quantify a burst period based on this overlapping distribution would be highly subjective, and hence the approach of BT has been used.

They compared the cumulative distribution of the time between ejections with an exponential distribution which is expected of random events. The exponential distribution was modified (see BT) to take into account the finite duration of ejections during which time interval the probe cannot possibly detect another ejection. A similar comparison for the present data can be seen in Figure 5.5. It can be seen that for smaller time intervals there are more ejections than predicted by the exponential distribution, whereas at larger separation there are fewer. The time corresponding to the crossover point, here 17 s, is taken as the maximum time between ejections from the same streak t_{max}.

Having set the value of t_{max}, the data were again passed through the detector function to group ejections occurring within the time of the set t_{max} from one another into a single burst. This grouping process produced the histogram of what are now bursts shown in Figure 5.6. The distribution has a roughly lognormal or a Γ-distribution shape. It is interesting to note that if the smaller time peak (ejections from the same burst) in Figure 5.4 corresponds to an exponential distribution, then subtracting such a distribution from the observed bimodal distribution would result in a distribution

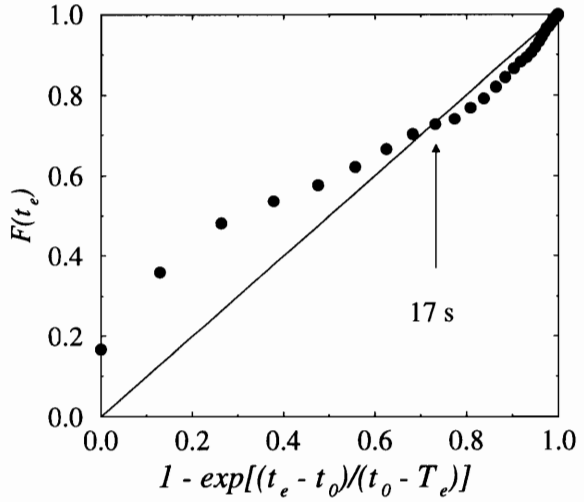

Figure 5.5: Cumulative probability distribution of time between ejections compared to the exponential distribution modified for the finite duration of an ejection. Crossing time determines t_{max}.

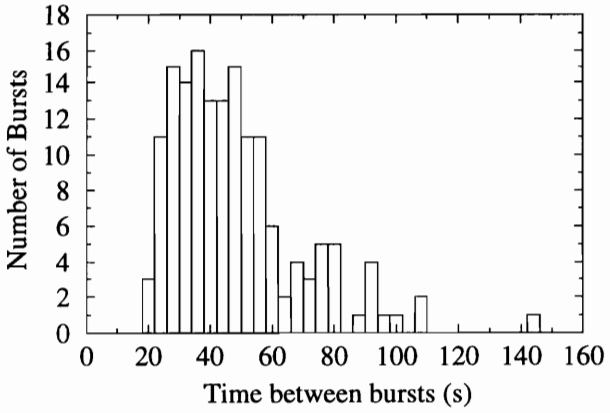

Figure 5.6: Histogram of the distribution of time between bursts; threshold $H = 1.0$.

close to the lognormal distribution seen in Figure 5.6. The mean burst period at $H = 1$ is 46 s based on the distribution in Figure 5.6. For comparison, Narasimha & Kailas [1987] estimated a burst period of 70 s in the atmospheric boundary layer over land and Gordon [1975] has estimated a burst period of 65–70 s in the tidal boundary layer.

Evaluating the mean burst period T_B and the mean ejection period T_e as a function of threshold H results in the values plotted in Figure 5.7. BT, and, later, many others have shown that the burst period is relatively constant for a wide range of threshold values. Although the number of ejections was a monotonic decreasing function of H, they grouped into roughly the same number of bursts over a broad range of H. This can be seen in Figure 5.7, where T_e rises steadily with increasing threshold but T_B is relatively insensitive to H. T_B shows a minimum at $H \approx 1$, rising slowly as H is increased further. The average value of T_B obtained between $H = 0.8$ and 1.4 is 47 s. The dashed lines on Figure 5.7 are at $\pm 5\%$ of this mean.

5.3 Determining Quasi-Periodicity

Autocorrelation of the streamwise component of the velocity signal. Quasi-periodicity in the signal can also be confirmed by performing an autocorrelation on the velocity signal. Kim *et al.* [1971] showed that bursting periods correspond to the lag time of the first small peak in a "short-time" autocorrelation. Figure 5.8 shows the autocorrelation of the u' signal calculated from three, consecutive, 8000-point (1600 s or roughly 30 burst periods) segments of the 2-hour data record. The variability in the first peak can be attributed to the variability of the burst period in the signal. This variability reduces the correlation of the u' signal if larger segments of the streamwise

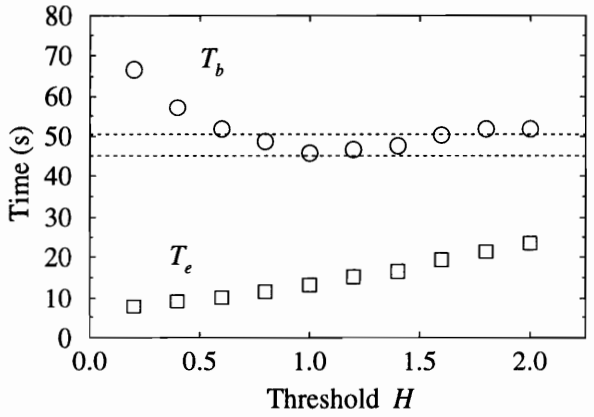

Figure 5.7: Variation of mean time between bursts T_B and mean time between ejections T_e with threshold H. T_B was determined using $t_{max} = 17$ s. Dotted lines indicate $\pm 5\%$ from the mean of T_B for $H = 0.8$–1.4.

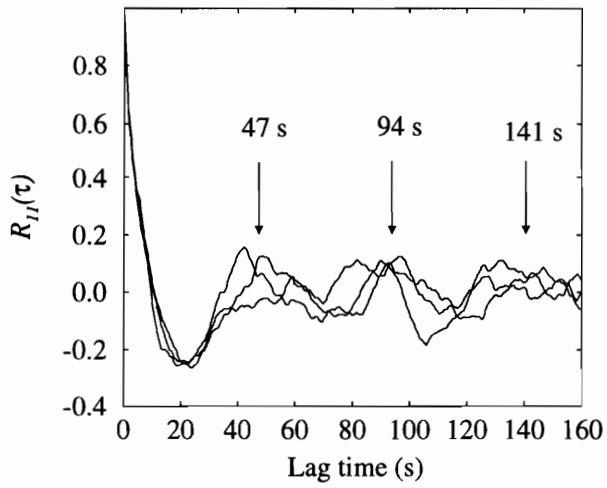

Figure 5.8: Autocorrelation of filtered streamwise velocity component for segments 1600 s long.

velocity record are used for autocorrelation. Though the location of the first peak varies quite a bit, it can be noted that it falls within the histogram of time between bursts (Figure 5.6). It can also be seen that the time lag between successive peaks is close to the mean burst period.

Spectral analysis of the velocity signal. Strickland & Simpson [1975] showed a direct correspondence between the peak of the first moment of the wall shear stress spectrum and the mean burst period obtained by short-time autocorrelation. Such a correspondence between the peak of the first moment of the uw cospectrum and the burst period, does seem to exist in the marine atmospheric surface layer. The spectral estimates were computed using a Hamming window with 500 samples per segment. Figure 5.9 shows the first moment of the u' autospectrum, S_u, and the stress cospectrum, C_{uw}, without the trend removal that was applied in conjunction with the ejection detection. The peak of the cospectrum falls close to the mean burst period of 47 s. It can be seen that removal of the low-frequency content in the velocity signal by the moving average results in a shift in the u' autospectrum peak toward higher frequency but has little effect on the stress cospectrum peak. The motions supporting the bulk of the stress are not affected by this filtering.

5.4 Phase Averages of the Velocity Signal

To educe the spatial structure of the ejection events, ensemble averages of the signal were performed. The ensemble average of a quantity q is given by

$$< q(\tau) >= \frac{1}{N} \sum_{j=1}^{N} q(t_j + \tau) \tag{5.3}$$

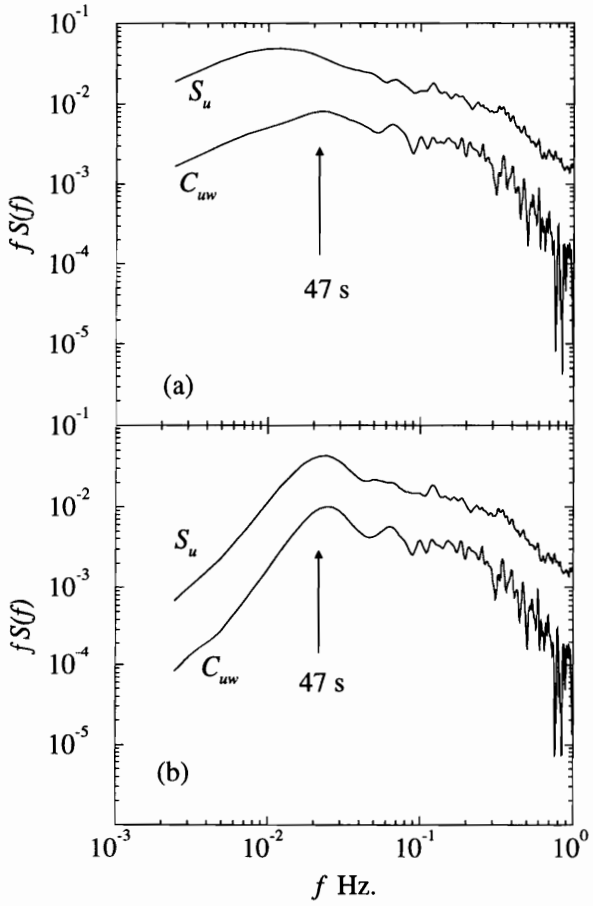

Figure 5.9: First moment of the streamwise component autospectra and stress cospectra. (a) Original file. (b) Filtered file.

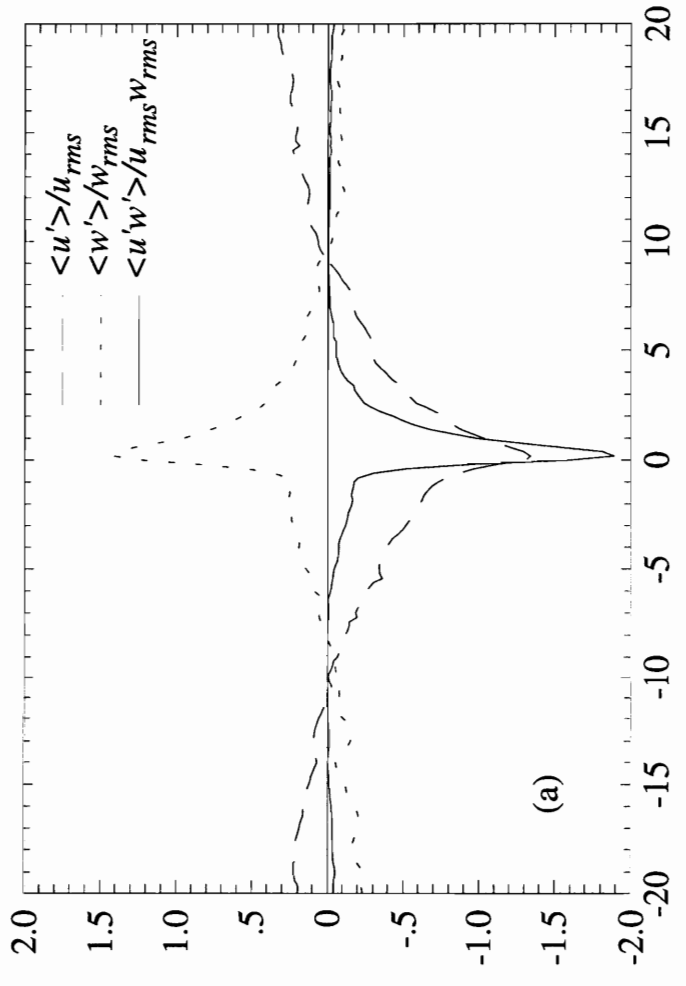

Figure 5.10: Ensemble averages of events detected by the quadrant technique.

where N is the number of events and τ is the time relative to the reference time t_j. The reference time here is taken as the point where the detector function is first turned on. Each time a detection was recorded, 20 s of data on either side were stored and finally averaged. Figure 5.10 shows normalized averages of u', w', and $u'w'$ produced using the quadrant technique. Averaging was done over the entire 2-hour record (546 ejections). Zero time is the leading edge of an ejection. These curves are very similar to corresponding averages of ejections in laboratory flow [e.g., Alfredsson & Johansson, 1984].

It is to be noted that conditional averages of u', w', and $u'w'$ obtained using the quadrant technique have their extreme values near the time of detection. It can be seen that the ejection events detected by this method are characterized by low streamwise velocity and a high value of the normal component of the velocity followed by a rapid streamwise acceleration. This is typical of near-wall, low-momentum fluid interacting with the outer flow. It was observed that the conditional averages of the cross-flow component of the velocity did not exhibit any peaks during the time frame where the u' and the w' signals showed the peaks, which seems to suggest that the ejection events do not contribute to the cross flow component in the mean. Examples of averages using other detection algorithms are given by Luchik & Tiederman [1987] (modified u-level), and Alfredsson & Johansson [1984] (VITA).

5.5 Scaling Burst Events in the Atmospheric Boundary Layer

The scaling of burst events has been a subject of controversy that has not been resolved to date. The turbulent boundary layer is a two-scale problem, with an inner and an outer layer having different scaling parameters. Studying burst events in a

turbulent channel flow, Luchik & Tiederman [1987] concluded that they scaled on inner variables. Scaling ejection events in the marine atmospheric surface layer using inner variables at a height of 8.2 m above the surface ($u_* = 0.19$ m/s, $z^+ = 1.03 \times 10^5$) leads to a nondimensional burst period of $O(10^5)$. This seems unreasonable when compared with laboratory values of ≈ 90 [Luchik & Tiderman, 1987], and hence the events detected here seem more likely to scale on outer variables. In laboratory flows this is done as $T_B U_e/\delta$, where U_e is the velocity at the edge of the boundary layer and δ is the thickness of the boundary layer.

Although the boundary layer thickness and U_e, as defined in the laboratory, do not have completely analogous counterparts in the atmospheric boundary layer, it is worthwhile to note that rough estimates of these quantities gives a nondimensional burst period which falls at least within an order of magnitude to the range of 2 to 6 obtained by various researchers (BT) using outer variables in the low Reynolds number laboratory flows. Although this study cannot assert that these events scale on outer variables, it appears that scaling these events using inner variables is inappropriate.

Chapter 6

WIND SPEED AND WAVE EFFECTS

In order to investigate the effects on ejection and burst periods of wind speed, surface wave height, and roughness variations, it is first necessary to consider the issue of obtaining these periods from the shorter 30 minute records. The quadrant, VITA, and modified u-level techniques were applied to the individual 30 minute records which made up the 2-hour record examined above and the results were compared with those obtained from the 2 hour record. It was found that the quadrant technique gave the most consistent results from the shorter records, with all four burst periods from the constituent records falling within 10% of that found for the longer record. It was concluded that the quadrant technique could be used to obtain reasonable burst period estimates from the shorter records.

One weather station and collocated wave array pair were chosen for analysis. The wave array data were analyzed for frequency spectra only. There were a total of 1090 wind records for which corresponding wave data were available.

6.1 Wind speed effect

Figure 6.1 shows the mean time between ejections as a function of wind speed. The ejection period is seen to decrease as wind speed increases. When these ejections are grouped into bursts (Figure 6.2), it appears that, except at very low wind speeds, the mean burst period is nearly constant with wide scatter. The constant nature of the burst period at higher wind speed may be due to the breakdown of the grouping technique at higher wind speeds. This breakdown could be attributed to a physical difference in the flow characteristics at higher wind speeds.

Figure 6.3 shows a timeline of u', w', the $u'w'$ product, the detected ejections, and the bursts into which they group for a portion of one of the data files. At lower wind speeds, as in Figure 6.3, where $U = 4.63$ m/s, the bursts are well separated in time (and, consequently, in space). At higher wind speeds the bursting rate increases to the point where the ejections are more closely and evenly spaced in time. Figure 6.4 is a timeline similar to Figure 6.3 for a record with mean wind speed $U = 10.56$ m/s. At higher wind speeds, the grouping algorithm is very sensitive to the value of t_{max} that is chosen. Since the ejections are so close together, they tend to group into about the same number of bursts for the same t_{max}, regardless of wind speed. Since t_{max} is statistically based and there are relatively few ejections in each record, there is a good deal of uncertainty in its value. (There is a limit to how narrow the time bins used in the calculation of Figure 5.5 can be made). For the low speed records, where the bursts are well spread out, this is not a problem, but the high speed records will group differently with a small change in t_{max}. Thus, for the higher-speed records the number of bursts that the ejections group into (and thus the mean burst period) is

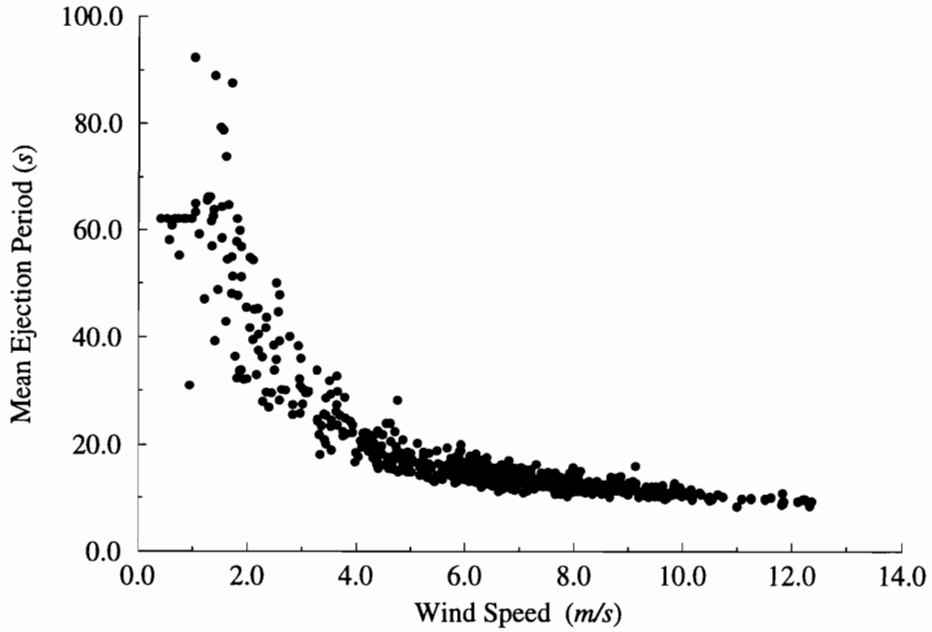

Figure 6.1: Variation of mean time between ejections with wind speed.

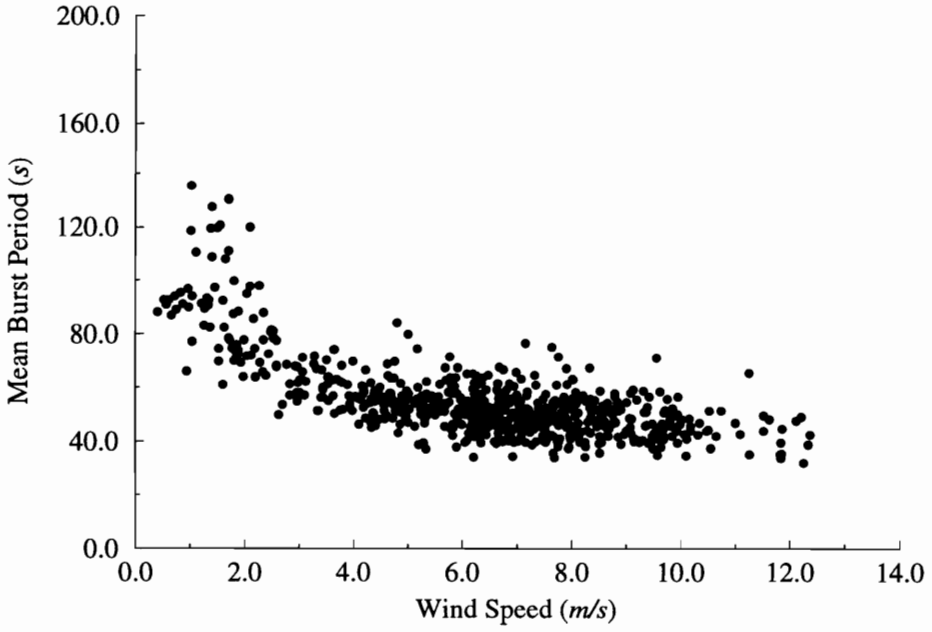

Figure 6.2: Variation of mean time between bursts with wind speed.

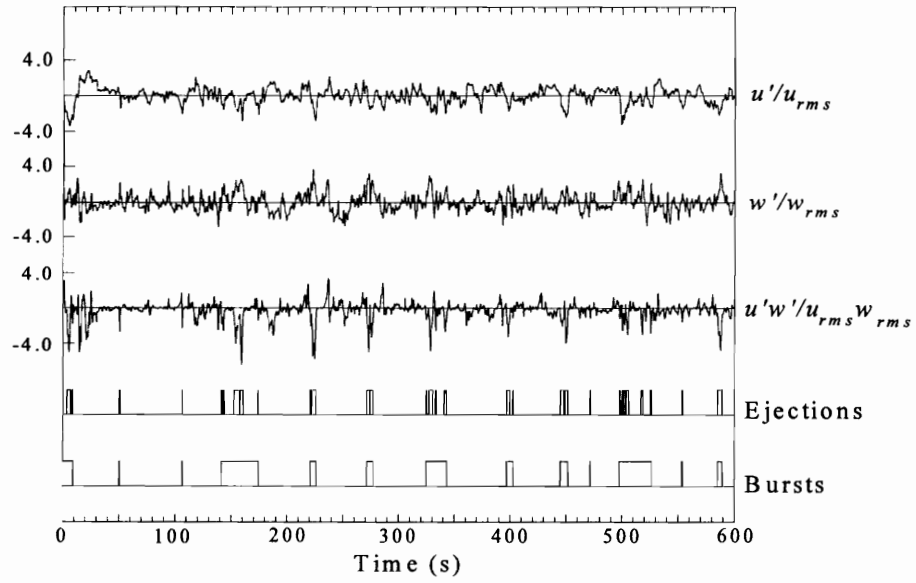

Figure 6.3: Timeline of u', w', the $u'w'$ product, the detected ejections, and the bursts into which they group for a portion of one of the low-speed data files, $U = 4.63$ m/s.

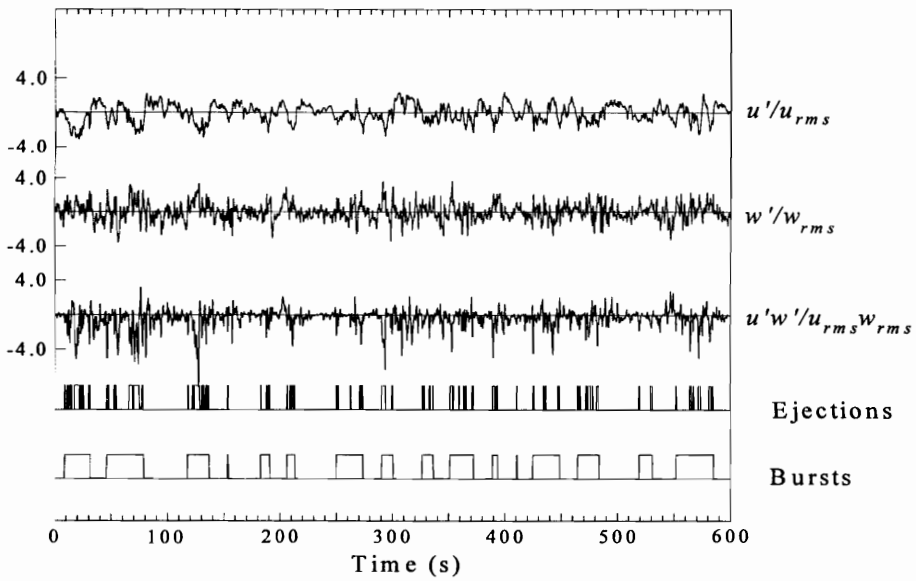

Figure 6.4: Timeline of u', w', the $u'w'$ product, the detected ejections, and the bursts into which they group for a portion of one of the high-speed data files, $U = 10.56$ m/s.

rather insensitive to the wind speed but is sensitive to the statistically chosen value of t_{max} that results for the record. This method of grouping fails for the higher-speed records.

Since the surface stress is largely supported by bursts, one will find that at lower wind speeds, the stress is highly intermittent. Stress pulses ($u'w'$) occur with a period on the order of a minute. As the wind speed increases, this pulsing will appear to diminish and the stress appears more continual.

In terms of vortical structures which may support the bursting process, at low wind speeds there are relatively few of these structures convecting in the flow but at high speeds there may be many more. At higher speeds they may appear in many different sizes, perhaps often overlapping, and give rise to an apparently more continual surface stress.

6.2 Wave field effects

Figures 6.5 and 6.6 depict the dependence of ejection period and burst period on the significant wave height. In order to increase the clarity of Figures 6.5 and 6.6, not all the data are plotted, however, those which are shown are representative of the entire set. The data in each figure are sorted and coded according to significant wave height. Within each 1 m/s wide wind speed band, the data with the lowest 20% of the wave heights in that band are plotted in one symbol, those with the next highest 20% in another symbol, and so on. Thus the symbols indicate wave height ranges relative to what is expected for the particular wind speed at which the data point falls.

If there were a strong significant wave height dependence, the symbols in Fig-

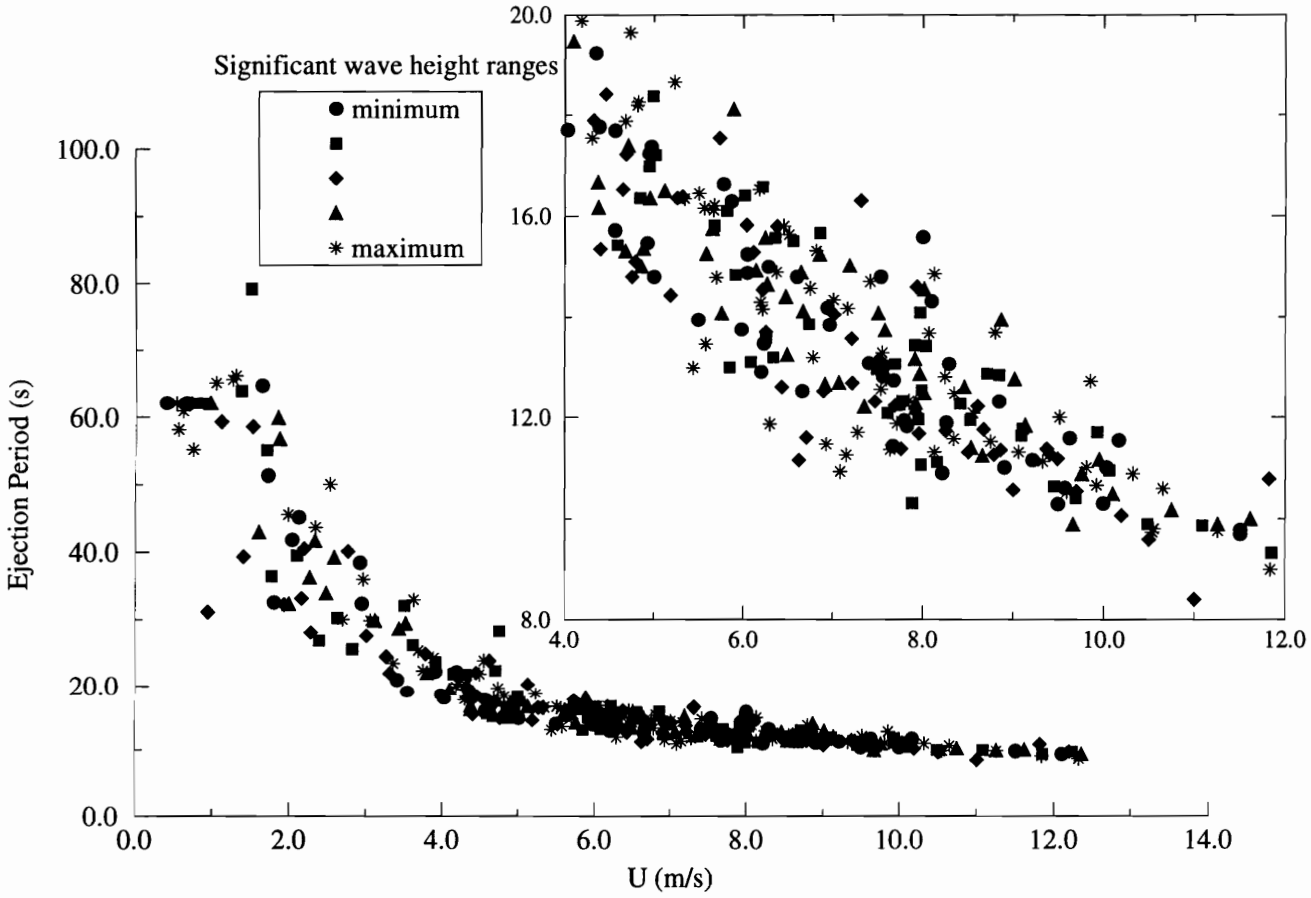

Figure 6.5: Ejection period versus wind speed sorted by significant wave height. The inset is an enlargement of the indicated range to show detail.

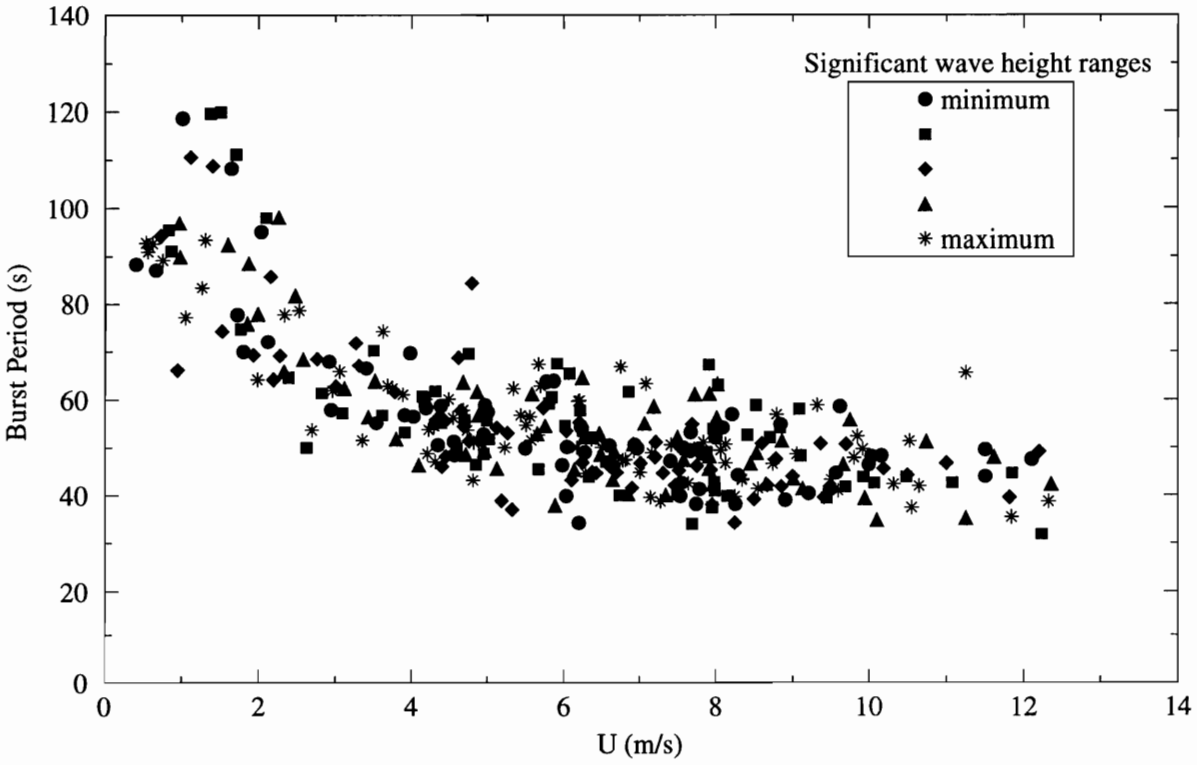

Figure 6.6: Burst period versus wind speed sorted by significant wave height. Technique for grouping ejections into bursts breaks down at higher wind speeds.

ures 6.5 and 6.6 would sort out in bands across the entire range of wind speeds. This does not seem to be the case; that is, there does not seem to be any discernible significant wave height dependence.

In Figure 6.7 the ejection period data are sorted according to a measure of the mean wave slope, $H_{\frac{1}{3}}\omega_m^2/g\pi$, where $H_{\frac{1}{3}}$ is significant wave height, ω_m is modal wave frequency, and g is the acceleration of gravity. Again, the symbols indicate the range of values present in each 1 m/s wind speed band. Also, again, there seems to be no apparent dependence on the wave field. A similar conclusion is reached when examining the burst periods. The modal wave frequencies (ω_m) here range from 0.88 to 5.33 s, thus the timescale of the surface motion is significantly shorter than the average burst or ejection periods.

Arya [1988] points out that air flow in the lowest region of the surface layer may see direct influences of the wave field. However, above the height of a few significant wave heights, the mean flow becomes essentially independent of the wave field. This may explain the absence of any noteworthy correlation between the bursting frequencies and the wave field as the anemometer is positioned at a height much greater than the mean significant wave height ($\approx$ .4 m). It must be noted, however, that there are a significant number of ejections which are separated by periods close to the modal wave periods. These ejections have been grouped together and are identified as ejections from the same burst structure. Surface wave influences on the structure of these motions are possible. In the open ocean, where the wave periods would be longer, there may be a discernible wave dependence on the mean ejection period.

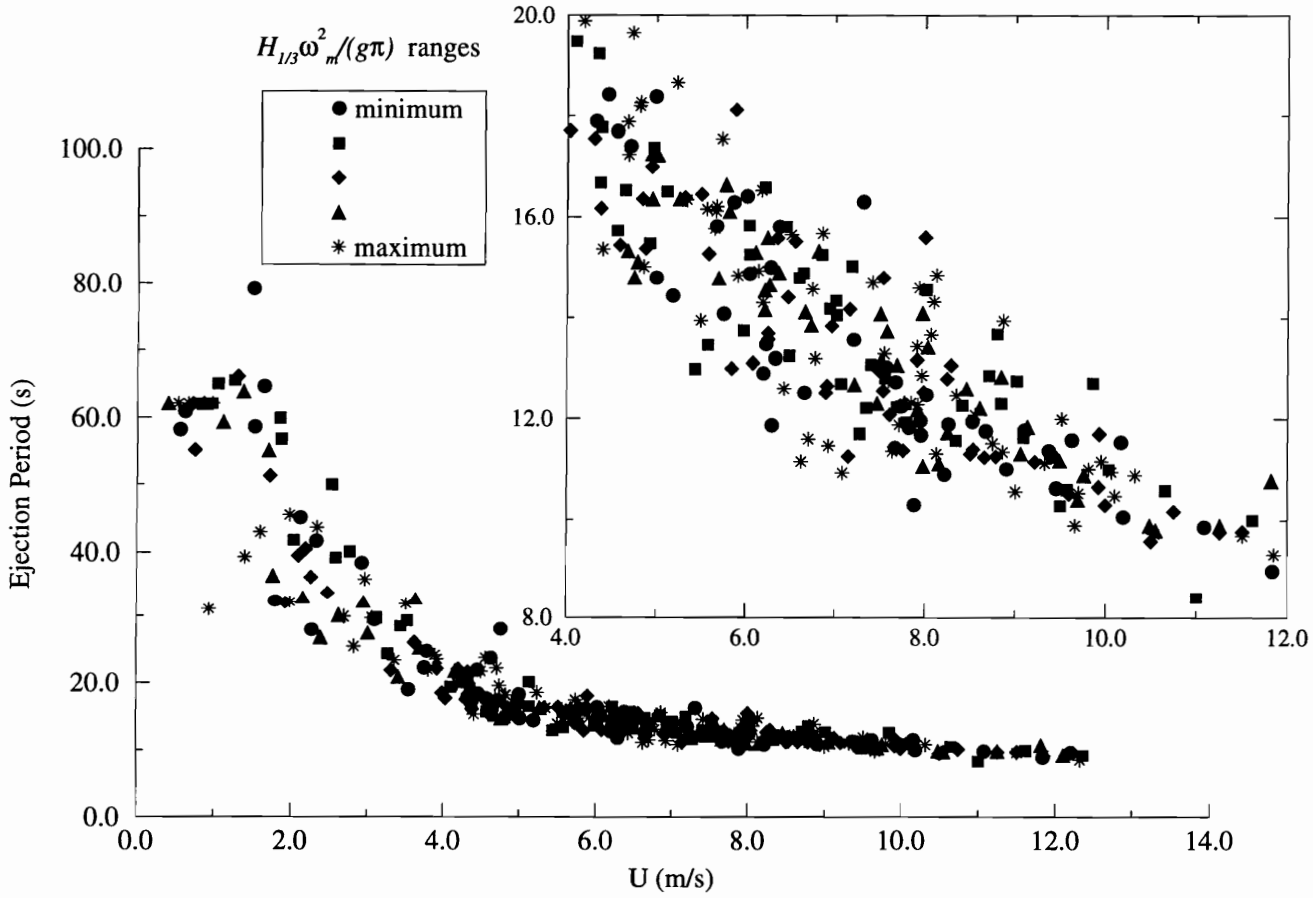

Figure 6.7: Ejection period versus wind speed sorted by a mean wave slope indicator. The inset is an enlargement of the indicated range to show detail.

Chapter 7

FRACTAL NATURE OF ATMOSPHERIC TURBULENCE

Having observed the existence of ejection and sweeps in large Reynolds number flows, it would be interesting to see if this phenomena coexists at different scales simultaneously in the marine atmospheric surface layer. The same record which was previously used to detect bursts in the atmospheric surface layer was chosen to investigate if ejection and sweep motion coexist at different scales, i.e, if they exhibit a fractal nature.

To see if ejection and sweep motions exist at a particular scale, it was necessary to isolate the corresponding scale from the other frequency components.

7.1 $u'w'$ Cospectrum

The $u'w'$ cospectrum, C_{uw}, was used to select the frequency bands for filtering the velocity signal. The frequency bands were chosen such that the energy content (i.e., the area under the cospectrum, Figure 7.1) for each band is roughly equal. Based

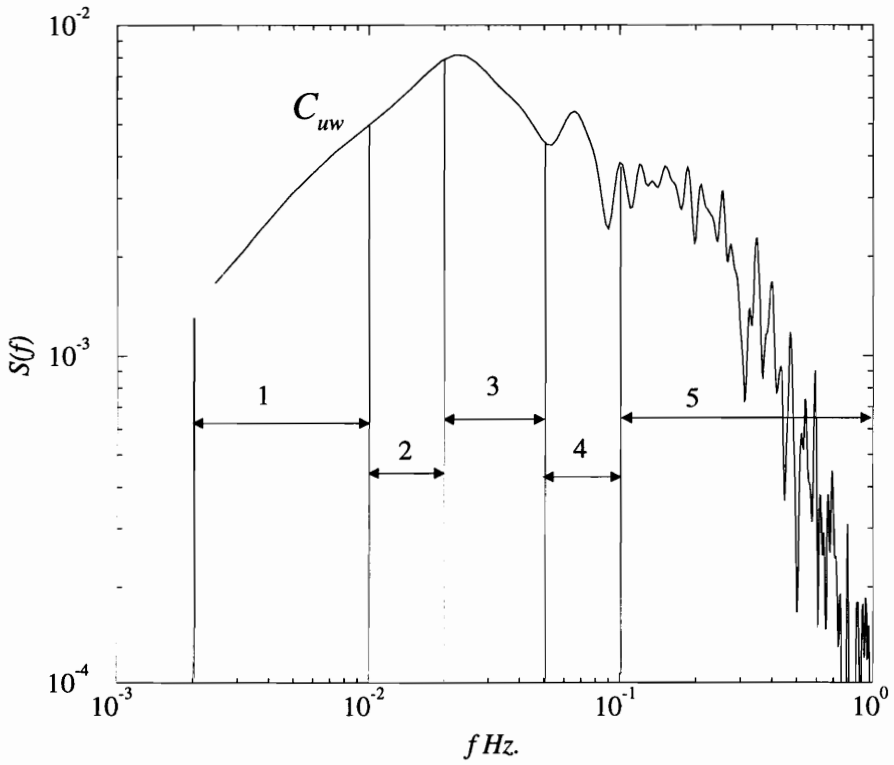

Figure 7.1: Frequency bands are chosen such that the energy content in each band under the $u'w'$ cospectrum (C_{uw}) is almost equal.

Table 7.1: Frequency ranges selected as passbands for filtering.

Band	Frequency Range
1	0.002 – 0.01 Hz.
2	0.01 – 0.02 Hz.
3	0.02 – 0.05 Hz.
4	0.05 – 0.1 Hz.
5	0.1 – 1 Hz.

on this rule, five bands (shown in Table 7.1) were selected which will be used as passbands for the signal.

7.2 Filtering

In order to isolate the specific frequency content, the signal, would have to be bandpass filtered for each of the selected frequency bands separately. Bandpass filtering could be achieved either by using a digital filter in the time domain or filtering in the frequency domain.

Digital Filter: Digital filtering is a process by which the input data $x(t)$ is transformed to the output data $y(t)$ by a linear relation such as

$$y(t) = \sum_{l=-\infty}^{\infty} h_l x(t-l) \tag{6.1}$$

It is worthwhile to note that such a filter need not conform to the condition of "physical realizability", as it assumes that future values of the time series are available at the time of filtering. The weights, h_l, are chosen suitably to define the characteristics of the filter.

A special case of such a filter is the *symmetric filter*, where $h_{-l} = h_l$. Using the

$\mathcal{Z}$ transform*, the transfer function of the filter is

$$H(\mathcal{Z}) = \sum_{l=-\infty}^{\infty} h_l \mathcal{Z}^{-1} \tag{6.2}$$

Substituting $\mathcal{Z} = e^{-j2\pi f\Delta}$, where Δ is the sampling interval, into the above equation gives the frequency response function, $H(f)$, of the filter. It can be seen that for a symmetric filter

$$H(f) = h_0 + 2\sum_{l=1}^{\infty} h_l \cos(2\pi f l\Delta); \quad -\frac{1}{2\Delta} \leq f \leq \frac{1}{2\Delta} \tag{6.3}$$

The phase shift between input and output is either 0 or π as the frequency response function contains no imaginary part. This was the main reason for choosing a symmetric moving average filter, so as not to distort the phase relation between the input and output signal.

Bandpass filtering: Bandpass filtering of the signal using a moving average was achieved in two steps. The moving average scheme is first used to remove frequencies below the lower cutoff frequency (highpass step) and then acts as a lowpass filter to remove frequencies above the upper cutoff frequencies. Such a filter is easy to implement and, as shown above, does not give rise to any phase distortions.

Consider a signal $x(t)$, sampled at f Hz. To bandpass $x(t)$ through a filter with a lower cutoff of F_l and an upper cutoff of F_u, the high pass filter would be

$$x_h[i] = x[i] - \sum_{j=i-\frac{f}{2F_l}}^{i+\frac{f}{2F_l}} x[j] \tag{6.4}$$

and the low pass filter would be

*refer Jenkins & Watts [1968]

$$x_b[i] = \sum_{j=i-\frac{f}{2F_u}}^{i+\frac{f}{2F_u}} x_h[j] \tag{6.5}$$

where $x_b[i]$ is the bandpass filtered signal. This is illustrated in Figure 7.2, which shows the u' as it passes through the filter.

To check if the filter performs reasonably, the cospectra of the velocity signal were checked after it was passed through each passband. In Figure 7.3, it can be seen that the filter is effective in eliminating energy outside the passbands.

7.3 Correlation in the u' and w' signal

The u' and w' signals when seen on a phase plane, Figure 7.4, reveal a distinct correlation at all frequencies. This is an important feature, which says that the turbulent fluctuations are not entirely random at any scale in the surface layer.

The low frequency fluctuations are more organized than the higher frequency fluctuations (due to smaller bandwidth) and hence have less scatter in those plots. Plots (a) through (e) can be compared to the unfiltered signal in (f) and are fairly similar.

7.4 Percentage contributions to the Reynolds stress

It was interesting to note that the percentage contributions to the Reynolds stress (Table 7.2) from each quadrant of the $u'w'$ plane of the bandpass filtered signal is about the same as that of the unfiltered signal. This is also comparable to the contributions seen in the laboratory and for the signal which was not passed through

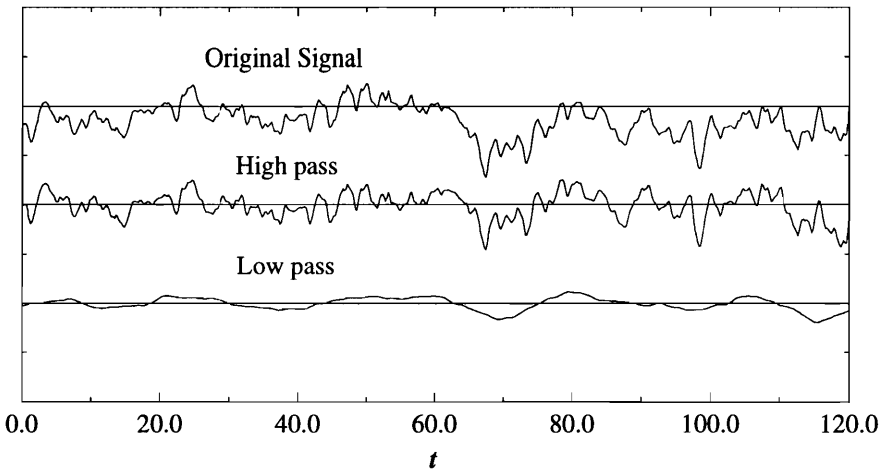

Figure 7.2: The u' signal as it passes through a bandpass filter of width 0.05 – 0.1 Hz.

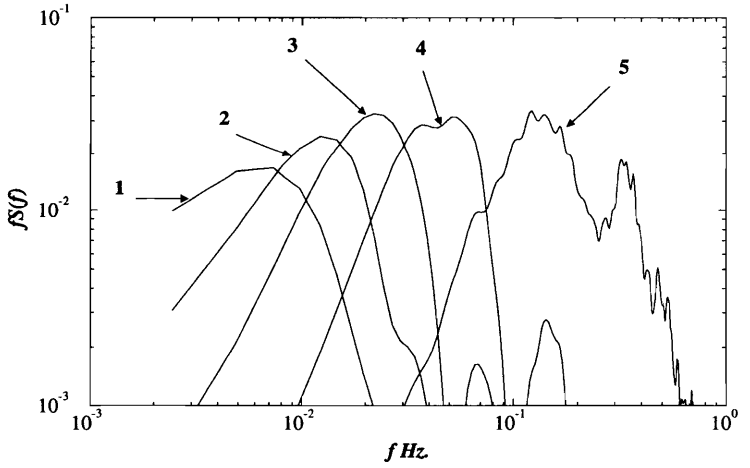

Figure 7.3: Spectra of the bandpass filtered data. 1) 0.002 – 0.01 Hz. 2) 0.01 – 0.02 Hz. 3) 0.02 – 0.05 Hz. 4) 0.05 – 0.1 Hz. 5) 0.1 – 1 Hz.

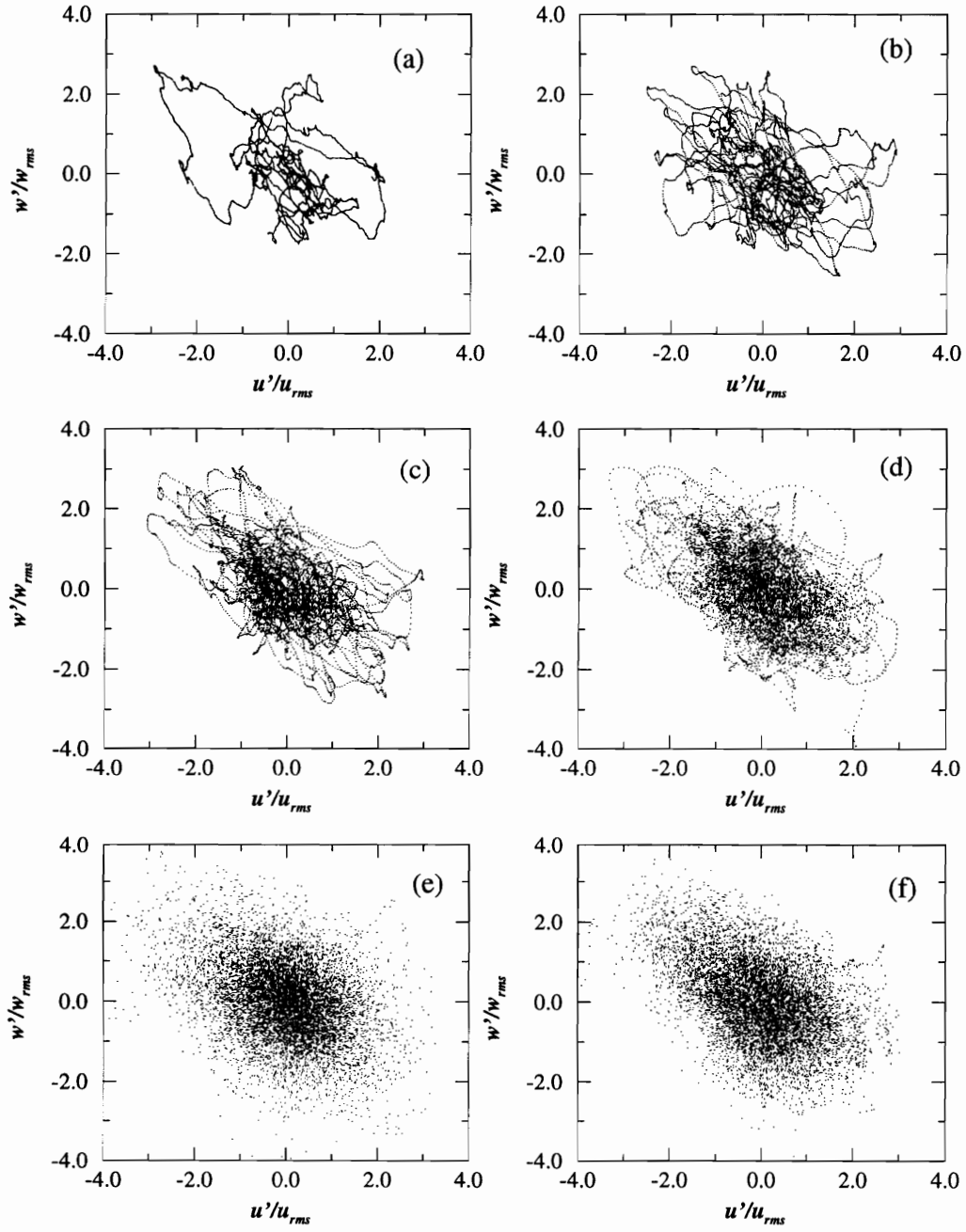

Figure 7.4: Scatter plots on the $u'w'$ plane for the different bandpass filtered signal. (a) 0.002 – 0.01 Hz. (b) 0.01 – 0.02 Hz. (c) 0.02 – 0.05 Hz. (d) 0.05 – 0.1 Hz. (e) 0.1 – 1 Hz. (f) Low pass filtered signal with cutoff at 1 Hz.

Table 7.2: Percentage contribution to the Reynolds stress from the different quadrants of the $u'w'$ plane.

	Q1	Q2	Q3	Q4
Band 1	-10.13	86.17	-9.49	33.46
Band 2	-14.32	69.25	-18.13	63.20
Band 3	-6.93	65.65	-8.37	49.65
Band 4	-10.58	67.11	-9.49	52.96
Band 5	-22.94	76.75	-20.01	66.20
Full Signal	-14.59	74.14	-12.74	53.20

the bandpass filtered signal. This seems to indicate that the mechanisms of ejection and sweep, which are major flux mechanisms in the surface layer, exist at all scales.

7.5 The Timelines

Since the percentage contributions to the Reynold's stress from different quadrants of the $u'w'$ plane are similar, it is possible that the bursting phenomena coexists (or is superimposed) at different scales in the turbulent signal. The ejection phenomena will manifest itself as a negative fluctuation in the u' signal with a simultaneous positive fluctuation in the w' signal. These are the events that are sought by conditional sampling techniques to register an ejection event.

The timelines of the velocity signal for the different bands are illustrated in Figures 7.5 through 7.10. The plots show the signals normalized by their corresponding root-mean-square value. The time axis, t^* has been scaled by the mid frequency (f_m) of the frequency band which was used to filter the signal. On such a plot, the signals passed through different frequency bands look "similar", suggesting the fractal nature of ejection and sweep like events. Events which contribute significantly to the Reynolds stress ($u' < 0$, $w' > 0$; $u' > 0$, $w' < 0$) are seen to exist at different scales.

Previous results suggest that bursting is a quasi-periodic phenomenon with a period on the order of a minute. However, the fractal nature of ejection and sweep motions suggests that these motions exist simultaneously at different scales. It is hypothesized that the dominant scale of the flux mechanism is the scale corresponding to the peak in the $u'w'$ cospectrum and the peaks in the autocorrelation function of the u' signal.

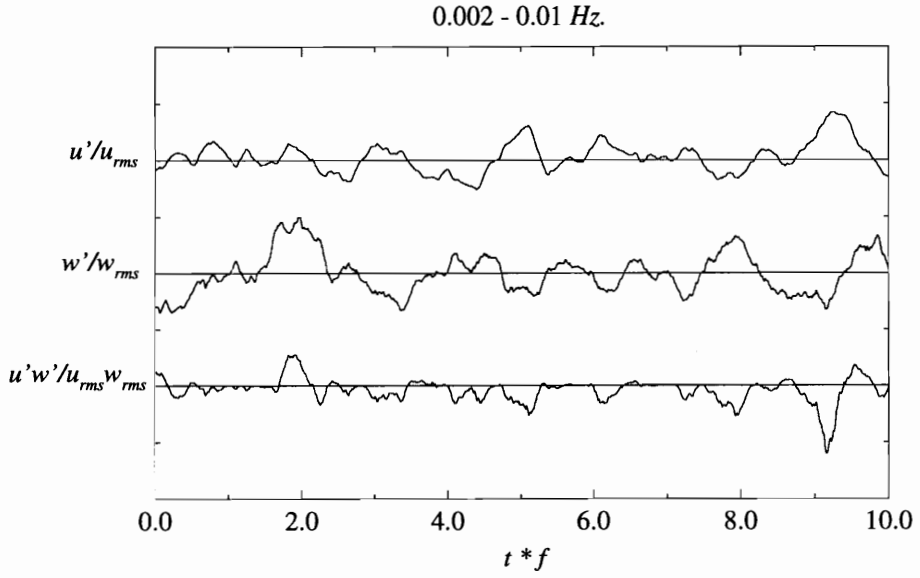

Figure 7.5: u' and w' signals for 0.002 – 0.01 Hz. band seen on normalized time axis.

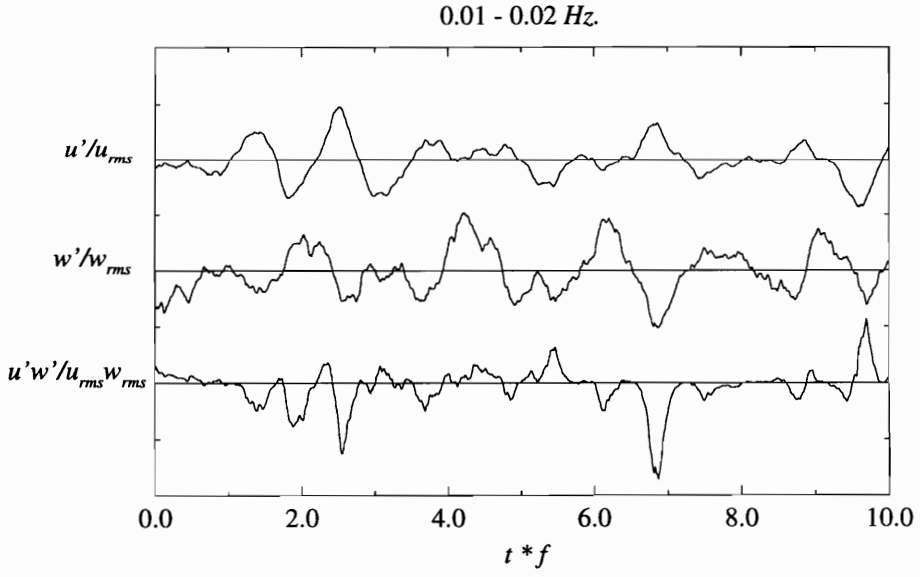

Figure 7.6: u' and w' signals for 0.01 – 0.02 Hz. band seen on normalized time axis.

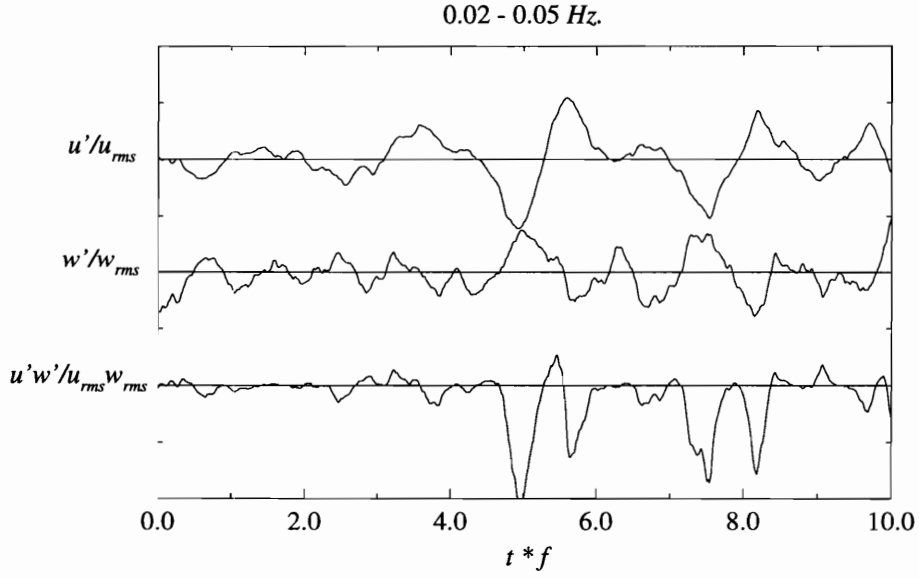

Figure 7.7: u' and w' signals for 0.02 – 0.05 Hz. band seen on normalized time axis.

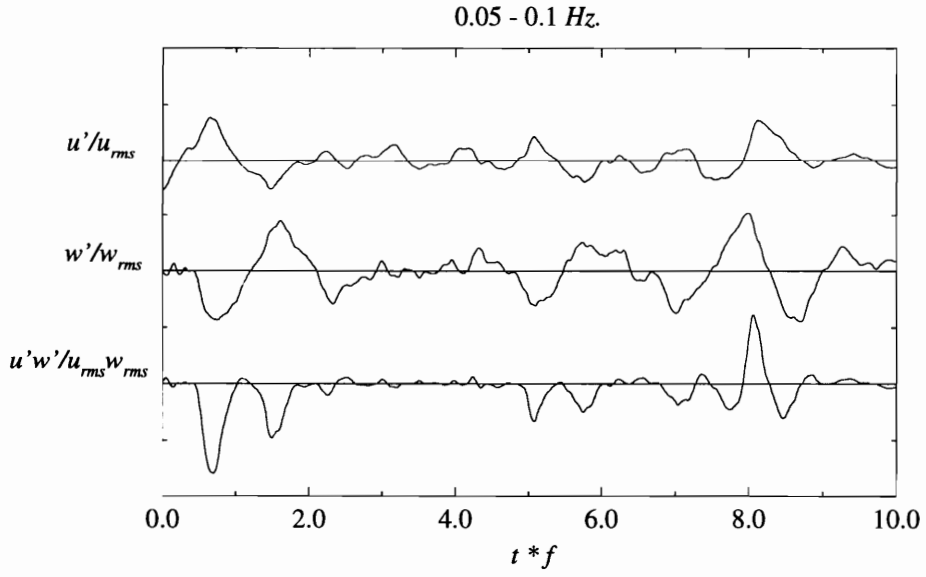

Figure 7.8: u' and w' signals for 0.05 – 0.1 Hz. band seen on normalized time axis.

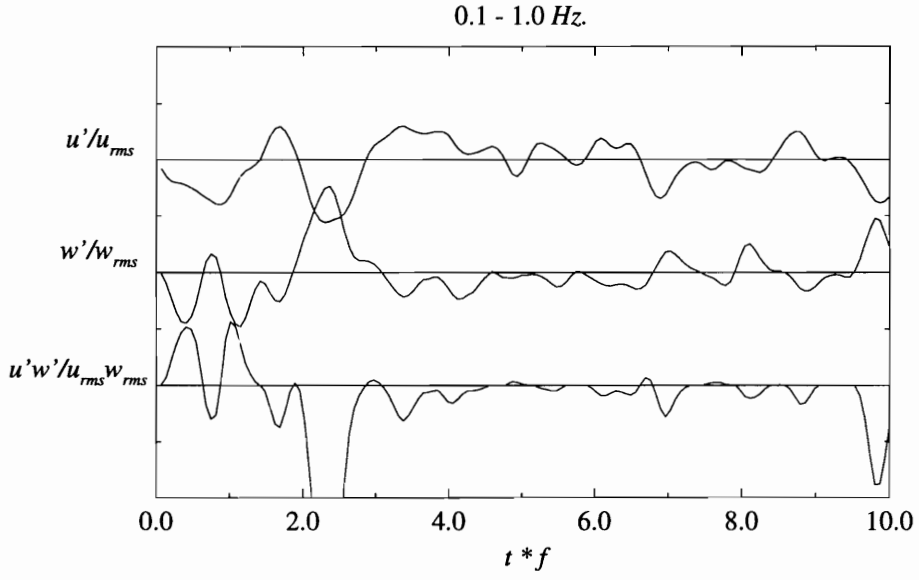

Figure 7.9: u' and w' signals for 0.1 – 1 Hz. band seen on normalized time axis.

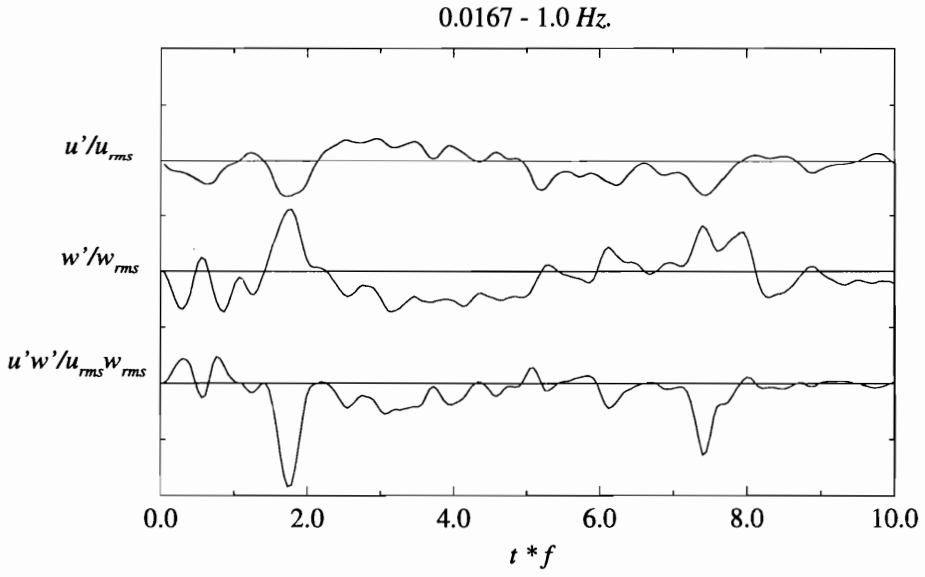

Figure 7.10: u' and w' signals for 0.0167 – 1 Hz. band seen on normalized time axis.

Chapter 8

IDENTIFYING LARGE SCALE MOTIONS

Burst structures seen in velocity probe data are typically associated with the ejection of low momentum fluid from the near wall region into the outer flow. It has been suggested (refer chapter 2) that these motions could be associated with the passage of large scale vortical motions. These vortical motions manifest themselves as a positive or negative fluctuation in the streamwise velocity, depending on where the probe is relative to the structure. As these structures are seen to play an important role in the flux dynamics, it would be worthwhile to identify and characterize these structures in a high Reynolds number flow, such as the atmospheric surface layer.

In turbulent shear flows, detection as well as detailed investigation of such structures is complicated by their three dimensional nature and their large deviations in shape, size, orientation and convection velocity. Furthermore, little is known about the growth and decay cycles of such structures at high Reynolds numbers. Thus identifying such structures in the flow is subjective despite making the assumption that evolution and decay is identical in each cycle. Ideally, one would like to be able to identify the structure in the flow and follow it in space (a Lagrangian approach)

in order to best study its dynamics, growth and decay. However, such an approach is not feasible until computers evolve, powerful enough to simulate the high Reynolds number flow using DNS, without prohibitive expense and effort. The alternative is to use the Eulerian approach and measure the flow field using velocity and temperature probes. It is interesting to note that, in order to fully capture the flow field associated with the large scale motions, a three-dimensional sensor array is needed. Even then, only those structures whose configuration matches the sensor setup would be recorded with any reliability [Hussain, 1981]. However, such a setup would be prohibitively expensive. Given all these constraints and hurdles, one has to be content with limited and partial available data.

The previous chapters describe characterizing such structures (associated with the bursting phenomena) in the marine atmospheric surface layer, using single point velocity measurements. As stated above, these measurements give no information on the spatial structure and orientation of the large scale motions correlated to the burst structures. The Risø data set [Barthelmie *et al.*, 1994] alleviates this situation to a certain extent. Velocity measurements were made at multiple heights which provides an opportunity to study the spatial structure (though only in one plane). This might shed light on the different sizes and orientation of these large scale structures.

Figure 8.1 is a schematic of the atmospheric boundary layer under stable or neutral conditions. This gives an idea of the eddy structures, which convect in the flow. It is hypothesized that these structures (e.g., a transverse vortical structure) embody the ejection and sweep motions. Figure 8.2 is a schematic of the unstable convective boundary layer showing its large eddies and convective plumes. The atmospheric surface layer is mostly unstable, however, the data record chosen for study is near

neutral stability where observed events are largely shear related. Ejections and sweep motions have also been associated with sharp gradients of large eddies which are called microfronts [Chen & Blackwelder, 1978; Robinson, 1990; Mahrt & Gibson, 1992; Mahrt & Lowell, 1994]. Figure 8.3 gives a schematic of a microfront and its associated motions in terms of Robinson's hypothesis of the form of theses structures. The following sections describe an attempt to identify the aforementioned structures in the marine atmospheric surface layer.

8.1 Data files

Wind velocities were measured at six different levels (3, 6, 10, 18, 32 and 45 m) in the atmospheric surface layer. Fall 1994 data files* were chosen to identify large scale motions. To avoid complications, care was taken to select the data file so that the atmosphere was near neutral stability during that period. It was desirable to have the fetch as long as possible to approach fully developed wave conditions. This may help, to a certain extent, in rationalizing the assumption of a statistically stationary flow field. The data files picked for analysis are coded 131216, which indicates that the data were collected during the 13th of October, starting at 1216 hrs.

8.2 Temporal fluctuations

A time history of the fluctuating component of the streamwise velocity (u'), at different levels, is seen in Figure 8.4. As expected, the turbulence intensity (proportional to u_{rms}) decreases with height. It can be seen, during certain time intervals,

*refer chapter 3 for data reduction information

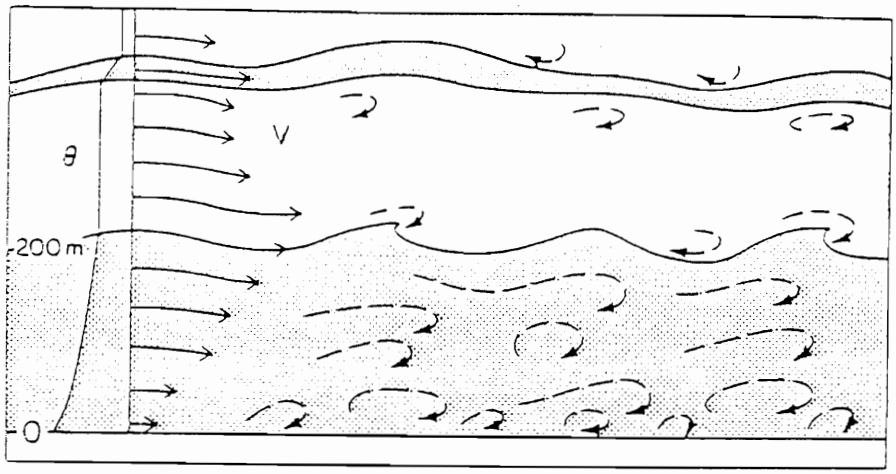

Figure 8.1: Schematic of a stable atmospheric boundary layer showing its eddy structure, [Wyngaard, 1992].

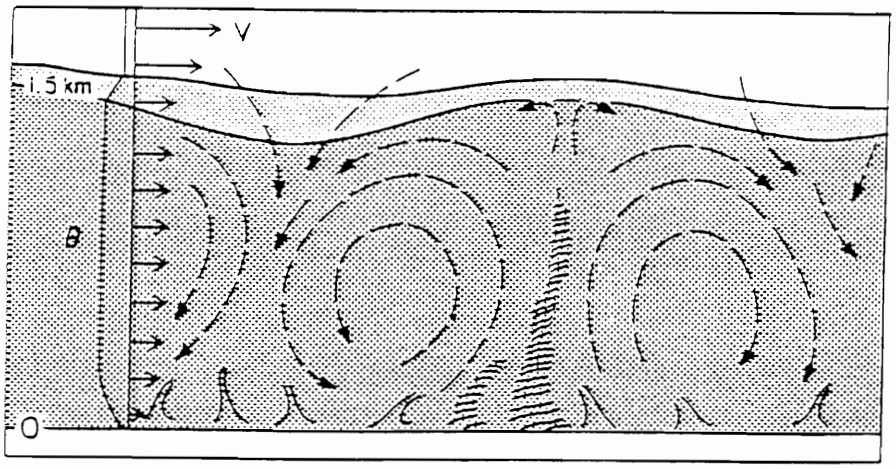

Figure 8.2: Schematic of an unstable atmospheric boundary layer showing its large eddies, convective plumes, flat wind profile, and the capping inversion layer. [Wyngaard, 1992].

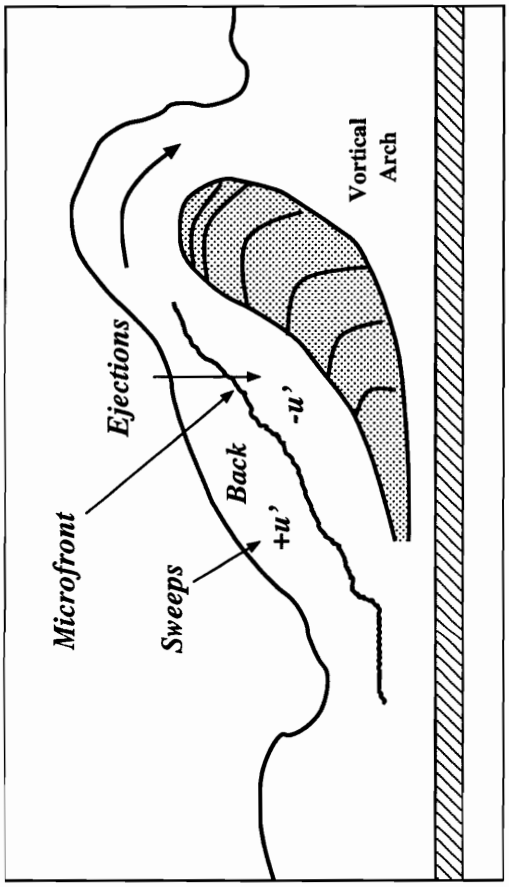

Figure 8.3: Schematic of eddy microfront giving rise to ejection and sweep motions, [after Robinson, 1990].

that fluctuations at different levels seem to be correlated with each other, with a certain time delay. In order to accentuate these correlations, wavelet filtering was performed. The threshold for the filter was kept high ($K^{\dagger}= 12$) in order to see only the strong motions. The filtered signals are seen in Figure 8.5. These "enhanced" signals facilitate the visual detection of the large organized motions. The time interval between 400 and 600 s in Figure 8.5 seems to have two structures which extend across the depth of the surface layer. These structures have been marked using the dashed lines on the figure. The dashed lines have been subjectively drawn by eye, but are held constant in the figures to follow to serve as a reference. The slope of the dashed line suggests the structure, associated with these strong motions, is inclined. The probes at the upper levels "see" this structure first. Subsequently, after a time delay, which may be the time required for the structure to convect downstream, the probes at the lower levels encounter the structure. The time delays can be used to estimate the orientation and size/shape of these structures.

For clarity, Figure 8.6 shows the streamwise velocity fluctuations for the time interval which contains the two structures. For the same time interval (Figure 8.7) the normal velocity fluctuations (w'), also show the expected correlation. The quadrant technique has been used to detect ejections. A threshold of $H = 2.0$, was used to detect ejections at all the heights. It is possible that decreasing the threshold with increasing height may result in detection of the weak ejections at higher levels, so as to better resolve the structure. It is interesting to note that the ejections, seen in Figure 8.8, also line up well with the reference (dashed) lines. Intuitively, this microfront, which gives rise to the negative and then a positive defect in the

[†]refer chapter 4

streamwise velocity could be associated with the "back" of a large eddy structure (Figure 8.3).

8.3 Spatial Structure

Having identified motions which seem to be associated with the passage of a large scale structures, it is worthwhile to educe the spatial nature of these motions. Taylor's hypothesis enables conversion of temporal measurements at a point to spatial patterns in space through the transformation $x = ct$. Implicit in the transformation is the assumption that the turbulence field is frozen in time and is transported horizontally past the probe at a speed c. It is obvious that turbulence in the atmosphere is not frozen. However, Taylor's hypothesis gives valuable insight into the spatial structure, as it has been found that the eddy life is typically long compared to the time it takes to travel across the sensor.

8.3.1 Orientation of the large scale motion

Researchers [Kaimal, 1974; Davidson, 1974; Wilczak & Businger, 1984; Perry & Li, 1990] have found that the large scale motions in a turbulent boundary layer convect at a speed different from the local wind speed. They also found that the convection velocity depends on the size of the structure, the stability of the boundary layer, the distance from the surface and its roughness condition. However, Kaimal & Finnigan [1994] suggest that the local mean wind $\overline{u}$ could be used as the convection velocity of organized structures, as long as reasonably good agreements between atmospheric measurements made with moving and stationary probes are found. For the present study, both the local mean wind and the average wind velocity across the measuring

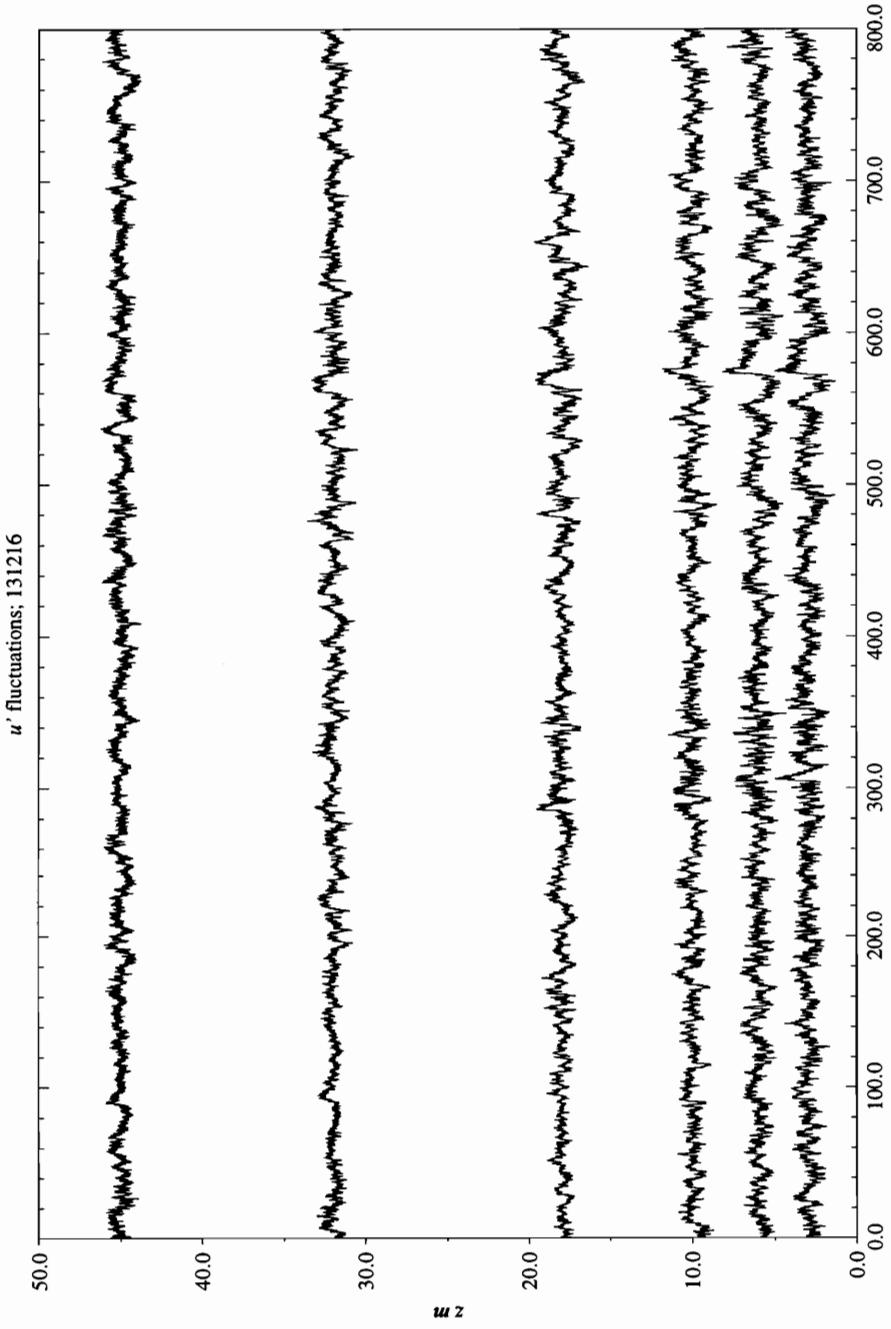

Figure 8.4: Fluctuations of streamwise velocity component.

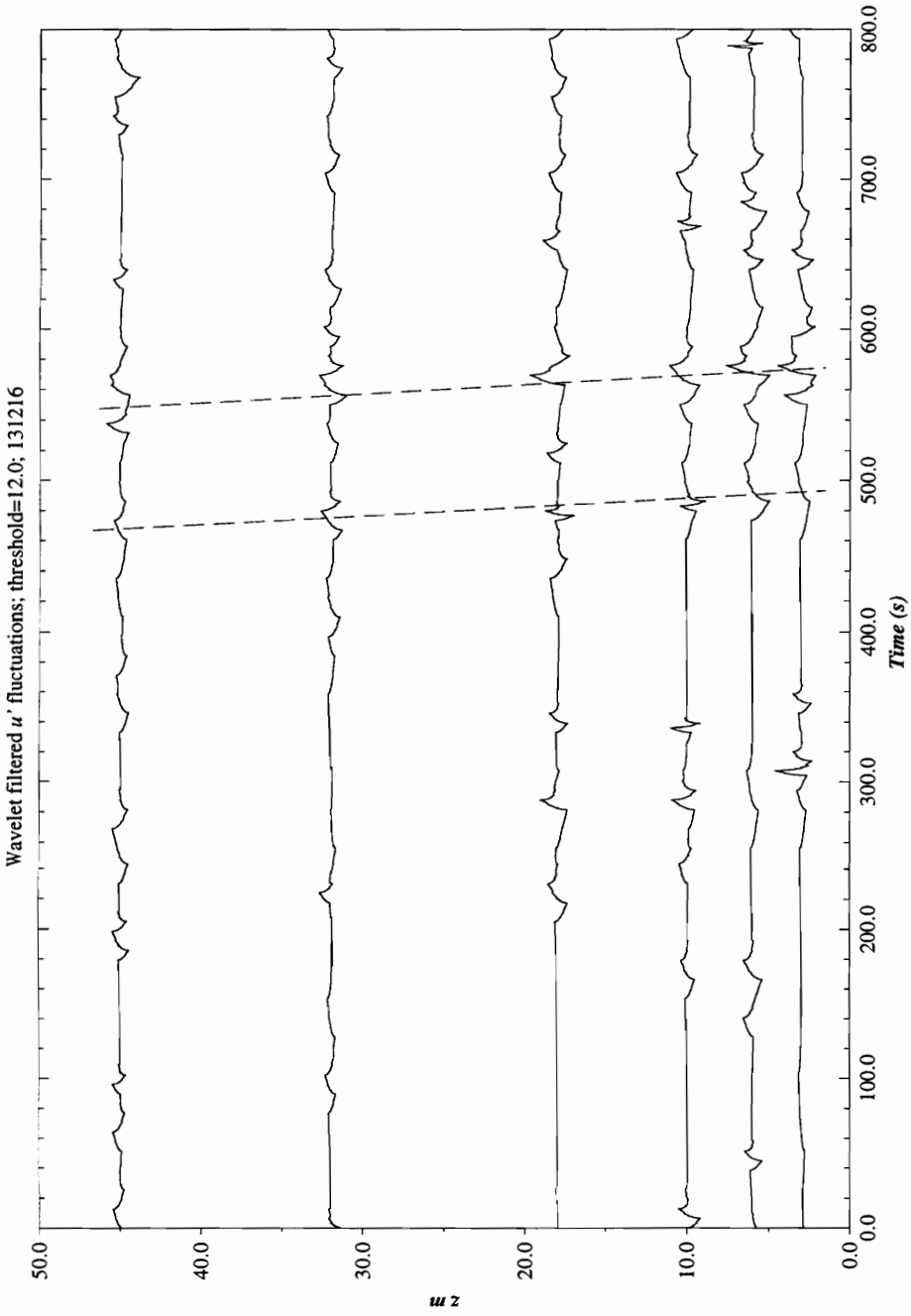

Figure 8.5: Wavelet filtered fluctuations of streamwise velocity component.

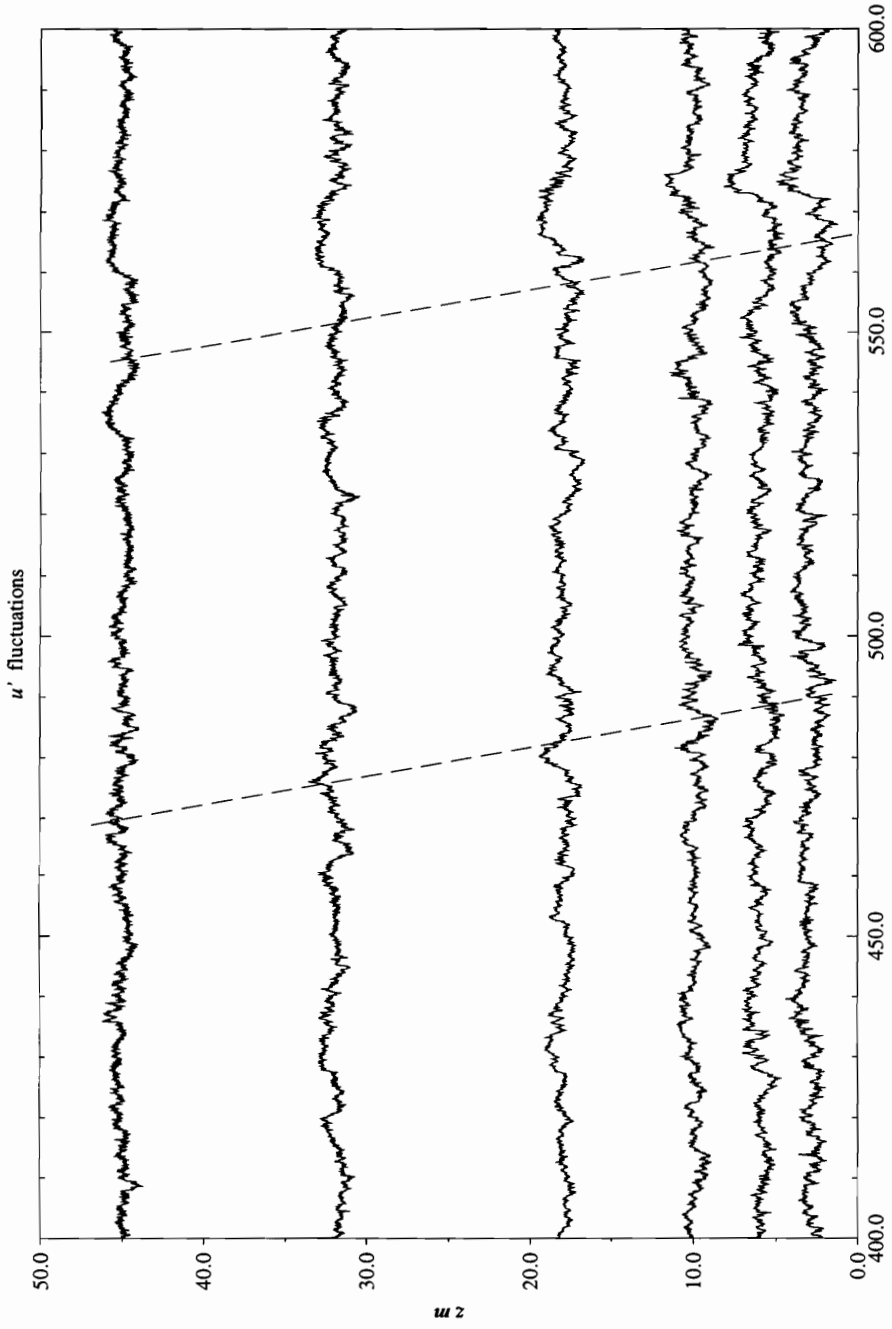

Figure 8.6: Fluctuations, in the selected time interval, of streamwise velocity component.

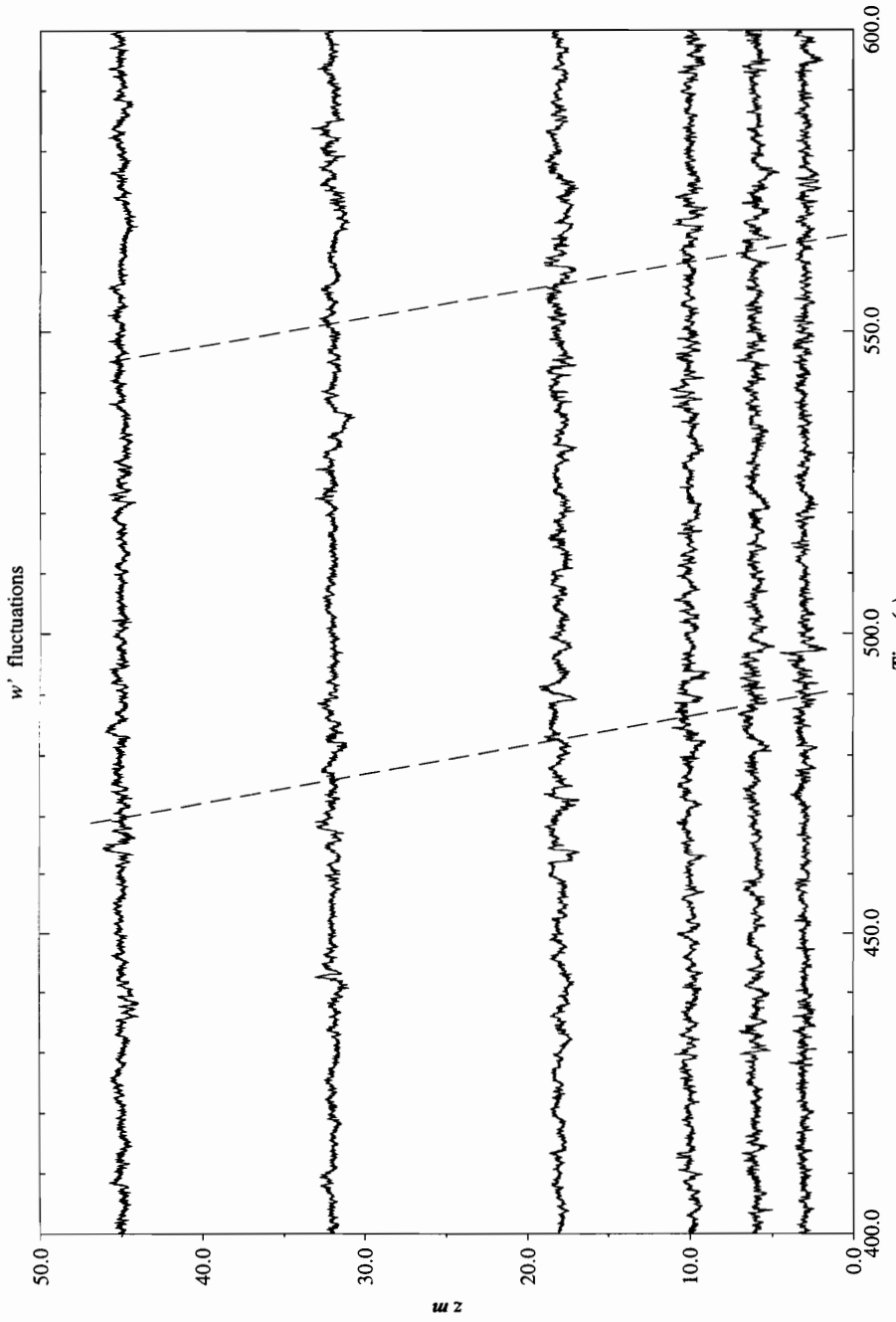

Figure 8.7: Fluctuations, in the selected time interval, of vertical velocity component.

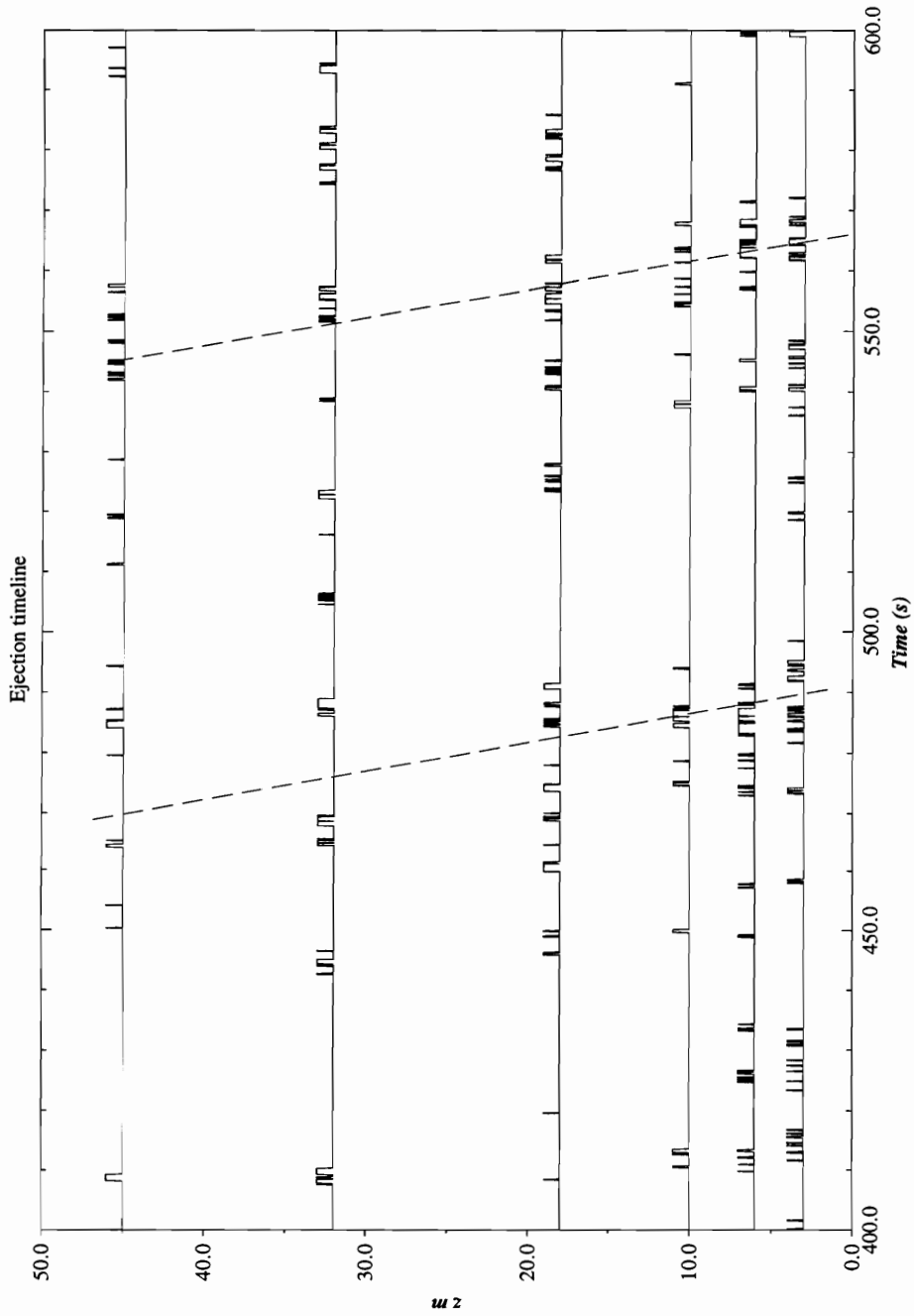

Figure 8.8: Timeline of ejections at different levels.

depth have been used as the convection velocities in order to estimate the orientation of the structure.

The orientation could be calculated by estimating the time delay between the encounter of the structure with probes at different heights. A rough estimate of such time delays could be done visually by looking at Figure 8.8. However, a more objective method is to use cross-correlation between the signals at different levels.

Data segments of length 50 s were selected (starting from $t = 530$; Figure 8.6) at each level. The reference signal picked is the 45 m u' signal, which has been assigned the index 1. Signals at successive depths have been assigned indices 2 through 6. The cross-correlation between signal 1 and signals at successive depths (viz., 32m through 3m), is given by,

$$R_{1j}(\tau) = \frac{\overline{u_1'(t)u_j'(t+\tau)}}{(u_1')_{rms}(u_j')_{rms}} \tag{8.1}$$

A shift in the peak of the cross-correlation gives an indication of how much an organized feature is lagging behind a corresponding feature at other levels. The cross-correlation can be seen in Figure 8.9. Curve R_{11} is the autocorrelation of the 45 m u' signal. It can be seen that peaks of the cross-correlations, are shifted by a positive lag. These shifts have been used to estimate the orientation (Table 8.1). Using Taylor's hypothesis, the time delay (τ), has been converted to distance ($u_z \cdot \tau$). A convention of negative distance is used to show that the organized part of the structure is upstream of the part encountered at the reference level ($z = 45$ m). These distances have been plotted on a 1:1 grid to give an idea of the orientation. Figure 8.10 shows the orientation estimates using both the local mean wind and the mean wind across the measuring depth (shown in dashed lines). It can be seen that for the observational depth for the experiments, the difference in estimates is insignificant. The structure

Table 8.1: Pseudo distance between the structure at different levels to estimate inclination.

Index	z m.	u_z (m/s)	R_{1j} Peak	Delay τ (s)	$u_z \cdot \tau$ m.	$\overline{u_z} \cdot \tau$ m.
1	45	7.66	0.0	0.0	0.0	0.0
2	32	7.70	0.9	-0.9	-6.9	-5.9
3	18	6.87	3.8	-3.8	-26.1	-25.0
4	10	6.37	7.5	-7.5	-48.1	-49.7
5	6	5.87	12.0	-12.0	-70.4	-78.9
6	3	5.12	14.9	-14.9	-76.3	-98.0

seems to be inclined at an angle of 45° above $z = 18$ m, and below that convects at very shallow angles ($\approx 15°$) to the surface. This suggests that the inclination increases with height. It should be noted, however, that the structure may be constantly stretching and changing orientation. Also, choosing a different reference level will lead to a different orientation estimate. For comparison, Phong-anant *et al.* [1980] estimate inclination angles ranging from 21 – 47°, for temperature "ramps" in the first 8 m of the atmospheric surface layer. Kaimal [1974] estimated angles between 35–56° with an average of 43° for convecting thermal plumes in the surface layer.

8.3.2 Spatial velocity fluctuations

Figures 8.11 and 8.12 show the spatial velocity fluctuations. These fluctuations are relative to a frame of reference moving with the average wind velocity across the measuring depth, in the streamwise direction. The abscissa marked "pseudo" x has been obtained by the transformation $x = \overline{u_z}t$, where $\overline{u_z}$ (= 6.58 m/s) is the mean wind velocity across the observational depth. The fluctuations have been color coded for ease in interpretation. Colors blue, red, yellow and green represent the first through fourth quadrant motions on the $u'w'$ plane, respectively, i.e. red lines represent the

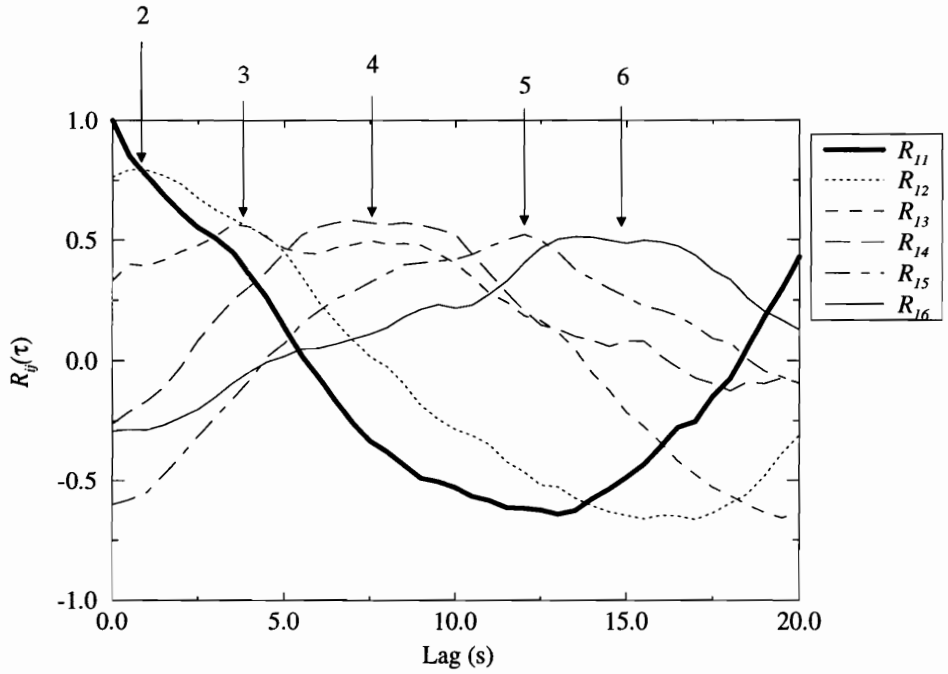

Figure 8.9: Cross-correlation of the u' signals at different levels. Refer Table for details.

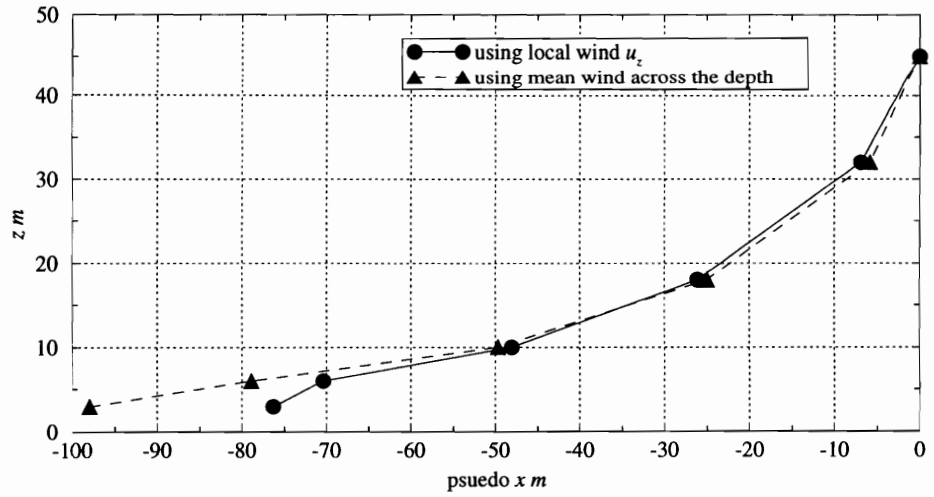

Figure 8.10: Spatial orientation of a large scale motion.

ejection motions and green lines represent sweeps. The time interval which has been transformed to spatial fluctuations contains one of the large scale motions identified in the temporal fluctuations (structure around 550 s in Figure 8.8). Following the fluctuations in space, the "back" of the large scale motion is quite apparent. As the schematic (Figure 8.3) suggests, the sweep like motions are seen from 150–250 on the pseudo x axis. This is the region of $+u'$. This is followed by the ejection like motions from 225–320 m. Downstream, a large eddy like motion is apparent from 380–440, which may be the "head" of a large vortical arch. Vortex like motions of smaller sizes can be picked out from these figures using visual observations. This suggests that large scale motions in the near neutral atmospheric surface layer may indeed be manifestations of transverse vortical arch like structures. The signature of these structures will be useful as a test bed for comparison with numerical simulation.

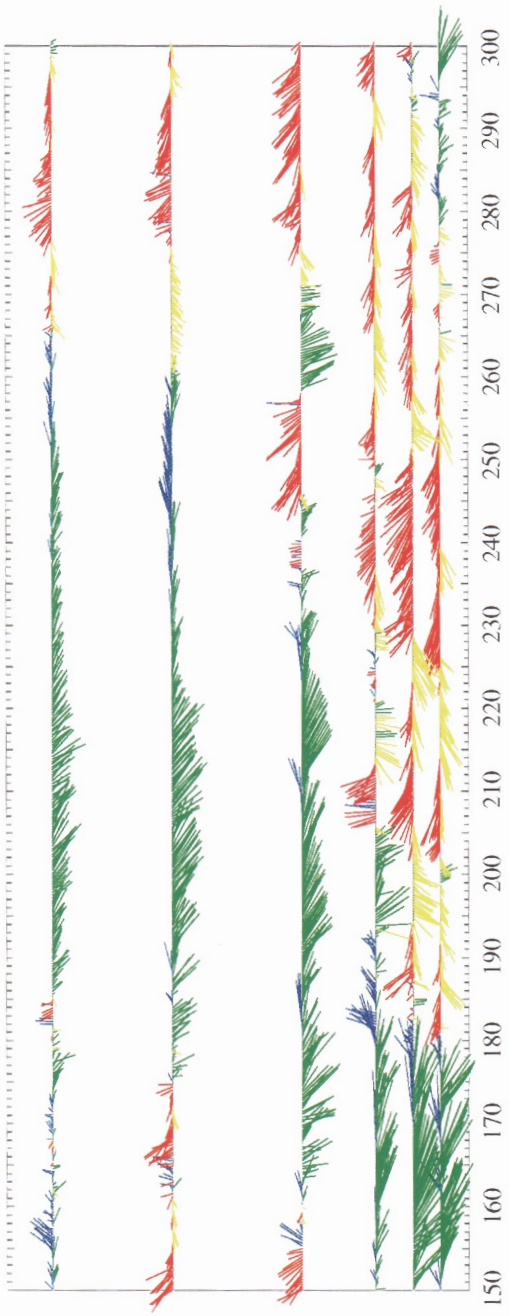

Figure 8.11: Velocity fluctuations in space (150 300).

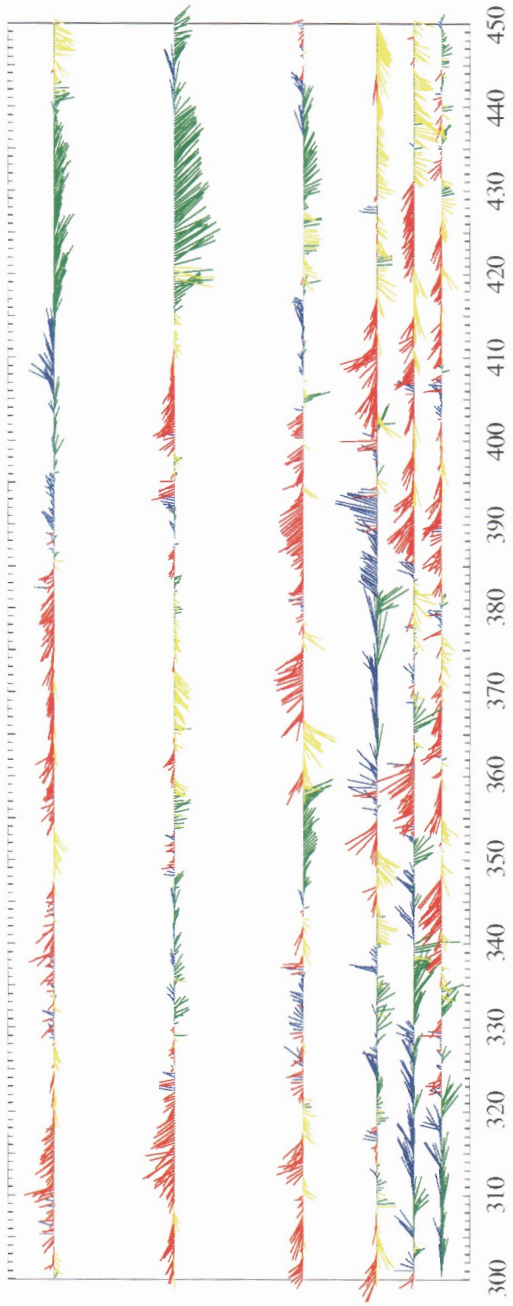

Figure 8.12: Velocity fluctuations in space (300 450).

Chapter 9

CONCLUSIONS

The quasi-periodic structures seen in turbulent laboratory flows also appear to be present in the marine atmospheric surface layer. These structures are also seen to have a major contribution to the Reynolds stress.

Although the probe is located at $z^+ \approx 10^5$, it is well within the log region or close to the wall in terms of the atmospheric boundary layer profile [e.g., Panofsky & Dutton, 1984] if not in terms of viscous lengths. Analysis suggests that the events detected in the velocity data are very similar to the ejection events observed in laboratory flow. It appears that these flow features are kinematically driven rather than being viscous effects.

The percentage contribution to the Reynolds stress from ejection events observed in the marine atmospheric surface layer is in close agreement to corresponding values obtained in the laboratory. As the Reynolds number of the laboratory flows is much smaller than the atmospheric boundary layer flow, it may be argued that the percentage contribution to the Reynolds stress from different quadrants of the $u'w'$ plane is independent of the Reynolds number.

Detection of these events using the various ejection detection techniques shows that these events occur in groups. These groups may be in accordance with the observations of Offen & Kline [1975] and Bogard & Tiderman [1986] (BT) that burst structures consist of one or more than one ejection resulting from the same streak instability. Following the technique of BT, the ejections were grouped into bursts resulting in a distribution of time between bursts having a mean of 47 s at a height of 8.2 m above the sea surface, where the mean wind velocity was 6.74 m/s. The bursts in the marine atmospheric surface layer occur on a much larger time (and space) scale than the bursts observed in the laboratory.

Although the number of ejections detected is a monotonic function of the threshold parameters used in the detection algorithms, the number of bursts these ejections group into is relatively insensitive to the threshold. This is an indication that each streak breakup has at least one "strong" ejection which is preceded and/or succeeded by other ejections of varying intensity.

The quasi-periodic nature of the bursting process in the marine atmospheric surface layer has been confirmed using the short-time autocorrelation of Kim *et al.* [1971] on the streamwise component of the velocity signal. The time between peaks in the autocorrelation corresponds very well with the mean burst period obtained by the distribution of bursts. The peak of the first moment of the $u'w'$ cospectrum is at a frequency close to the mean burst frequency.

Conditional averages of the velocity signal during the time of ejection suggests that the ejections are events which are characterized by a deceleration in the streamwise velocity followed by a sudden acceleration during which time the normal fluctuating velocity increases and then suddenly drops. This is similar to the ejection event seen

in laboratory flows. The cross-flow component of the velocity signal was not observed to have any correlation with the ejection events.

Scaling of burst periods using inner variables (u_*, ν) produces far different results than seen in laboratory flows. This suggests that the molecular viscosity may not have an important role in determining the flow structure. The unavailability of data on the outer variables precludes drawing any absolute conclusions on the appropriateness of outer variable scaling.

Both ejection and burst periods decrease with increasing wind speed. There is a significant difference in the pattern of ejections found between the cases when the wind speed is low and when the wind speed is higher. At low speeds the ejections occur in well-separated groups of one or more which group well into bursts. As wind speed increases, the number of ejections per unit time also increases. At higher speeds the spacing between them shrinks to the point that when using the shorter, 30 min records, it is difficult to assign the ejections to individual bursts. The transition between these low and high-speed cases occurs gradually beginning in the 6-7 m/s range. Since the surface stress is largely supported by the bursts, one will find that at low wind speeds the stress is highly intermittent. Stress pulses occur with a period of the order of a minute. As the wind speed increases, however, this period shortens, the pulsing will appear to diminish and the stress appears more continual. In the case of higher wind speeds, it makes less sense to try to group the ejections into bursts, at least using the BT scheme. In terms of the vortical structures which may support the bursting process, at low wind speeds there are relatively few of these structures being swept along in the wind, but at high speeds, there may be many more. At high speeds they may appear in many different sizes, perhaps often overlapping, and give

rise to an apparently more continual surface stress.

The mean ejection and burst periods are seen to have little if any dependence on the significant wave height or mean wave slope present at the sea surface. The modal wave periods here range from 0.88 to 5.33 s, thus the timescale of the surface motion is significantly shorter than the average burst or ejection periods. There are a significant number of ejections falling less than 10 s apart which have been identified as ejections from a single burst. Surface wave influence on these is possible which may affect the structure of a burst. In the open ocean, where the wave periods would be longer, there may be a discernible wave dependence on the mean ejection and burst periods.

Ejection and sweep motions seem to exist simultaneously at all scales suggesting the fractal nature of turbulence. Though previous results indicate that bursting is quasi-periodic with a period on the order of a minute, the fractal nature of the ejection motions suggests that the dominant scale of the flux mechanism is the scale corresponding to the peak in the $u'w'$ cospectrum. This may help to better understand the cascading process.

Using velocity measurements at multiple heights, large scale motions in the marine atmospheric surface layer have been identified. Eddy like structures of various sizes could be identified by visual observations of the velocity fluctuations. Analysis of the velocity signals, suggests that the ejection and sweep motions may be "backs" of large transverse vortical arch like structures. These structures convect at shallow angles ($\approx 15°$) near the surface. The inclination increases with height and they are seen to convect with a 45° inclination above $z = 20$ m. Further analysis is required to characterize these structures which could be used as a test bed for comparison

with large-eddy or direct numerical simulations. These large scale motions (which are qualitatively similar to their laboratory counterparts) may indeed be a universal feature of wall bounded turbulent shear flows.

REFERENCES

[1] Alfredsson, P. H., and A. V. Johansson, On the Detection of Turbulence-Generating Events, *J. Fluid Mech.*, *139*, 325–345, 1984.

[2] Arya, S. P., *Introduction to Micrometeorology*, Academic Press, San Diego, 1988.

[3] Barthelmie, R. J., M. S. Courtney, J. Høstrup, and P. Sanderhoff, The Vindeby Project: A Description. **RISO-R-741(EN)**, Risø National Laboratory, Roskilde, Denmark, March 1994.

[4] Blackwelder, R. F., and R. E. Kaplan, On the Bursting Phenomenon Near the Wall in Bounded Shear Flows, *J. Fluid Mech.*, *76*, 89–112, 1976.

[5] Bogard, D. G., and W. G. Tiederman, Burst Detection With Single Point Velocity Measurements, *J. Fluid Mech.*, *162*, 389–413, 1986.

[6] Chambers, A. J., and R. A. Antonia, Wave-Induced Effect on the Reynolds Shear Stress and Heat Flux in the Marine Surface Layer, *J. Phys. Oceanogr., 11,* 116–121, 1981.

[7] Chen, C. H. P., and R. F. Blackwelder Large-scale Motion in a Turbulent Boundary Layer: A Study Using Temperature Contamination. *J. Fluid Mech.*, *89*, 1–31, 1978.

[8] Comte-Bellot, G., J. Sabot, and I. Saleh, Detection of Intermittent Events Maintaining Reynolds Stress, *Dynamic measurements in unsteady flows; Proceedings of the Dynamic Flow Conference*, Skovlunde, Denmark, 1979.

[9] Corino, E. R., and R. S. Brodkey, Visual Investigation of the Wall Region in Turbulent Flow, *J. Fluid Mech.*, *37*, 1–30, 1969.

[10] Daubechies, I., Orthonormal bases of compactly supported wavelets. *Commun. Pure Appl. Math., 41*, 909-996, 1988.

[11] Davidson, D. S., The Translation Velocity of Convective Plumes, *Quart. J. Roy. Meteor. Soc.,*, 100, 572–592, 1974.

[12] Duncan, M. R., and P. H. Shuepp, A Method to Delineate Extreme Structures Within Airborn Flux Traces Over the FIFE site, *J. Geophys. Res.*, *97*, 18487–18498, 1992.

[13] Falco, R. E., and C. P. Gendrich, The Turbulence Burst Detection Algorithm of Z. Zarić. *Near Wall Turbulence: 1988 Zarić Memorial Conference*, Hemisphere Pub. Corp., New York, 1990.

[14] Farge, M., Wavelet Transforms and their Application to Turbulence. *Annu. Rev. Fluid Mech., 24*, 395–457, 1992.

[15] Gao, W., R. H. Shaw, and K. T. Paw U, Conditional Analysis of Temperature and Humidity Microfronts and Ejection/Sweep Motions Within and Above a Deciduous Forest, *Boundary Layer Meteorol., 59*, 35–57, 1992.

[16] Garratt, J. R., *The Atmospheric Boundary Layer*, Cambridge University Press, Cambridge, 1992.

[17] Gordon, J. R., Intermittent Momentum Transport in a Geophysical Boundary Layer, *Nature, 248*, 392–394, 1974.

[18] Gordon, M. C., Period Between Bursts at High Reynolds Number, *Phys. Fluids, 18*(2), 141–143, 1975.

[19] Grass, A. J., Structural Features of Turbulent Flow Over Smooth and Rough Boundaries, *J. Fluid Mech., 50*, 233–255, 1971.

[20] Grossmann, A., Kronland-Martinet, R., and Morlet, J., Reading and understanding Continuous Wavelet Transforms, in J. M. Combes *et al.* (eds.), *Wavelets: Time-Frequency Methods and Phase Space*, Springer-Verlag, New York, 2–20, 1989.

[21] Head, M. R., and P. Bandyopadhyay, New Aspects of Turbulent Boundary Layer Structure, *J. Fluid Mech., 107*, 297–338, 1981.

[22] Heathershaw, A. D., "Bursting" Phenomena in the Sea, *Nature, 248*, 394–395, 1974.

[23] Hussain, A. K. M. F., Coherent Structures and Studies of Perturbed and Unperturbed Jets, *The Role of Coherent Structures in Modelling Turbulence and Mixing*, 252–291, Springer-Verlag, New York, 1981.

[24] Jackson, R. G., Sedimentological and Fluid-Dynamic Implications of the Turbulent Bursting Phenomenon in Geophysical Flows, *J. Fluid Mech., 77*, 531–560, 1976.

[25] Jenkins, G. M., and D. G. Watts, *Spectral Analysis and its Applications*, Holden-Day, San Franscisco, 1968.

[26] Johansson, A. V., and P. H. Alfredsson, On the Structure of Turbulent Channel Flow, *J. Fluid Mech., 122*, 295–314, 1982.

[27] Kaimal, J. C., Translation Speed of Convective Plumes in the Atmospheric Surface Layer. *Quart. J. Roy. Meteor. Soc.,*, 100, 46–52, 1974.

[28] Kaimal, J. C., and J. J. Finnigan, *Atmospheric Boundary Layer Flows: Their Structure and Measurement*, Oxford University Press, New York, 1994.

[29] Kawamura, H., K. Okuda, S. Kawai, and Y. Toba, Structure of Turbulent Boundary Layer Over Wind Waves in a Wind Wave Tunnel, *Tohoku Geophys. J.*, *28*, 69–86, 1981.

[30] Katul, G. G., J. Albertson, M. Parlange, and H. Stricker, Conditional Sampling, Bursting, and the Intermittent Structure of Sensible Heat Flux. *J. Geophys. Res.*, *99*(D11), 22869–22876, 1994.

[31] Kim, H. T., S. J. Kline, and W. C. Reynolds, Production of Turbulence Near a Smooth Wall in a Turbulent Boundary Layer, *J. Fluid Mech.*, *50*, 133–160, 1971.

[32] Kline, S. J., and S. K. Robinson, Quasi-Coherent Structures in the Turbulent Boundary Layer: part I. Status report on a community–wide summary of the data, *Near Wall Turbulence: 1988 Zarić Memorial Conference*, Hemisphere Pub. Corp., New York, 1989.

[33] Kline, S. J., W. C. Reynolds, F. A. Schraub, and P. W. Runstadler, The Structure of Turbulent Boundary Layer. *J. Fluid Mech.*, *30*, 741–773, 1967.

[34] Lu, S., and W. W. Willmarth, Measurements of the Structure of the Reynolds Stress in a Turbulent Boundary Layer, *J. Fluid Mech.*, *60*, 481–511, 1973.

[35] Luchik, T. S., and W. G. Tiederman, Timescale and Structure of Ejections and Bursts in Turbulent Channel Flow, *J. Fluid Mech.*, *174*, 529–552, 1987.

[36] Mahrt, L., and W. Gibson, Flux Decomposition into Coherent Structures, *Boundary Layer Meteorol.*, *60*, 143–168, 1992.

[37] Mahrt, L., and J. F. Howell, The Influence of Coherent Structures and Microfronts on Scaling Laws Using Global and Local Transforms, *J. Fluid Mech.*, *260*, 247–270, 1994.

[38] Narasimha, R., and V. S. Kailas, Energy Events in the Atmospheric Boundary Layer, *Perspectives in Turbulence Studies : International Symposium DFVLR Research Center*, Springer-Verlag, New York, 1987.

[39] Narasimha, R., and V. S. Kailas, Turbulent Bursts in the Atmosphere, *Atmos. Environ.*, Part A, *24*(7), 1635–1645, 1990.

[40] Offen, G. R., and S. J. Kline, A Comparison and Analysis of Detection Methods for the Measurements of Production in a Boundary Layer, paper presented at Third Biennial Symposium of Turbulence in Liquids, Univ. of Mo.-Rolla, 1975.

[41] Panofsky, H. A., and J. A. Dutton, *Atmospheric Turbulence: Models and Methods for Engineering Applications,* John Wiley, New York,1984.

[42] Paw U, K. T., Y. Brunet, S. Collineau, R. H. Shaw, T. Maitani, J. Qiu, and L. Hipps, On Coherent Structures in Turbulence above and Within Agricultural Canopies, *Agric. For. Meteorol.*, *61*, 55–68, 1992.

[43] Perry, A. E., and J. D. Li, Experimental Evidence for the Attached-Eddy Hypothesis in Zero Pressure Gradient Turbulent Boundary Layers. *J. Fluid Mech.*, *218*, 405–438, 1990.

[44] Phong-anant, D., R. A. Antonia, A. J. Chambers, and S. Rajagopalan, Features of the Organized Motion in the Atmospheric Surface Layer, *J. Geophys. Res.*, *85*(C1), 424–432, 1980.

[45] Press, W. H., S. A. Teukolsky, W. T. Vellerling, and B. P. Flannery, *Numerical Recipes in Fortran: The Art of Scientific Computing*, Cambridge, 1992.

[46] Robinson, S. K., Instantaneous Velocity Measurements in a Turbulent Boundary Layer. *Chem. Eng. Comm.*, *43*, 347–369, 1986.

[47] Robinson, S. K., Coherent Motions in the Turbulent Boundary Layer. *AIAA*, *23*, 601–639, 1990.

[48] Robinson, S. K., Coherent Motions in the Turbulent Boundary Layer. *Annu. Rev. Fluid Mech.*, *23*, 601–639, 1991.

[49] Snyder, R. L., W. L. Neu, R. B. Long, and W. J. P. de Voogt, A Long Range Program to Parameterize the Two–Dimensional Evolution of the Surface Gravity Wave Field, Tech. Rep. *90–2*, Nova Univ. Oceanogr. Cent., Fort Lauderdale, Fl., 1990.

[50] Spalart, P. R., Direct Simulation of a Turbulent Boundary Layer up to $Re_\theta = 1410$, *J. Fluid Mech.*, *187*, 61–98, 1988.

[51] Strickland, J. H., and R. L. Simpson, "Bursting" Frequencies Obtained from Wall Shear Stress Fluctuations in a Turbulent Boundary Layer, *Phys. Fluids*, *18*(3), 306–308, 1975.

[52] Stull, R. B., *Introduction to Boundary Layer Meteorology*, Kluwer Academic, Norwell, Mass., 1988.

[53] Takeuchi, K., E. Leavitt, and S. P. Chao, Effects of Water Waves on the Structure of Turbulent Shear Flows, *J. Fluid Mech.*, *80*, 535–559, 1977.

[54] Turner, B. J., and M. Y. Leclerc, Conditional Sampling of Coherent Structures in Atmospheric Turbulence Using the Wavelet Transform, *J. Atmos. Oceanic Tech.*, *11*, 205–209, 1994.

[55] Wallace, J. M., H. Eckelmann, and R. S. Brodkey, The Wall Region in Turbulent Shear Flow, *J. Fluid Mech.*, *54*, 39–48, 1972.

[56] Wei, C., Evaluation of the Dynamic Characteristics of the K-Gill Anemometer. M.S. thesis, Va. Polytech. Inst. and State Univ., Blacksburg, 1990.

[57] Wilczak, J. M., and J. A. Businger, Large-Scale Eddies in the Unstably Stratified Atmospheric Surface Layer. Part II: Turbulent Pressure Fluctuations and Budgets of Heat Flux, Stress, and Turbulent Kinetic Energy. *J. Atmos. Sci.*, *41*, 3551–3567, 1984.

[58] Willmarth, W. W., and S. S. Lu, Structure of the Reynolds Stress Near the Wall. *J. Fluid Mech.*, *55*, 65–92, 1972.

[59] Wyngaard, J. C., Cup, Propeller, Vane, and Sonic Anemometers in Turbulence Research. *Annu. Rev. Fluid Mech.*, *13*, 399–423, 1981.

[60] Wyngaard, J. C., Atmospheric Turbulence, *Annu. Rev. Fluid Mech.*, *24*, 205–233, 1992.

VITA

The author was born in India on 23^{rd} of August 1969. He received his Bachelor of Technology (Hons.) in Naval Architecture from the Indian Institute of Technology, Kharagpur, India, in May 1991. He entered the Aerospace & Ocean Engineering department at Virginia Tech in August 1991 and received his M. S. degree in Aerospace Engineering in December 1992. He enrolled in the doctoral program in the same the same department in January 1993.